Biogeosciences

High-field NMR spectroscopy and FTICR mass spectrometry: powerful discovery tools for the molecular level characterization of marine dissolved organic matter

N. Hertkorn[1], **M. Harir**[1], **B. P. Koch**[2], **B. Michalke**[1], **and P. Schmitt-Kopplin**[1]

[1]Helmholtz Zentrum Muenchen, German Research Center for Environmental Health, Research Unit Analytical Biogeochemistry (BGC), Ingolstaedter Landstrasse 1, 85764 Neuherberg, Germany
[2]Alfred Wegener Institute, AWI, Am Handelshafen 12, 27570 Bremerhaven, (Building Co-5), Germany

Correspondence to: N. Hertkorn (hertkorn@helmholtz-muenchen.de)

Abstract. High-performance, non-target, high-resolution organic structural spectroscopy was applied to solid phase extracted marine dissolved organic matter (SPE-DOM) isolated from four different depths in the open South Atlantic Ocean off the Angola coast (3° E, 18° S; Angola Basin) and provided molecular level information with extraordinary coverage and resolution. Sampling was performed at depths of 5 m (Angola Current; near-surface photic zone), 48 m (Angola Current; fluorescence maximum), 200 m (still above Antarctic Intermediate Water, AAIW; upper mesopelagic zone) and 5446 m (North Atlantic Deep Water, NADW; abyssopelagic, ∼ 30 m above seafloor) and produced SPE-DOM with near 40 % carbon yield and beneficial nuclear magnetic resonance (NMR) relaxation properties, a crucial prerequisite for the acquisition of NMR spectra with excellent resolution. ^{1}H and ^{13}C NMR spectra of all four marine SPE-DOM showed smooth bulk envelopes, reflecting intrinsic averaging from massive signal overlap, with a few percent of visibly resolved signatures and variable abundances for all major chemical environments. The abundance of singly oxygenated aliphatics and acetate derivatives in ^{1}H NMR spectra declined from surface to deep marine SPE-DOM, whereas C-based aliphatics and carboxyl-rich alicyclic molecules (CRAM) increased in abundance. Surface SPE-DOM contained fewer methyl esters than all other samples, likely a consequence of direct exposure to sunlight. Integration of ^{13}C NMR spectra revealed continual increase of carboxylic acids and ketones from surface to depth, reflecting a progressive oxygenation, with concomitant decline of carbohydrate-related substructures.

Aliphatic branching increased with depth, whereas the fraction of oxygenated aliphatics declined for methine, methylene and methyl carbon. Lipids in the oldest SPE-DOM at 5446 m showed a larger share of ethyl groups and methylene carbon than observed in the other samples.

Two-dimensional NMR spectra showed exceptional resolution and depicted resolved molecular signatures in excess of a certain minimum abundance. Classical methyl groups terminating aliphatic chains represented ∼ 15 % of total methyl in all samples investigated. A noticeable fraction of methyl (∼ 2 %) was bound to olefinic carbon. Methyl ethers were abundant in surface marine SPE-DOM, and the chemical diversity of carbohydrates was larger than that of freshwater and soil DOM.

In all samples, we identified sp[2]-hybridized carbon chemical environments with discrimination of isolated and conjugated olefins and α,β-unsaturated double bonds. Olefinic proton and carbon atoms were more abundant than aromatic ones; olefinic unsaturation in marine SPE-DOM will be more directly traceable to ultimate biogenic precursors than aromatic unsaturation. The abundance of furan, pyrrol and thiophene derivatives was marginal, whereas benzene derivatives, phenols and six-membered nitrogen heterocycles were prominent; a yet unassigned set of six-membered N-heterocycles with likely more than one single nitrogen occurred in all samples. Various key polycyclic aromatic hydrocarbon substructures suggested the presence of thermogenic organic matter at all water depths.

Progressive NMR cross-peak attenuation from surface to deep marine SPE-DOM was particularly strong in COSY NMR spectra and indicated a continual disappearance of biosignatures as well as entropy gain from an ever increased molecular diversity. Nevertheless, a specific near-seafloor SPE-DOM signature of unsaturated molecules recognized in both NMR and Fourier transform ion cyclotron mass spectrometry (FTICR/MS) possibly originated from sediment leaching. The conformity of key NMR and FTICR/MS signatures suggested the presence of a large set of identical molecules throughout the entire ocean column even though the investigated water masses belonged to different oceanic regimes and currents.

FTICR/MS showed abundant CHO, CHNO, CHOS and CHNOS molecular series with slightly increasing numbers of mass peaks and average mass from surface to bottom SPE-DOM. The proportion of CHO and CHNO negative ions increased from surface to depth, whereas CHOS and especially CHNOS molecular series markedly declined. While certain rather aliphatic CHOS and CHNOS ions were observed solely in the surface, deep marine SPE-DOM was enriched in unique unsaturated and rather oxygenated CHO and CHNO molecular series. With the exception of abyssopelagic SPE-DOM at 5446 m, which showed a peculiar CHOS chemistry of unsaturated carbon and reduced sulphur (black sulphur), CHO and CHNO molecular series contributed $\sim 87\%$ to total positive electrospray ionization FTICR mass peak integral, with a near constant ratio of CHNO / CHO molecular compositions near 1.13 ± 0.05. In case of all four marine SPE-DOM, remarkably disparate average elemental compositions as determined from either MS and NMR spectra were observed, caused by a pronounced ionization selectivity in electrospray ionization FTICR/MS.

The study demonstrates that the exhaustive characterization of complex unknowns in marine DOM will enable a meaningful classification of individual marine biogeosignatures. Future in-depth functional biodiversity studies with a clear understanding of DOM structure and function might eventually lead to a novel, unified perception of biodiversity and biogeochemistry.

1 Introduction

The concentrations and molecular character of marine dissolved organic matter (DOM) in a given ocean water result from the combined action of biotic and abiotic reactions at different depths of the water column and are further mediated by physical distribution of water masses (Hansell and Carlson, 1998). DOM is one of the most abundant contributors to the global carbon and several other element cycles; nevertheless, marine DOM still ranges among the least characterized natural organic matter (NOM) fractions known (Dittmar and Kattner, 2003a; Hedges and Oades, 1997; Hernes and Ben-

ner, 2006). Local biochemical activity maxima in upwelling regimes, near deep sea vents or near large river plumes, and processing of terrestrial precursor molecules in coastal areas (Dittmar and Kattner, 2003b; Hernes and Benner, 2006) contribute extensively to marine DOM biosynthesis; yet, our current knowledge and definition of major contributors, like bacteria, archeae and viruses, to marine DOM synthesis and decomposition remain poorly constrained (Jiao et al., 2010). Yet, the open ocean is responsible for $\sim 70\%$ of marine production (Geider et al., 2001) and $>50\%$ of this net primary production is estimated to be funnelled through DOM into the microbial loop (Del Giorgio et al., 1997; Carlson et al., 2007).

The recently proposed concept of the microbial carbon pump (MCP) (Jiao et al., 2010) supplements the classical view of marine carbon processing by the conventional biological pump. Here, regenerated production of organic matter by microbial heterotrophic activity is considered as a main source for accumulation of recalcitrant dissolved organic carbon. Significant primary production occurs in nutrient-rich surface waters, whereas successive and perhaps repetitive processing of DOM by MCP will operate in a more diffuse manner throughout the entire ocean column. Vertical mixing, especially the downward transport of rather fresh particulate organic matter (POM) (Hedges et al., 2001) and DOM (Hopkinson and Vallino, 2005), meets with horizontal long-range transport of DOM with average ^{14}C ages of several millennia (Walker et al., 2011) and imposes a complex distribution pattern of DOM production and degradation reactions (Hansell and Carlson, 1998). Prominent abiotic reactions like photochemistry (Schmitt-Kopplin et al., 1998; Zepp et al., 2011) and atmospheric deposition (both influential near the surface) (Andreae and Crutzen, 1997; Jimenez et al., 2009; Paytan et al., 2009), (metal-mediated) redox chemistry (Schmidt et al., 2011), and thermogenic processing of organic matter (Dittmar and Koch, 2006; Dittmar and Paeng, 2009; Falco et al., 2011) attenuate and diminish the biological signatures (i.e. the complement of all primary and secondary metabolites of the marine food chain) of marine DOM which ultimately arise from primary production.

Degradative DOM analysis has revealed carbohydrates, amino acids and lipids as key biological constituents of marine DOM (Benner, 2002); at increasing water depth, the proportion of assigned carbon covered by these classes of molecules progressively diminishes from 20 % to less than 2 % of total carbon (Benner, 2002). Recently, thermogenic organic carbon (TMOC) of considerable ^{14}C age (on average, several ten thousands of years), which shows abundance in hydrogen-deficient aromatic molecules, has been detected in appreciable amounts (a few percent of total DOM) throughout the oceans (Dittmar and Koch, 2006; Dittmar and Paeng, 2009; Ziolkowski and Druffel, 2010). TMOC may originate from deep sea vents or other oceanic underground sources (Dittmar and Koch, 2006) and from riverine transport (Battin et al., 2009) of terrestrial black carbon into the ocean

(Falco et al., 2011). TMOC passively correlates with salinity, suggesting photodegradation in the surface ocean as a plausible degradation mechanism (Dittmar and Paeng, 2009). While comprehensive molecular level characterization of marine DOM remains elusive, large-scale variance of marine DOM concentration and composition and disparate reactivities across DOM fractions are well established (Hansell, 2009, 2013). Microbe-DOM interactions decisively govern DOM composition and turnover (Kujawinski, 2011; Gilbert et al., 2012; Kaiser and Benner, 2012; Hansman et al., 2009; Nagata et al., 2010); however, familiar biosignatures of marine metabolites are continually attenuated by combined action of biotic and abiotic reactions. Moreover, the majority of marine DOM resides in the deep ocean (Hansell, 2009), whereof little is known in general.

Non-target organic structural spectroscopy of DOM attempts to unselectively characterize the entire carbon present in DOM by means of information-rich detection methods such as Fourier transform ion cyclotron resonance (FTICR) mass spectrometry and NMR spectroscopy (Einsiedl et al., 2007; Hertkorn et al., 2006, 2007, 2008; Mopper et al., 2007; Schmitt-Kopplin et al., 2010a,b). FTICR mass spectrometry of DOM allows for an unprecedented resolution of thousands of molecular formulae direct out of the DOM mixture, however with considerable selectivity depending on sample handling and ionization method applied (Hertkorn et al., 2008; Koch et al., 2005; Kujawinski, 2002; Stenson et al., 2003; Flerus et al., 2012; Kujawinski et al., 2009). NMR on the other hand allows for a successive acquisition of multiple informative complementary NMR spectra at however lesser sensitivity (Simpson et al., 2002, 2011; Hertkorn and Kettrup, 2005). One dimensional NMR spectra provide near-quantitative data when carefully acquired. While acquisition of NMR spectra at high magnetic field strength (B_0) is desirable because of excellent resolution and intrinsic sensitivity and dispersion gain, transverse relaxation (loss of coherence and entropy gain because of atomic motion) may become faster at larger B_0 (Kleckner and Foster, 2011). Higher dimensional NMR spectra of complex organic mixtures of polar and ionisable molecules like those present in marine DOM may show convoluted signatures of chemical composition and physical interactions which could attenuate cross-peak integrals at high resolution if magnetization is lost with fast relaxation.

Molecular level NOM composition and structure often exhibit far more variance than anticipated from often more uniform bulk parameters, which are subject to intrinsic averaging (Ritchie and Perdue, 2008; Kelleher and Simpson, 2006; Mahieu et al., 1999; Hertkorn et al., 2007). This study aims to use high-field NMR spectroscopy with cryogenic detection and high-field FTICR mass spectrometry as non-target discovery tools to resolve characteristic molecular signatures of a specific, representative set of four selected marine DOM samples obtained by solid-phase extraction (SPE). These four SPE-DOM samples were collected during an ex-tensive SPE mapping study of marine waters across the east Atlantic Ocean (Koch and Kattner, 2012) and shared the common extraction material used (PPL, a styrene divinyl copolymer) and the position of sampling (3.1° E, 17.7° S). The water sampling depth was 5 m (near surface), 48 m (fluorescence maximum), 200 m (upper mesopelagic zone) and 5446 m (30 m above seafloor) to represent major characteristic oceanic regimes of global relevance (Koch and Kattner, 2012).

2 Methods

2.1 Sampling area and SPE-DOM extraction

Atlantic Ocean water samples were collected during the R/V *Polarstern* cruise ANT XXV/1 on 27 November 2008 at 3.126° E, −17.737° S by means of a Teflon lined, towed "fish" sampler and CTD cast, as described in Koch and Kattner (2012). Immediately after sampling, the water (50 L aliquots) was filtered (Whatman GF/F glass fiber; precombusted at 450 °C) and subjected to solid phase extraction by means of PPL, a styrene divinyl copolymer which is tailored for the retention of highly polar to non-polar substances from large volumes of water (Dittmar et al., 2008; Kaiser et al., 2003). Water was acidified (pH 2) with 10 M HCl and gravitationally loaded into 6 g PPL solid-phase extraction cartridges (PPL, Varian Bond Elut; Table 1) (Dittmar et al., 2008; Kaiser et al., 2003). Finally, the SPE-DOM was eluted with about 50 mL of pure methanol (Merck, Darmstadt, Germany). The eluted samples were stored at −27 °C in the dark until use. Four marine SPE-DOM samples were processed from 5 m depth (near-surface photic zone, Angola Current), 48 m (fluorescence maximum, Angola Current), 200 m (upper mesopelagic zone, still above Antarctic Intermediate Water, AAIW) and 5446 m (abyssopelagic; 30 m above seafloor; North Atlantic Deep Water, NADW). For NMR spectroscopy, aliquots of original methanol solutions of marine SPE-DOM samples were evaporated in vacuo to dryness and deuterated methanol (CD_3OD) was added; this cycle was repeated three times to largely exchange methanol-h_4 with methanol-d_4. Here, yellow, somewhat grainy solid marine SPE-DOM was obtained, sometimes accompanied by tiny amounts of white materials evenly distributed in the flask at the level of initial liquid phase. DOC and DON were determined as described in Flerus et al. (2012) and Schmidt et al. (2009).

2.2 NMR analysis

All proton detected NMR spectra were acquired immediately after sample preparation with a Bruker Avance III NMR spectrometer operating at 800.13 MHz ($B_0 = 18.8$ Tesla) and TopSpin 3.0/PL3 software with samples from redissolved solids (9–36 mg solid SPE-DOM in typically 120–225 μL CD_3OD (99.95 % ^{2}H), Aldrich, Steinheim,

Table 1. Details of marine SPE-DOM isolation and NMR sample preparation by PPL solid phase extraction; volume/weight ratios for methanolic extract were based on the methanol density at $20\,°C = 0.7915\,\mathrm{g\,mL^{-1}}$; asterisk: only one experiment performed.

Water depth	Marine water used for SPE	DOC of water (μM C)	Original methanolic SPE-DOM solution obtained (g/mL)	Volumetric concentration factor from solid phase extraction SPE	C extraction yield carbon (μM C L^{-1})	N extraction yield nitrogen (μM N L^{-1})
5 m	50 L	71	38.16/48.22	1037	27 199 ± 71	1088 ± 27
48 m	50 L	76	71.57/90.42	553	20 151 ± 741	816 ± 50
200 m	50 L	63	68.80/86.93	575	18 579*	723*
5446 m	50 L	47	39.37/49.74	1005	14 408 ± 377	533 ± 4

C / N ratio of SPE-DOM	Extraction yield carbon (%)	Extraction yield nitrogen (%)	Original CD$_3$OD solution used for NMR (mg)	Dry matter of SPE-DOM used for NMR (mg)	CD$_3$OD used to dissolve SPE-DOM for NMR (mg)	Total computed SPE-DOM dry matter of extract (mg)
25.0 ± 0.7	37	24.8	23 484.8	21.9	104.7	35.6
24.7 ± 2.4	44	28.3	34 225.4	36.2	190.0	75.7
25.7 ± 0.1	40	11.3	30 716.4	33.9	153.9	75.9
27.0 ± 0.9	43	10.2	16 609.4	9.2	151.9	21.8

Germany; Table 1) in sealed 2.5 and 3.0 mm Bruker Match tubes. Proton NMR spectra were acquired with an inverse geometry 5 mm z-gradient ^{1}H/^{13}C/^{15}N/^{31}P QCI cryogenic probe (**q**uaternary **c**ryogenic **i**nverse; 90° excitation pulses: ^{13}C $\sim$ ^{1}H $\sim$ 10 µs), whereas carbon detected NMR spectra were also acquired with a 3 mm z-gradient QCO ^{13}C(^{15}N,^{31}P)/^{1}H cryogenic probe (**q**uaternary **c**ryogenic **o**bserve; 90° excitation pulses: ^{13}C $\sim$ 5.3 µs and ^{1}H $\sim$ 17 µs). NMR chemical shift reference: ^{1}H NMR, HD$_2$OD: 3.30 ppm; HD$_2$SOCD$_3$, DMSO-d$_6$: 2.49 ppm; ^{13}C NMR, CD$_3$OD: 49.00 ppm. All spectra were acquired at 283 K to impede side reactions during NMR acquisitions. Comparison of ^{1}H NMR spectra acquired before and after lengthy acquisitions showed negligible alterations (Flerus et al., 2011). 1-D ^{1}H NMR spectra were recorded with a spin-echo sequence (10 µs delay) to allow for high-Q probe ring-down (Q: quality factor), classical presaturation *zgpr* and *zg-purge* (Simpson and Brown, 2005) and solvent suppression with presaturation and 1 ms spin-lock (*noesypr1d*), 5 s acquisition time, 15 s relaxation delay (d1), typically 512 scans, 1 Hz exponential line broadening. Another set of ^{1}H NMR spectra of marine SPE-DOM was acquired in dry DMSO-d$_6$ under exclusion of moisture (Kovalevskii et al., 2000; Hertkorn et al., 2006) in sealed 5 mm tubes from 500 µg of SPE-DOM in 750 µL DMSO-d$_6$ (99.95 % ^{2}H, Aldrich, Steinheim, Germany) at $B_0 = 18.8$ T and 11.7 T; an acquisition time of 5 s and a relaxation delay of 5 s was used with a spin echo sequence (10 µs delay time).

Surprisingly, ^{13}C NMR spectra of our marine SPE-DOM could not readily be acquired with acceptable baseline with an inverse 5 mm QCI probehead (optimized for ^{1}H NMR sensitivity with an outer ^{13}C and an inner ^{1}H coil) in

which the 90° ^{13}C excitation hard pulse ranged near 10 µs at $B_0 = 18.8$ T (carbon frequency: 201.26 MHz). This applied to a range of experimental conditions, including single pulse excitation and spin-echo sequences (Buddrus et al., 1989), with 10 µs delay and various adiabatic refocusing pulses (up to 70 kHz bandwidth) (Xia et al., 2008). The available composite 180° refocusing pulses with a duration of several µs to diminish effects of fast transverse NMR relaxation exhibited limited excitation bandwidth (Martin et al., 2010), which so far were not sufficient to evenly excite the full range of the ^{13}C NMR spectrum (here 235 ppm, analogous to 47 kHz). This behaviour appeared specific to these marine SPE-DOM because mixtures of small molecules in a repertory of organic solvents including CD$_3$OD could be readily detected with the same NMR experimental setup. Several delay periods from 8 µs to 40 µs were employed in single pulse sequences between pulse and first acquisition data point to account for ringdown which takes longer time for high-Q NMR probeheads. However, acceptable baseline could again not be reached, also with use of backward linear prediction (data not shown). Because of extensive molecular intricacy, marine SPE-DOM harbours arrays of superimposed narrow and broad NMR resonances which do not reach the baseline across nearly the entire chemical shift range in ^{1}H and ^{13}C NMR spectra. The Avance III NMR console offers options for digital signal enhancements (Moskau, 2002) to likely overcome these problems in the future; these are, however, beyond the scope of this publication.

^{13}C NMR spectra used inverse gated WALTZ-16 decoupling (**w**ideband **a**lternating-phase **l**ow-power **t**echnique for **z**ero residual splitting; 19 s relaxation delay; typically 10 000–35 000 scans) with an acquisition time (aq) of 1 s

and an exponential line broadening of 12.5 Hz. Methanol-d_4 NMR resonances could be fitted with Lorentzian line shapes in the chemical shift range from $\delta_C \sim 48$–49.5 ppm and subtracted from the ^{13}C NMR spectra (data not shown). However, excellent line shape and high magnetic field made this a cosmetic exercise for interest rather than a mandatory visual improvement. ^{13}C DEPT NMR spectra (**d**istortionless **e**nhanced **p**olarization **t**ransfer) were acquired with aq = 1 s and d1 = 2 s; the one bond coupling constant ^{1}J(CH) used in 1-D ^{13}C DEPT and 2-D ^{1}H,^{13}C DEPT-HSQC spectra (**h**eteronuclear **s**ingle **q**uantum **c**oherence) was set to 145 Hz and 135 Hz (the latter for CH$_3$ subspectra). DEPT-HSQC spectra were acquired with 16 scans and 1024 increments with a carbon sweep width of 40 kHz (200 ppm). Individual ^{1}H and multiplicity-edited ^{13}C NMR traces obtained from linear combinations of DEPT NMR spectra were integrated with a bucket width of 0.01/1 ppm (AMIX software, version 3.9.4) to produce the ^{1}H NMR overlay spectra (Figs. 2 and S3) and the NMR section integrals provided in Tables 2 and 3. Carbon decoupled ^{1}H, ^{13}C HSQC spectra (*hsqcetgpsisp2.2*) were acquired under the following conditions: acquisition time: 250 ms; ^{13}C 90° decoupling pulse, GARP (70 μs); 50 kHz WURST 180° ^{13}C inversion pulse (**w**ideband, **u**niform, **r**ate, and **s**mooth **t**runcation; 1.2 ms); F2 (^{1}H): spectral width (SW) of 9615 Hz, ^{1}J(CH) = 150 Hz, 1.25 s relaxation delay; F1 (^{13}C): SW = 40 253 Hz (200 ppm); number of scans (F2)/F1-increments (^{13}C frequency) for SPE-DOM (400–1800/137–142). HSQC-TOCSY (*hsqcetg-psisp.2*) NMR spectra used dipsi-2 mixing of 70 ms. Non-decoupled absolute value accordion (^{1}J$_{CH}$ = 135–165 Hz; ^{n}J$_{CH}$ = 5–10 Hz) HMBC spectra (**h**eteronuclear **m**ultiple **b**ond **c**oherence; *hmbcacbigplnd*) were acquired with aq = 250/750 ms and d1 = 1.25/0.75 s. All HSQC-derived NMR spectra were computed to a 8192 × 1024 matrix (HMBC: 16 384 × 512) with exponential line broadening of 3 Hz in F2 (SPE-DOM) and a shifted sine bell (π/2.5) in F1. Gradient (1 ms length, 200 μs recovery) and sensitivity enhanced sequences were used for all HSQC, DEPT-HSQC and TOCSY NMR spectra. COSY and TOCSY NMR spectra (**c**orrelation **s**pectroscopy; **to**tal **c**orrelated **s**pectroscopy) used acquisition times of 750 ms at a spectral width of 9615 Hz with 70 ms dipsi-2 mixing sequence (TOCSY with solvent suppression: *dipsi2etgpsi19*; **d**ecoupling **i**n the **p**resence of **s**calar **i**nteractions), and absolute value (COSY) and echo–antiecho selection (TOCSY) with variable relaxation delay d1, ranging from 750 ms to 3.25 s, depending on T_1 noise attenuation and induced temperature variance; 8–64 scans/1600 increments were acquired. COSY/TOCSY spectra were computed to a 8192 × 2048 matrix with 2.5 Hz exponential multiplication in F2 and a shifted sine bell (π/2.5; TOCSY) and squared shifted sine bell (π/2.5; COSY) in F1.

NMR chemical shifts and NMR spectra for the proposed model of substituted polycyclic aromatics (Figs. 11 and S6 and Table S4) were computed from ACD HNMR and CNMR predictor software, version 5.0 (Advanced Chemistry Development, Toronto, Canada). Further NMR acquisition parameters are provided in the Table S3; see also Table 1.

2.2.1 NMR-based reverse mixing model to determine H / C and O / C elemental ratios

A ^{13}C NMR-based reverse mixing model (Hedges et al., 2002) served to compute the NMR-derived elemental H / C and O / C ratios of the four marine SPE-DOM samples. Seven carbon NMR regions of chemical shift (cf. Table 3) attributed to certain fundamental building blocks with given H / C and O / C ratios (Table 3) were multiplied with their relative carbon abundances to provide the NMR-derived H / C and O / C elemental ratios shown in Table 3. Feasible correction for carbon multiplicity as derived from ^{13}C DEPT NMR spectra (Fig. 4) would leave these computed values nearly unchanged: a near 50 % reduction of the H / C ratio for aromatic carbon (to account for the presence of quaternary carbon atoms) would be compensated by an elevated H / C ratio for the proposed HC-O units (presence of H$_2$**C**-O and H**C**-O units in the respective chemical shift section) and for the proposed CH$_2$ units (more methyl than methine carbon was present in the C**C**H region of marine SPE-DOM).

2.3 FTICR mass spectrometry

Ultrahigh-resolution Fourier transform ion cyclotron resonance (FTICR) mass spectra were acquired using a 12 T Bruker Solarix mass spectrometer (Bruker Daltonics, Bremen, Germany) and an Apollo II electrospray ionization (ESI) source in negative and positive mode. Diluted marine SPE-DOM (5 μg mL^{-1} in methanol) were injected into the electrospray source using a micro-liter pump at a flow rate of 120 μL h^{-1} with a nebulizer gas pressure of 138 kPa and a drying gas pressure of 103 kPa. A source heater temperature of 200 °C was maintained to ensure rapid desolvation in the ionized droplets. Spectra were first externally calibrated on clusters of arginine in MeOH (0.57 mol L^{-1}), and internal calibration was systematically done in the presence of natural organic matter, reaching accuracy values lower than 500 ppb. The spectra were acquired with a time domain of 4 megawords in ESI($-$) and 2 megawords in ESI($+$), and 1000 scans were accumulated for each spectrum. Calculation of elemental formulae for each peak was done in a batch mode by an in-house written software tool and with the *NetCalc* network approach described previously (Tziotis et al., 2011). The generated formulae were validated by setting sensible chemical constraints (N rule, O / C ratio $\leq$ 1, H / C ratio $\leq 2n + 2$ (C$_n$H$_{2n+2}$), element counts (C $\leq$ 100, H $\leq$ 200, O $\leq$ 80, N $\leq$ 3, S $\leq$ 2, P $\leq$ 1) and mass accuracy window (set at $\pm$ 0.5 ppm)). Final formulae were generated and categorized into groups containing CHO, CHNO, CHOS or CHNOS molecular compositions, which were used to reconstruct the group-selective mass spectra (Schmitt-Kopplin

et al., 2010a,b). The computed average values for H, C, N, O and S (atom %) and the H/C and O/C elemental ratios given in Tables 5 and 6 were based upon intensity-weighted averages of mass peaks with assigned molecular formulae. The frequency analysis of mass differences and attribution to various functional groups was performed from computed compositional networks as described in Tziotis et al. (2011).

2.4 Metal analysis of methanolic SPE-DOM extract

From each original methanolic SPE-DOM extract, exactly weighted (range 40–50 mg) solutions were gently evaporated using a "DigiPREP system" (S-Prep, Germany), and the residuals were redissolved with very pure 30 mL 1 % HNO_3. These solutions were used for analysis with ICP-AES (inductive coupled plasma atom emission spectroscopy; Optima 7300, Perkin Elmer, Rodgau-Jügesheim, Germany) or, in case when concentrations were found below the instrument limit of detection (LoD), with a high-resolution ICP-sf-MS (inductive coupled plasma sector field mass spectrometer; Element-1, Thermo-Finnigan, Bremen). Instrument parameters for ICP-AES: the RF power was 1000 W, the plasma gas was 15 L Ar min^{-1}, and the nebulizer gas was 0.6 L Ar min^{-1}. A micromist nebulizer was connected to a cyclon spray chamber. The measured spectral element lines were (nm): Al: 396.153, As: 193.696, B: 249.772, Ca: 393.366, Cu: 324.752, Fe: 259.939, K: 766.490, Mn: 257.610, Mo: 202.031, Na: 589.592, Ni: 231.604, P: 213.617, S: 181.975, and Zn: 213.857.

High-resolution ICP-sf-MS: Sample introduction was carried out using a peristaltic pump equipped with an "anti-pulse-head" (SPETEC, Erding, Germany), connected to a micromist nebulizer with a cyclon spray chamber. The RF power was 1200 W, the plasma gas was 15 L Ar min^{-1}, and the nebulizer gas was 0.9 L Ar min^{-1}. The measured isotopes were ^{9}Be, ^{209}Bi, ^{114}Cd, ^{59}Co, ^{52}Cr, ^{133}Cs, ^{202}Hg, ^{7}Li, ^{24}Mg, ^{55}Mn, ^{58}Ni, ^{208}Pb, ^{121}Sb, ^{120}Sn, ^{88}Sr, ^{232}Th, ^{48}Ti, and ^{238}U.

Quality control was performed for ICP-AES and ICP-sf-MS: Before and after sample measurements, control determinations of blanks and certified standards for all mentioned elements were performed. Calculation of results was carried out on a computerized lab-data management system, relating the sample measurements to calibration curves, blank determinations, control standards and the weight of the digested samples.

3 Results and discussion

3.1 Details of solid phase extraction of marine SPE-DOM from seawater

A large volume of seawater (∼ 50 L each) was processed to eventually obtain NMR spectra with a good S/N ratio; hence, the amount of isolated marine SPE-DOM at last outbalanced conceivable organic impurities possibly originating from the SPE cartridge itself. SPE extraction discriminated against DON, especially at deep waters; the C/N ratio for all extracts ranged around 25 (Table 1, placing credible restraints on the maximum occurrence of peptides in isolated marine SPE-DOM).

The water masses covered by our sampling represent Atlantic surface water (5 m, 48 m, 200 m) and North Atlantic Deep Water (NADW, 5446 m). The depth profile (Fig. 1) was characterized by the typical decreasing DOC/DON concentration induced by primary production in the surface, whereas older water masses (North Atlantic Deep Water, NADW, Fig. 1) carried predominantly refractory DOM in the deeper layers (Koch and Kattner, 2012).

3.2 Key transfer functions in the isolation and characterization of marine dissolved organic matter

Transfer functions define the relationships between measured variable and atomic/molecular/physical/chemical processes. Owing to the polydispersity of marine DOM, transfer functions referring to its isolation and characterization will be complex, non-linear and mainly ill-defined. Any method of DOM extraction out of seawater will exhibit structure-selective individual proportions of irreversibly adsorbed, not retained at all, and eventually isolable organic matter. Therefore, these transfer functions have to be constrained indirectly by a series of experiments, e.g. by using various techniques of isolation, followed by complementary physical and chemical characterization (Hertkorn et al., 2007; Mopper et al., 2007).

Mass spectrometry detects gas phase ions of marine SPE-DOM, whereas NMR spectroscopy evaluates atomic environments of dissolved SPE-DOM molecules; hence, their transfer functions are governed by different factors. Relevant previous NMR and mass spectrometry characterization of marine organic matter is described in the Supplement (SI 3 and SI 4). Further key aspects of NMR experiment selection, sensitivity and resolution in polydisperse marine SPE-DOM that are indispensable for understanding of the following text are described in the Supplement (SI 1 and SI 2).

Transfer functions referring to isolation of marine DOM

Marine dissolved organic matter (DOM) accounts for roughly 95 % of the organic carbon in the oceans and occurs as a highly diluted mixture (∼ 0.5–2 mg L^{-1} DOM) of likely millions of organic compounds (a polydisperse size–reactivity continuum) in highly saline (20–35 g L^{-1} salt) aqueous solution.

Three major methods, tangential- and cross-flow ultrafiltration (UF; 8–45 % DOC yield), solid phase extraction (SPE: 10–75 % DOC yield), and reverse osmosis/electrodialysis (ROED; 70–85 % DOC yield), are currently in use to overcome the remarkable challenges of
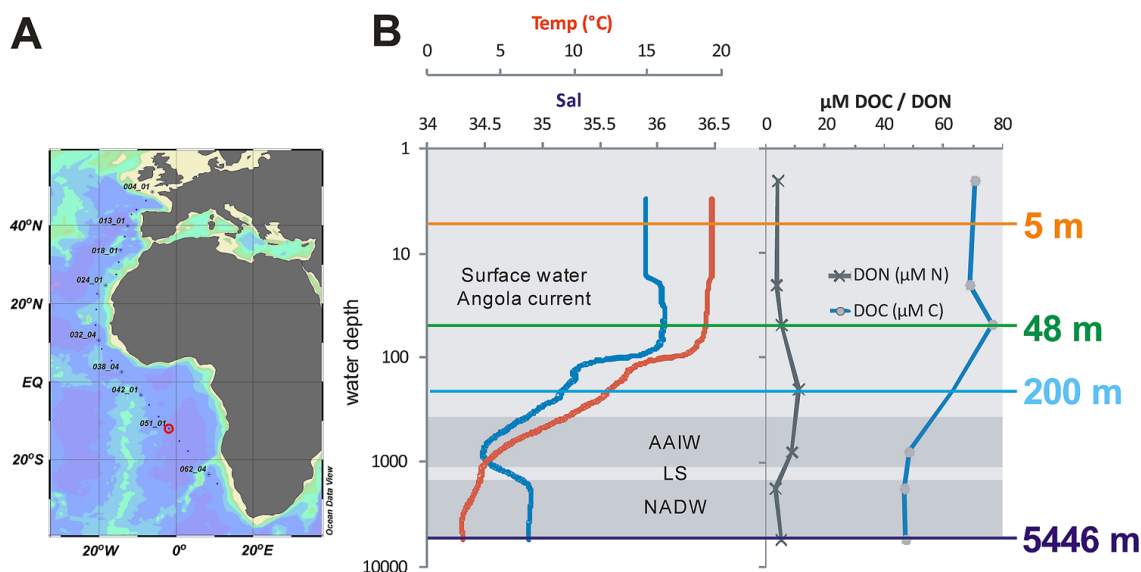
Fig. 1. (A) Sampling location of SPE-DOM during the R/V *Polarstern* cruise ANT XXV/1 on 27 November 2008 at 3.126° E, −17.737° S; figure courtesy of Gerd Rohardt, AWI. (B) Conditions of oceanic waters; AAIW: Antarctic Intermediate Water, which is derived from the Weddell Sea and Labrador Sea; LS: Labrador Sea (Tomczak and Godfrey, 2003); NADW: Nort Atlantic Deep Water.

isolating reasonable ash-free, unbiased marine DOM from seawater in acceptable yield (Mopper et al., 2007).

At present, marine DOM isolated by means of ROED (ROED-DOM) appears to be most representative, and is comprised of both hydrophobic moieties preferentially isolated by SPE, and more polar and carbohydrate derivatives primarily isolated by UF (Koprivnjak et al., 2009). However, large fractions of collateral inorganic components in ROED-DOM remain (commonly >50 %; Mao et al., 2012) that strongly interfere with key methods of organic structural spectroscopy like NMR (imposing strong differential NMR relaxation from metal coordination) and FTICR mass spectrometry (extensive formation of cluster ions with exceptional ionization selectivity that will suppress mass peaks from ROED-DOM itself).

In contrast to ROED, isolation of marine SPE-DOM requires no major instrumentation and is readily adapted to field conditions; it represents a fair compromise between low expenditure and satisfactory recovery of carbon (in this study about 40 %; cf. Table 1) (Dittmar et al., 2008). In particular, marine SPE-DOM is thoroughly desalinated. This is a huge indirect benefit for further spectroscopic characterization of marine SPE-DOM because bothersome interferences with potential to severely deplete significance of data will be strongly attenuated.

3.3 ^{1}H NMR spectra of marine SPE-DOM

The ^{1}H NMR spectra of the four SPE-DOM samples acquired with and without (data not shown) solvent suppression showed the smooth bulk envelopes familiar from other marine DOM spectra (Fig. 2) (Aluwihare et al., 2002; Repeta

et al., 2002; Hertkorn et al., 2006). From higher to lower field (from right to left), abundant (a) aliphatic, (b) "acetate-analogue", (c) carboxyl-rich alicyclic molecules CRAM, (d) "carbohydrate-like" and methoxy, (e) olefinic, and (f) aromatic NMR resonances showed clearly recognizable and rather broad maxima (letters given according to Fig. S3). Superimposed small NMR resonances indicative of comparatively abundant biological (marine metabolites) and biogeochemical molecules (abiotic alteration products) were most significant in the aromatic section (f), well noticeable in sections (d) and (e) and of continual lesser occurrence in the order (c) > (b) > (a).

In general, the abundance of proton NMR recognizable molecular signatures declined in the order 48 m > 5 m ≫ 200 m > 5446 m. The signatures correlated with the supposed biological activity and primary production in the photic zone. With the bulk envelopes dominating the NMR spectra, the relative intensity distributions nevertheless showed appreciable variation which appeared more conspicuous in the spectral overlay (Fig. 2a–d) than in the relative NMR section integrals (Table 2, Fig. S2). In fact, given the extent of mandatory intrinsic averaging in proton 1-D NMR spectra, the observed variance across the ^{1}H NMR spectra of the four marine SPE-DOM has to be appraised as relevant (Fig. 2d).

The proton NMR spectra of four marine SPE-DOM shown (Fig. 2 and S3) were normalized to identical areas of total integral from $\delta_{H} \sim 0$–10.5 ppm. The signal envelopes showed smooth overall distribution with nearly coinciding methyl resonances near $\delta_{H} \sim 0.9$ ppm (methyl, terminating purely aliphatic chains), variable intensity maxima at $\delta_{H} \sim 1.3$ ppm
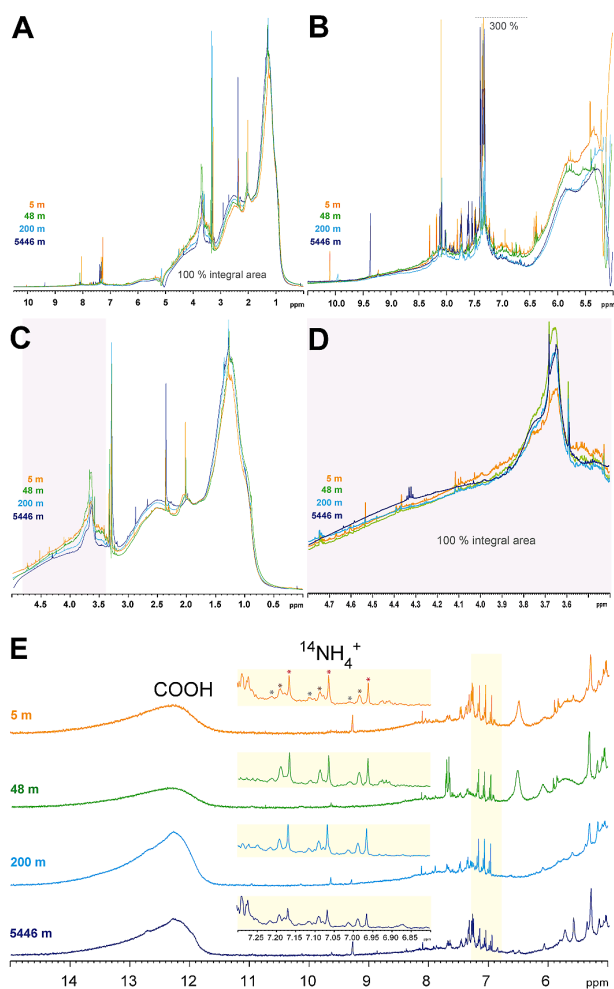
Fig. 2. (A) ^{1}H NMR spectra of marine SPE-DOM obtained by solid phase extraction (PPL) at different depths according to color: orange: 5 m (near surface photic zone); green: 48 m (fluorescence maximum); blue: 200 m (upper mesopelagic zone); and dark blue: 5446 m (30 m above seafloor). In **(A–C)**, the respective spectral intensities were scaled to 100 % total integral within the entire region of chemical shift ($\delta_H \sim 0$–10.5 ppm; with residual water and methanol excluded). **(A)** Entire spectral range, $\delta_H \sim 0$–10.5 ppm; **(B)** unsaturated protons, bound to sp^2-hybridized carbon, $\delta_H \sim 5$–10.5 ppm, and anomeric protons ($\delta_H < 5.5$ ppm); truncated at 33 % maximum intensity; cf. Figs. S2 and S3; **(C)** protons bound to sp^3-hybridized carbon, $\delta_H \sim 0$–5 ppm; **(D)** section of **H**C-O protons, normalized to 100 % integral within the chemical shift indicated ($\delta_H \sim 3.4$–4.8 ppm); note the different relative NMR resonance amplitudes compared with **(C)**, which is normalized to the entire range of chemical shift ($\delta_H \sim 0$–10.5 ppm). **(E)** ^{1}H NMR spectra of marine SPE-DOM in dry DMSO-d$_6$, downfield section $\delta_H > 5$ ppm; acquired at $B_0 = 11.7$ T, showing both exchangeable and non-exchangeable protons; aside from the large carboxylic acid NMR resonance near $\delta_H \sim 12.3$ ppm ($\delta_H \sim 11.6$–14.7 ppm), a minimum of three different ammonium (^{14}NH$_4^+$) chemical environments were observed near $\delta_H \sim 7.07$ ppm with an ostentatious coupling between ^{14}N and ^{1}H ($^1J_{NH} = 51.2$ Hz; 1 : 1 : 1 triplet, because of nuclear spin for ^{14}N = 1, denoted with colored asterisks).

(methylene and other purely aliphatics, **H**C ≥ 4 bonds away from next heteroatom) and progressively increasing downfield shoulders ranging from $\delta_H \sim 1.4$–1.7 ppm in the order 5 m < 48 m < 200 m < 5446 m, which represented mostly alicyclic rings with a large proportion of methyl groups (cf. DEPT-HSQC spectra; Figs. 7 and 8). The abundance of acetate derivatives near $\delta_H \sim 2.1$ ppm declined from surface to deep SPE-DOM, whereas functionalized aliphatics including those with remote carboxylic substitution typical of carboxyl-rich alicyclic molecules (CRAM; heteroatoms ≥ 2 bonds away from protons; $\delta_H \sim 2.2$–3.2 ppm) showed the opposite trend. The sum of purely aliphatic (heteroatoms ≥ 4 bonds away; $\delta_H \sim 0$–1.9 ppm) and functionalized (heteroatoms ≥ 3 bonds away; $\delta_H \sim 1.9$–3.1 ppm) protons increased from surface to bottom SPE-DOM, however slightly. Singly oxygenated units (**H**C-O) in marine SPE-DOM divided in methoxy derivatives ($\delta_H \sim 3.6$–3.8 ppm), carbohydrates, alcohols, esters, ethers and others ($\delta_H \sim 3.4$–4.8 ppm). When scaled to the total integral across the entire chemical shift range, methoxy derivatives showed maximum occurrence at the 48 m SPE-DOM and otherwise declined from surface to bottom, whereas general oxygenated units declined from surface to bottom SPE-DOM (Fig. 2, Table 2). When normalized to 100 % abundance within the **H**C-O chemical shift section from $\delta_H \sim 3.4$–4.8 ppm (Fig. 2d), methoxy peaks declined in the order 48 m > 200 m $\sim$ 5446 m > 5 m. Here, classical carbohydrates ($\delta_H \sim 3.4$–4.1 ppm) appeared most abundant for the 5 m surface sample (Fig. 2d).

Variable proportions of olefins ($\delta_H \sim 5$–7 ppm) and aromatics ($\delta_H \sim 7$–10 ppm) contributed to unsaturated chemical environments of protons. The combined abundance of protons bound to sp^2-hybridized carbon (i.e. olefins and aromatics) decreased from surface to 200 m, consistent with FTICR/MS findings (Flerus et al., 2012) and slightly increased near the ocean bottom. A group of NMR resonances with small J$_{HH}$ couplings ($^nJ_{HH} < 3$ Hz; cf. JRES and COSY NMR spectra) at $\delta_H \sim 6.3$ ppm (Figs. 2b, S4 and S5) with declining abundance from surface to deep marine SPE-DOM (McCaul et al., 2011), recognized earlier in ultrafiltered marine NOM (Hertkorn et al., 2006) and lake sediments (data not shown) but not previously assigned, can now be attributed to (remotely substituted) olefins by positions of their HSQC cross peaks (near $\delta_C \sim 110$ ppm). Analogous isolated double bonds can be found in linear terpenoids and double bonds within alicyclic systems, suggesting (in line with its declining distribution pattern from surface to depth) biological origin of these olefins. The olefinic NMR envelopes of surface samples from 5 m and 48 m on the one hand and of the deep samples from 200 m and 5446 m on the other hand nearly coincided (Fig. 2b), and the olefinic/aromatic proton NMR integral ratio varied from 1.78 (5 m), 1.89 (48 m), 2.11 (200 m) to 1.41 (5446 m; Table 2). Hence, the abundance of olefinic protons in marine SPE-DOM always exceeded that of aromatic protons (note that oxygenated aromatics

Table 2. ^{1}H NMR section integrals (percent of non-exchangeable protons) and key substructures from four marine SPE-DOM samples.

$\delta(^1\text{H})$ [ppm]	10–7.0	7.0–5.3	4.9–3.1	3.1–1.9	1.9–0.0	$H_{olefinic}/$ $H_{aromatic}$	10–5.3 ($\underline{H}C_{sp2}$)
Key substructures	$\underline{H}_{ar}$	$\underline{H}C=C$, $\underline{H}CO_2$	$\underline{H}CO$	$\underline{H}C\text{-}N$, $\underline{H}C\text{-}C\text{-}X$	$\underline{H}C\text{-}C\text{-}C\text{-}$		
5 m	1.82	4.56	22.20	28.97	42.45	2.50	6.38
48 m	1.44	2.22	23.09	28.12	45.13	1.54	3.66
200 m	0.73	2.20	19.91	30.13	47.03	3.01	2.93
5446 m	1.59	1.91	19.61	30.55	46.34	1.20	3.50

resonate at $\delta_H > 7$ ppm and polarized double bonds in part at $\delta_H > 7$ ppm). The aromatic section (f; Fig. S3) showed the largest proportion of recognizable NMR signatures, the most extensive variation in NMR resonance distribution, and therefore the most pronounced distinct signature (cf. also COSY NMR spectra). Here, the deep sea aromatic protons differed most from all other groups and suggest the presence of an unique deep sea molecular signature which could have resulted from long-term DOM processing or, alternatively, DOM leaching from bottom sediments across the expansive seafloor.

NMR resonances indicative of $\underline{H}C\text{-}O$ environments ($\delta_H \sim 3.1$–4.9 ppm) occurred in the order 48 m > 5 m > 200 m > 5446 m and commonly showed an intensity maximum near $\delta_H \sim 3.65$ ppm, probably caused by methoxy groups ($\delta_H \sim 3.6$–3.8 ppm; cf. discussion of JRES, TOCSY and (DEPT) HSQC NMR spectra). However, the relative intensity distributions within this group of NMR resonances changed considerably (Fig. 2d): The deep SPE-DOM (5446 m) exhibited a noticeable downfield shoulder which progressively developed from marine SPE-DOM at 48 m to bottom SPE-DOM (cf. assignment in DEPT-HSQC NMR spectra). Both surface (5 m and 48 m) samples showed abundant resolved $\underline{H}C\text{-}O$ NMR resonances with almost identical distribution in the chemical shift range from $\delta_H \sim 3.35$–4.7 ppm, with however much more prevalent OCH_3-derived NMR resonances (from $\delta_H \sim 3.6$–3.8 ppm) present in the SPE-DOM at 48 m. Both deep SPE-DOM samples (200 m and 5446 m) showed rather smooth and nearly coinciding NMR envelopes from $\delta_H \sim 3.35$–4.1 ppm with abundant methyl ester resonances at $\delta_H \sim 3.6$–3.8 ppm; in case of the 5446 m sample, possibly a few aromatic methyl esters ($\delta_H > 3.75$ ppm) appeared with a more distinct shoulder. After scaling the ^{1}H NMR spectra of the two surface and two deep SPE-DOM to maximum accordance across the entire $\underline{H}C\text{-}O$ chemical shift range (Fig. 2d), the intensity maxima for SPE-DOM were in the order 48 m > 5446 m $\sim$ 200 m > 5 m, with the surface SPE-DOM at 5 m strongly (by >20 %) attenuated. The lower abundance of methyl esters in surface SPE-DOM at 5 m (cf. DEPT-HSQC NMR spectra) could be plausibly explained by selective photodegradation from strong exposure to direct sunlight (Zepp et al., 2011; Schmitt-Kopplin et al., 1998).

3.4 ^{13}C NMR spectra of marine SPE-DOM

Meaningful ^{13}C NMR spectra of the four marine SPE-DOM at $B_0 = 18.8$ T (carbon frequency: 201.26 MHz) with acceptable baseline could be acquired by overcoming considerable difficulties (cf. Sect. 2.2) with a 3 mm QCO probehead with classical geometry (optimized for observation of heteronuclei with an inner X (^{13}C, ^{15}N, ^{31}P) and an outer ^{1}H coil) with a 90° ^{13}C excitation hard pulse of 5.3 µs, allowing for a sufficient excitation bandwidth with a spin echo sequence using 10 µs delay (Fig. 3) and a composite refocusing 180° pulse.

Initially, the individual ^{13}C DEPT-45, -90 and -135 NMR spectra of all four marine SPE-DOM (Buddrus et al., 1989; Hertkorn et al., 2006, Einsiedl et al., 2007; Lam et al., 2007) appeared inconspicuous on visual inspection, but revealed systematic intensity distortions which precluded facile computation of meaningful methylene (CH_2) and methyl (CH_3) subspectra by means of linear combination (Fig. 4). These were most likely caused by intrinsic variations of $^1J_{CH}$ in CH, CH_2 and CH_3 chemical environments of marine SPE-DOM. This applied for ^{13}C DEPT NMR spectra acquired with both QCI and QCO probeheads.

All SPE-DOM showed similar overall ^{13}C NMR resonance envelopes, typical of an intricate mixture of natural organic matter, with noticeable peaks of anomerics and C-aromatics for surface SPE-DOM whereas oxygenated aromatics and ketones were of too low abundance to result in noticeable humps at the S / N ratio provided (Fig. 3). Exceptional S / N ratio allowed apodization with weakly attenuating exponential multiplication (Fig. 3a) to reveal groups of sharp NMR resonances helpful to elucidate significant clustering of abundant molecular signatures. Integration according to major substructure regimes revealed continual increase of carboxylic acids and ketones from surface to deep marine SPE-DOM, reflecting a progressive oxygenation of marine SPE-DOM, with concomitant decline of carbohydrate-related substructures (Table 3).

The dominance of carboxylic acids (COOH) over peptides (CONH) and esters (COOR) was independently corroborated by ^{1}H NMR spectra of marine SPE-DOM acquired in dry DMSO-d_6 under exclusion of moisture in which COOH appeared as a broad signal near $\delta_H \sim 12.3$ ppm
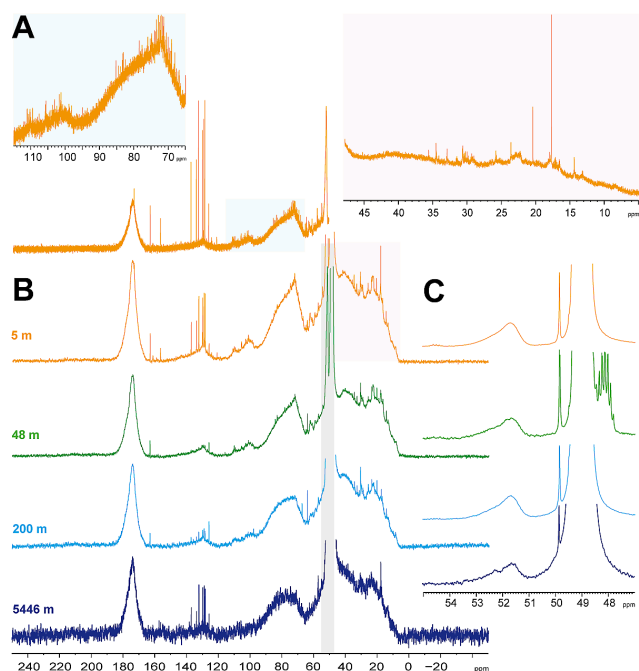
Fig. 3. ^{13}C NMR spectra of marine SPE-DOM (^{12}CD$_3$OD solution) obtained by solid phase extraction (PPL) at different depths indicated by color: 5 m (near-surface photic zone), 48 m (fluorescence maximum), 200 m (upper mesopelagic zone), and 5446 m (30 m above seafloor). **(A)** Apodization, exponential multiplication with LB = 1 Hz, showing resolved NMR resonances from abundant molecules; **(B)** apodization, exponential multiplication with LB = 12.5 Hz, fair compromise between decent resolution and S / N ratio; **(C)** apodization, exponential multiplication with LB = 5 Hz (methoxy NMR resonances).

($\delta_H \sim 11.6$–14.7 ppm), with a remarkably strong increasing abundance from surface to depth (% COOH/total proton NMR integral, 5 m: 4.7 %; 48 m: 4.5 %; 200 m: 7.5 %; 5446 m: 12.1 %). The fraction of CONH could not exceed 4 % of total carbon even if all DON would occur as peptides/proteins because the C / N ratio has been found to be >25 for all four SPE-DOM extracts (Table 1). Exclusive occurrence of all marine DON as peptides is, however, an unlikely presumption (McKee and Hatcher, 2010; Maie et al., 2006; see also discussion of sp^2-hybridized carbon in marine SPE-DOM (Sect. 3.10.1)). In addition, ^{1}H NMR spectra of marine SPE-DOM in dry DMSO-d$_6$ revealed at least three chemical environments of ammonium (^{14}NH$_4^+$) near $\delta_H \sim 7.07$ ppm with an ostentatious coupling between ^{14}N and ^{1}H ($^1J_{NH} = 51.2$ Hz; 1 : 1 : 1 triplet, because of nuclear spin for ^{14}N = 1; % ^{14}NH$_4^+$ signal/total proton NMR integral, 5 m: 0.8 %; 48 m: 0.6 %; 200 m: 0.6 %; 5446 m: 0.9 %). Furthermore, upper limits for carbonyl carbon derived from methyl esters ($\delta_C \sim 51$–54 ppm; Table 3, Fig. 3) were lower than one third of the ^{13}C NMR COX resonance. It is noteworthy that esters in marine organic matter more likely survive

SPE conditions rather than the drastic chemical alteration imposed by the IHSS humic substances extraction protocol.

Carbohydrate related NMR resonances (i.e. HCO and HCO$_2$ groups) decreased from surface to deep SPE-DOM in line with the expectation that these labile constituents will be more easily degraded with increasing DOM age. A certain section of carbon NMR resonances with $\delta_C \sim 70$–78 ppm (Figs. 3 and 4) present in both surface marine SPE-DOM samples was found virtually absent in both deep SPE-DOM samples. CRAM aliphatic carbon ($\delta_{C, max} \sim 42$ ppm) appeared somewhat depleted in SPE-DOM at 48 m compared with all other marine SPE-DOM. Aromatics were of little abundance in all marine SPE-DOM, and became more oxidized with increasing water depth. DEPT-90 NMR spectra representing solely methine (CH) carbon showed a remarkable increase of aliphatic branching from surface to deep marine SPE-DOM: HCC$_3$, the most prominent substructure to represent aliphatic branching, increased from 45.7 % (5 m) to 56.7 % (5446 m) of total methine (Table 3). A notable fraction of methine carbon (CH) resonated at $\delta_C > 140$ ppm, a strong indication for the presence of six-membered N-heterocycles, because simple aromatics, including polycyclic aromatic hydrocarbons, very rarely resonate beyond $\delta_C > 140$ ppm (see later discussion of sp^2-hybridized carbon chemical environments in marine SPE-DOM).

3.5 JRES NMR spectra of marine SPE-DOM

^{1}H, ^{1}H J-resolved (JRES) NMR spectra provided well resolved patterns for all four marine SPE-DOM, indicative of rather abundant molecular signatures (Fig. 5). The number of JRES cross peaks declined in the order SPE-DOM 48 m > 5 m > 200 m > 5446 m, and the adjacent pairs of SPE-DOM showed more similarity in JRES cross-peak patterns than distant ones, implying a rather continual evolution of DOM composition. Remarkably, numerous JRES cross peak have been observed even for the deep 5446 m SPE-DOM in which fast transverse NMR relaxation has strongly attenuated COSY cross peaks (cf. Fig. 6g and h). A rather large proportion of surface marine SPE-DOM (5 m and 48 m) methyl groups ($\delta_H < 1.6$ ppm) was connected to methine (CH; produced doublets in F1) rather than to methylene (CH$_2$; only a few triplets recognizable). With increasing water depth however, the fraction of methyl groups bound to methylene markedly increased and then dominated the upfield chemical shift range of pure aliphatics at $\delta_H < 1.1$ ppm (Fig. 5h). Rather isolated methyl groups, perhaps adjacent to quaternary carbon, with a few small vicinal $^3J_{HH}$ couplings appeared most prominent in SPE-DOM 48 m and 200 m samples ($\delta_H \sim 1.5$ ppm). Analogous considerations applied to methoxy groups near $\delta_H \sim 3.3$–3.7 ppm with strong centred JRES cross peaks with tiny couplings ($^3J_{HH} < 2$ Hz), which appeared in the order 48 m > 5 m ≥ 200 m > 5446 m SPE-DOM, thereby corroborating assignment from DEPT-HSQC
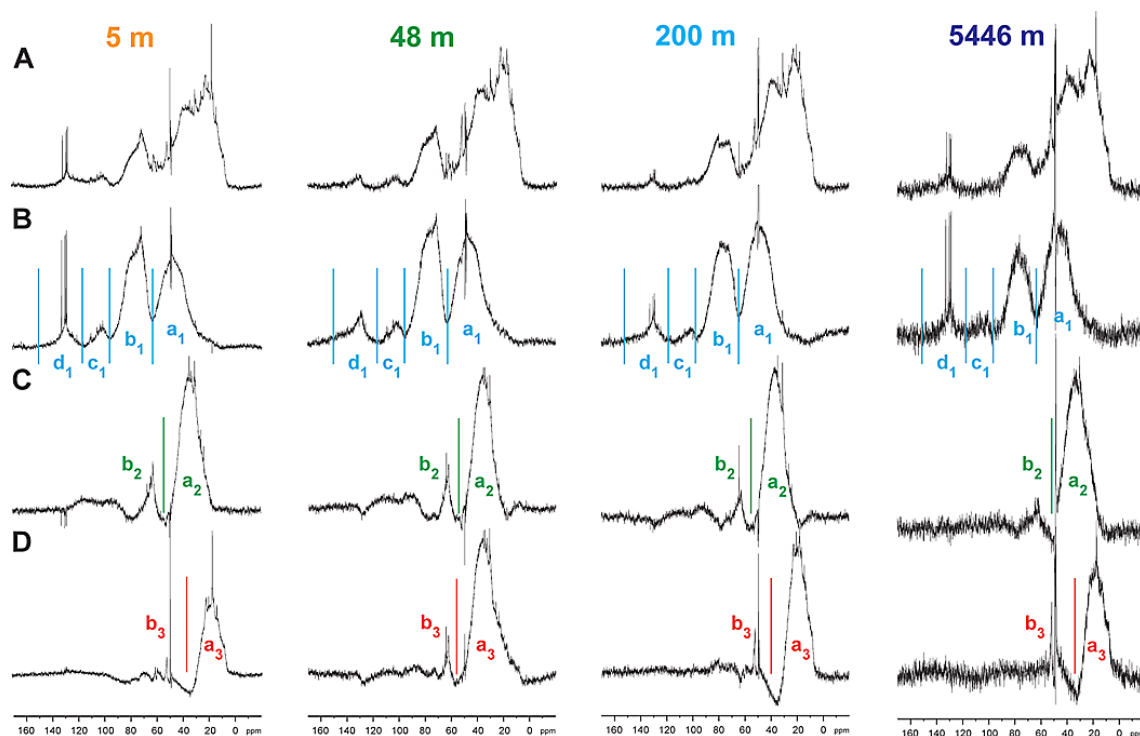
Fig. 4. ^{13}C NMR spectra for marine SPE-DOM obtained by solid phase extraction (PPL) at different depths (from left to right). **(A)** Superimposed protonated carbon NMR resonances (CH$_{123}$; DEPT-45 ^{13}C NMR spectra); multiplicity-edited ^{13}C NMR spectra are **(B)** CH: methine, with indices a_1–d_1 denoting the following chemical environments: **H**$\underline{\text{C}}_{\text{ar}}$-C/O-**H**$\underline{\text{C}}$-O/**H**$\underline{\text{C}}$-O/**H**$\underline{\text{C}}$-C; **(C)** CH$_2$: methylene, with indices a_2 and b_2 denoting the following chemical environments: **H**$_2$$\underline{\text{C}}$-O/**H**$_2$$\underline{\text{C}}$-C; and **(D)** CH$_3$: methyl, with indices a_3 and b_3 denoting the following chemical environments : **H**$_3$$\underline{\text{C}}$-O/**H**$_3$$\underline{\text{C}}$-C. The respective NMR section integrals are provided in Table 3.

NMR spectra (Figs. 7 and 8), which discriminated between aliphatic methyl esters and ethers, with ^{4}J$_{\text{HH}}$ for methyl ethers and ^{5}J$_{\text{HH}}$ for methyl esters, respectively. The complex spin systems characteristic of carbohydrates and other extended spin systems declined in the order SPE-DOM 48 m > 5 m > 200 m > 5446 m. The section of unsaturated protons (δ_{H} > 5.5 ppm) showed several olefinic protons with small ^{n}J$_{\text{HH}}$ couplings (δ_{H} ∼ 6.2 ppm, ^{n}J$_{\text{HH}}$ < 3 Hz), likely from olefins at aliphatic ring junctions with restricted conformational mobility; others showed COSY cross peaks with other olefinic protons (Fig. S5, panel A and C). Similar signatures have been previously recorded in ^{1}H NMR spectra of ultrafiltered marine organic matter (Hertkorn et al., 2006; Fig. 3) and sediment extracts (data not shown). Large vicinal scalar couplings (^{3}J$_{\text{HH}}$ > 12 Hz) from δ_{H} ∼ 6.7–7.6 ppm indicated α,β-unsaturated olefins present in all marine SPE-DOM.

3.6 COSY NMR spectra of marine SPE-DOM

The COSY NMR spectra of surface SPE-DOM from 5 m and 48 m displayed a few thousand intense cross peaks and slightly lesser counts of barely visible ones. The two COSY NMR spectra shared approximately 75 % of their intense cross peaks in the aliphatic section (Figs. 6, S4 and S5),

whereas only slightly more than half of the observed aromatic COSY cross peaks were common to both NMR spectra. About 4500 COSY off-diagonal cross peaks appeared resolved in the SPE-DOM sample from 48 m, of which ∼ 85 % derived from sp^3-hybridized carbon (**H**$\underline{\text{C}}_{\text{sp}^3}$-C$_{\text{sp}^3}$**H**, **H**$\underline{\text{C}}_{\text{sp}^3}$(O)-C$_{\text{sp}^3}$**H**, and **H**-C$_{\text{sp}^3}$(O)-C$_{\text{sp}^3}$(O)**H**) and the remainder from sp^2-hybridized carbon (**H**$\underline{\text{C}}_{\text{sp}^2}$-C$_{\text{sp}^2}$**H**; δ_{H} > 5 ppm). Corrected for symmetry across the diagonal (50 %) and average spin system size (∼ 3.5 protons per spin system; approximate value), the COSY signature in the marine SPE-DOM sample from 48 m suggested the presence of several hundreds of individual "signature" molecules of either biochemical or biogeochemical origin. Overall, the COSY NMR spectrum of SPE-DOM at 48 m showed about 25 % more abundant cross peaks than that derived from SPE-DOM at 5 m. This remarkable richness of COSY cross peaks in marine SPE-DOM is unprecedented because meaningful COSY NMR spectra of marine organic matter have not been acquired previously.

With increasing water depth, the observed COSY signature of marine SPE-DOM became progressively attenuated; this specifically applied for the 200 m and 5446 m SPE-DOM (Figs. 6 and S5). However, the position of all major aliphatic COSY cross peaks of SPE-DOM samples from 200 m and
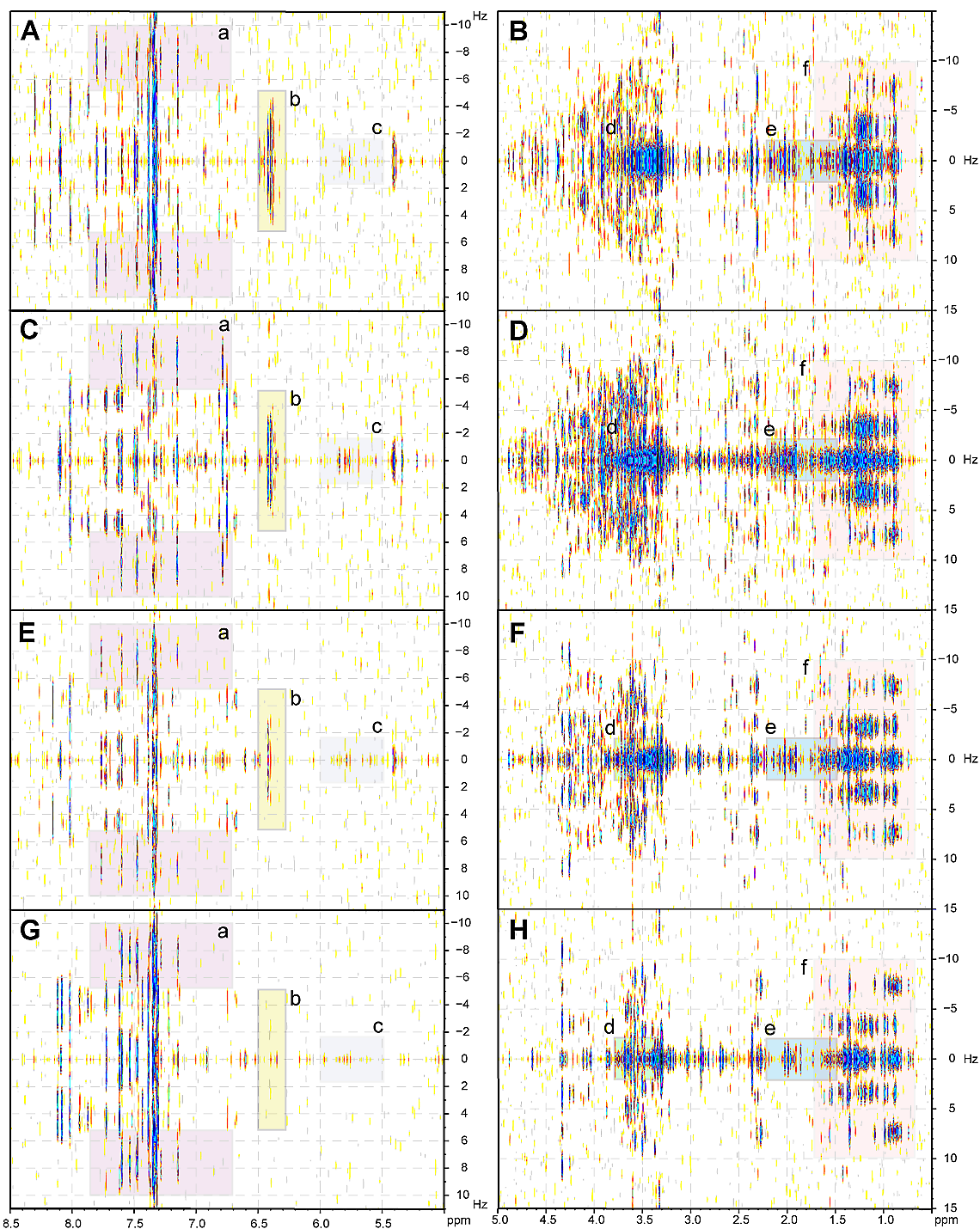
Fig. 5. ^{1}H,^{1}H JRES NMR spectra of **(A, C, E, G)** downfield ($\delta_H = 5.0$–8.5 ppm; aromatic and olefinic C-C_{sp2}**H**-C_{sp2}**H**-C cross peaks) and **(B, D, F, H)** upfield ^{1}H NMR chemical shift region ($\delta_H = 0.5$–5.0 ppm; aliphatic C-**H**C-**H**C-X (X: C, N, O)) cross peaks of marine SPE-DOM. **(A, B)** 5 m (near-surface photic zone); **(C, D)** 48 m (fluorescence maximum); **(E, F)** 200 m (upper mesopelagic zone); **(G, H)** 5446 m (30 m above seafloor). (a) α,β-unsaturated carbonyl compounds with $^nJ_{HH} > 12$ Hz; (b) olefinic protons with small (remote) couplings of $^nJ_{HH} \leq 3$ Hz, indicative of natural products; (c) isolated olefinic protons with small couplings of $^nJ_{HH} < 1$ Hz, possibly at quaternary bridgehead carbon; (d) methoxy groups, which only exhibit long-range couplings $^nJ_{HH}$ ($n = 4$ for methyl ethers and $n = 5$ for methyl esters; cf. Fig. 8c); (e) methyl protons: acetate derivatives ($\delta_H > 1.9$ ppm) and aliphatic methyl ($\delta_H < 1.6$ ppm); (f) methyl bound to methine (doublet, $^3J_{HH} \sim 7$ Hz) and methylene (triplett, $^3J_{HH} \sim 7$ Hz).

Table 3. Top: ^{13}C NMR section integrals (percent of total carbon) and key substructures of marine DOM. Middle: substructures used for NMR-derived reverse mixing model with nominal H / C and O / C ratios given. Bottom: percentage of methine, methylene and methyl carbon related to total protonated ^{13}C NMR integral as derived from ^{13}C DEPT NMR spectra of marine SPE-DOM according to carbon multiplicity (left 3 columns) and relative proportions of these CH$_n$ units binding to oxygen versus carbon chemical environments (cf. Figs. 8a and b).

$\delta(^{13}C)$ ppm	220–187	187–167	167–145	145–108	108–90	90–47	47–0	H / C ratio	O / C ratio
Key substructures	$\underline{C}=O$	$\underline{C}OX$	$\underline{C}_{ar}$-O	$\underline{C}_{ar}$-C,H	$O_2\underline{C}H$	O$\underline{C}$H	$\underline{C}\underline{C}H$		
5 m	0.91	11.00	0.33	4.80	5.91	38.05	39.00	1.378	0.731
48 m	1.95	12.43	0.16	4.21	4.90	34.88	41.46	1.393	0.717
200 m	1.13	11.62	0.34	4.15	5.33	37.22	40.20	1.387	0.726
5446 m	2.15	13.34	1.16	3.41	4.73	34.61	40.60	1.373	0.741

NMR mixing model	C=O	COOH	C_{ar}-O	C_{ar}-H	O_2CH	OCH	CH_2		
H / C ratio	0	1	0	1	1	1	2		
O / C ratio	1	2	1	0	2	1	0		

SPE-DOM (depth)	CH total	CH$_2$ total	CH$_3$ total	Ratio (d$_1$/c$_1$/b$_1$/a$_1$) H$\underline{C}_{ar}$-C/O-H$\underline{C}$-O/H$\underline{C}$-O/H$\underline{C}$-C	Ratio (b$_2$/a$_2$) H$_2\underline{C}$-O/H$_2\underline{C}$-C	Ratio (b$_3$/a$_3$) H$_3\underline{C}$-O/H$_3\underline{C}$-C
5 m	39	29	31	7.3/4.0/43.0/45.7	15/85	9/91
48 m	38	28	34	8.0/3.3/41.5/47.2	12/88	9/91
200 m	42	28	30	6.1/2.2/39.1/52.6	9/91	4/96
5446 m	35	39	26	8.1/2.3/32.9/56.7	3/97	5/95

5446 m agreed with strong COSY cross peaks observed for the SPE-DOM samples from 5 m and 48 m. Given the appreciable conformity of one-dimensional ^{1}H NMR spectra (Fig. 2, S2 and S3) and discernible COSY cross-peak positions for all four SPE-DOM, the disappearance of COSY signatures in the sample order 48 m ∼ 5 m > 200 m > 5446 m most likely related to ever increasing prevalence of fast transverse relaxation.

Two mutually non-exclusive and possibly cooperative mechanisms of COSY NMR cross-peak attenuation for deep marine SPE-DOM deserve evaluation in further experiments.

(1) Antiphase cancellation of COSY cross peaks (Cavanagh et al., 2007) in marine SPE-DOM from deeper waters might be induced by genuine line broadening resulting from accelerated T_2 relaxation. This at first could arise from a growing size of marine SPE-DOM molecules with increasing age at depth (the ^{14}C age places a minimum constraint on DOM turnover since successive internal reworking of aged DOM in the deep ocean will not modify the apparent ^{14}C age of DOM). Larger molecules of lesser atomic mobility, which could show compositions and structures similar to their smaller precursors, could not to be easily differentiated by means of their 1-D NMR spectra. Notably, FTICR mass spectra of Atlantic Ocean SPE-DOM showed both increased average mass, with a, however, small apparent displacement by about 10 Dalton, and a relative increase of unsaturation (Flerus et al., 2012; cf. Sect. 3.12).

Alternatively, the continual incorporation of metals into the sizable DOM molecules, which typically exhibit multiple oxygen-, nitrogen- and sulphur-containing functional groups capable of forming coordination compounds with metal ions, would lead to acceleration of transverse NMR relaxation. The likelihood of incorporating and retaining metals grows with molecular size of NOM because of better opportunities to form chelating coordination compounds with large binding constants. The long ocean residence time of DOM may induce progressive metal complexation because metal ions with lesser binding constants will increasingly become displaced by such with stronger binding constants (e.g. higher charged and kinetically stable metal ions) (Vraspir and Butler, 2009; Witter et al., 2000). While coordination of marine organic ligands with diamagnetic metal ions causes merely restrictions of molecular mobility, leading to moderately accelerated NMR transverse relaxation, coordination with paramagnetic ions such as 3d transition metals (notably Fe$^{2/3+}$) will impose fast longitudinal and transverse NMR relaxation from the large magnetic moment of free electrons (cf. Sect. 3.13.3).

(2) However, progressive loss of overall COSY cross-peak integral of SPE-DOM as observed with ever deeper marine waters (Figs. 6 and S6) might as well originate from entropy gain as a consequence of increased molecular diversity. Hence, when a given total number of marine SPE-DOM atoms is distributed across a larger diversity of
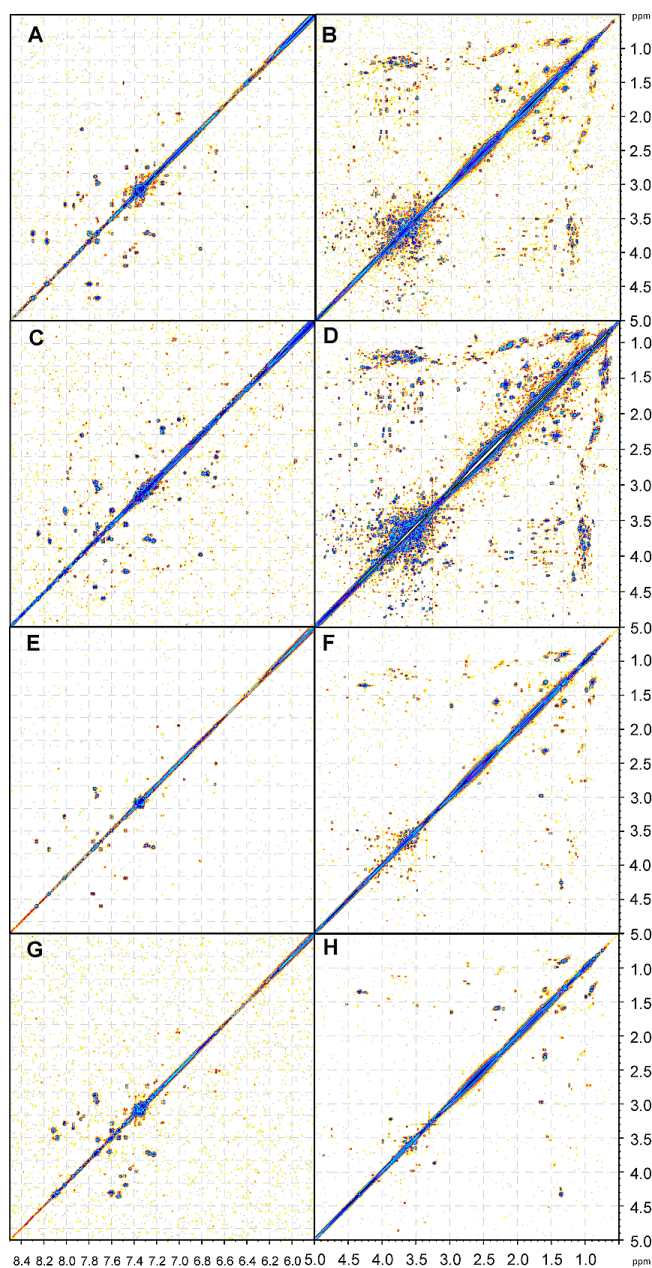
Fig. 6. ^{1}H,^{1}H COSY NMR spectra of marine SPE-DOM with **(A, C, E, G)** downfield ($\delta_H = 5.8$–8.5 ppm; aromatic and olefinic C-$C_{sp^2}\underline{H}$-$C_{sp^2}\underline{H}$-C cross peaks) and **(B, D, F, H)** upfield ^{1}H NMR chemical shift region ($\delta_H = 0.5$–5.0 ppm; aliphatic C-$\underline{HC}$-$\underline{HC}$-X (X: C, N, O) cross peaks; **(A, B)** 5 m (near-surface photic zone); **(C, D)** 48 m (fluorescence maximum); **(E, F)** 200 m (upper mesopelagic zone); **(G, H)** 5446 m (30 m above seafloor).

organic molecules, the probability for NMR resonances to appear within a defined (limited) bandwidth will decrease. The probability of incidental overlap in NMR spectra scales with the ratio of linewidth and spectral range in 1-D NMR spectra and with the ratio of cross-peak area and available nominal pixel space in 2-D NMR spectra (cf. Table S2),

and, in addition, with the magnetic field strength (apparent resolution $\sim B_0{}^n$). Hence, coincidental overlap of 2-D NMR cross peaks (indicates atom pairs in marine SPE-DOM) is considerably less probable than coincidental overlap of respective 1-D NMR resonances (which indicates single atoms).

Owing to strong biological activity, surface ocean SPE-DOM contains a rather large share of biomolecules – which show far lesser compositional variance than natural biogeochemical mixtures (Hertkorn et al., 2007, 2008). In general, progressive loss of NMR signature from surface to deep SPE-DOM was in line with decreasing proportions of common biomolecules and increased abundance of extensively reworked biogeochemical molecules present in deep SPE-DOM. These could have originated from more diffuse sources throughout the entire ocean column, produced on average with longer timescales and different mechanisms than those from surface biochemical reactions (McCollom and Seewald, 2007).

The conspicuous signature resonances which appear in 1-D NMR spectra of deep SPE-DOM at 5446 m (preferentially from $\delta_H \sim 6.2$–8.5 ppm) do not contradict this view because these likely represent a few abundant unsaturated signature molecules, possibly indicating interaction of deep marine SPE-DOM with bottom sediment.

Lower concentrations of certain molecules correspond to a lesser S / N ratio available for individual COSY cross peaks, with inevitable attenuation of recognizable COSY cross-peak signatures. Even if antiphase cancellation within 2-D NMR cross peaks is specific to COSY NMR spectra (Cavanagh et al., 2007), considerations based on relative chemical diversity within various marine SPE-DOM will probably apply for the observed attenuation of JRES (Fig. 5), TOCSY (Fig. 12), DEPT-HSQC (Fig. 7), and HSQC (Fig. 13) cross-peak amplitudes with increasing water depth. Entropy gain in marine SPE-DOM from ever increased molecular diversity will cause a continual attenuation of analytical signature patterns which may be mistaken as an apparent recalcitrance of marine organic matter. Progressive disappearance of signature patterns will make discrimination of complex mixtures ever more difficult. Eventually, discrimination capacity to enable meaningful differentiation of extremely complex supermixtures has to be restored by hyphenation of analytical methods such as combining separation and organic structural spectroscopy (Hertkorn et al., 2007; Woods et al., 2011).

3.7 Comparison of homonuclear 2-D NMR spectra of marine SPE-DOM (JRES, COSY and TOCSY NMR spectra)

The excellent COSY NMR cross-peak resolution of marine SPE-DOM was not readily available in TOCSY NMR spectra (Fig. S1, see also Fig. 12). At first, more numerous cross peaks with higher S / N ratio were expected in TOCSY than

in COSY NMR spectra. However, the superposition of abundant in-phase TOCSY cross peaks almost completely filled the entire accessible area of chemical shift with a near continuous assembly of cross peaks, especially in the aliphatic section (i.e. from $\delta_H \sim 0.5$–4.5 ppm; Fig. S1, see also Fig. 12a–d). The application of strongly apodizing functions in F1 and F2 of TOCSY NMR spectra resulted in considerably enhanced apparent resolution, primarily for -O-**H**C-**H**C-O- and aromatic cross peaks (Fig. S1c–d). However, purely aliphatic cross peaks then became somewhat blurred and showed less definition than COSY cross peaks, likely a consequence of superposition of very many aliphatic cross peaks with, for themselves, minor abundance (in part from higher order spin systems), overlaid with vertical T_1 noise from spectrometer instabilities and parallel diagonals from thermal noise.

JRES NMR spectra, on the other hand, produced fewer numbers of cross peaks than both COSY and TOCSY NMR spectra for several reasons. At first, the overall nominal resolution of JRES NMR spectra was only $< 1/300$ compared with that of COSY and TOCSY NMR spectra (cf. Table S2), and hence allowed for a far lesser disposable peak dispersion. In addition, the long duration of F1 increments in JRES NMR spectra (here 10 ms, as opposed to TOCSY: 104 µs and COSY: 104 µs) imposed mandatory loss of magnetization from prolonged operative NMR relaxation at high F1-resolution. In fact, the discretionary resolution of JRES NMR spectra obtained from SPE-DOM was limited to detect spin couplings of $^nJ_{HH} > 2.5$ Hz (Fig. 5), considerably larger than active and passive J_{HH} operating in COSY and TOCSY NMR spectra of SPE-DOM. Furthermore, a shorter total acquisition time of JRES as compared with COSY/TOCSY NMR spectra (because of limited useful numbers of F1 increments) will accumulate a lesser overall S / N ratio, attenuating weak cross peaks even further. Hence, JRES NMR spectra were only capable of depicting abundant molecular signatures in marine SPE-DOM, whereas COSY NMR spectra were (and will be in the future) best suited to reveal diversity of organic composition. TOCSY NMR spectra, on the other hand, will be best suited to reveal faint NMR signatures of low abundance like those derived from unsaturated biogeochemical mixtures (cf. discussion of sp^2-hybridized carbon in marine SPE-DOM).

3.8 DEPT-HSQC NMR and HSQC-TOCSY NMR spectra of marine SPE-DOM

The expansive aliphatic HSQC cross peak of all four SPE-DOM (Fig. 13, cf. also Fig. 9), which represented superimposed **H**C-C and **H**C-X (X: O, N, S) chemical environments, lacked peak discrimination, which could be vastly improved by spectral editing according to carbon multiplicity. The combination of methyl- and methylene-selective DEPT-HSQC NMR spectra revealed well resolved cross peaks for all three types of protonated carbon, i.e. CH₃, CH₂ and CH, although with decreasing amplitude (Fig. 7). Ef-

fects of differential relaxation influenced relative peak amplitudes in CH₂- and CH₃-edited DEPT-HSQC NMR spectra without affecting the significance of cross-peak assignments. Methyl groups bound to carbon (C-CH₃), sulphur (S-CH₃), nitrogen (N-CH₃) and oxygen (O-CH₃) occupied different sections of chemical shift, which were unambiguous for the latter two and rather extended for C-methyl groups. S-CH₃ groups and methyl attached to olefins resonated in the same chemical shift region and were potentially superimposed (Fig. 8a). Methoxy groups could be discriminated into aliphatic and at most a few aromatic methyl esters and aliphatic methyl ethers according to their specific chemical shift regions (Fig. 8c). Methyl groups terminating nonfunctionalized aliphatics, e.g. peptide side chains, resonated at $\delta_H < 1$ ppm and constituted a small minority (approximately 15 %) of methyl found in all marine SPE-DOM investigated here. Downfield chemical shift displacement of methyl cross peaks caused by chemical shift anisotropy from proximate carbonyl derivatives, which is favoured in alicyclic rings because of abundant short range connectivities, was rather common and responsible for the bulk of C-**CH**₃ NMR cross peaks in the region of $\delta_H \sim 1.0$–1.6 ppm.

3.9 HMBC NMR spectra of marine SPE-DOM

HMBC NMR spectra acquired from surface SPE-DOM from 5 m and 48 m showed extensive (~ 80 %) conformity of HMBC cross-peak patterns with excellent NMR cross-peak dispersion. The relatively low sensitivity of HMBC NMR spectra (Table S2) (Crouch et al., 2001) precluded so far the acquisition of meaningful HMBC spectra of deep marine SPE-DOM at 200 m and 5446 m. HMBC cross peaks indicated numerous complex aliphatics with (**H**C(C)**C**O) and without oxygen (**H**C(C)**C**C), indicative of alkylated and standard carbohydrates (with anomeric CH pairs), and unsaturated (i.e. olefinic and aromatic) and carbonyl carbon with a broad range of C- and oxygenated alkyl substitution. HMBC cross peaks are less sensitive than HSQC and homonuclear (^{1}H, ^{1}H) NMR cross peaks (Table S2), but showed superior connectivity information and better resolution, enabling the assembly of extended spin systems across quaternary carbon and heteroatoms. In future, separate studies, HMBC cross peaks will be very valuable for assignment confirmation of relatively abundant molecular signatures proposed by COSY and other NMR spectra.

3.10 Structural detail of carboxyl-rich alicyclic molecules (CRAM) in marine SPE-DOM

Marine SPE-DOM appears at first composed of four major constituents: peptides/proteins, carbohydrates, lipids and thermogenic organic carbon (TMOC). The latter originates from thermal decomposition of organic compounds via a succession of complex chemical degradations under harsh conditions, which from the onset have largely obviated
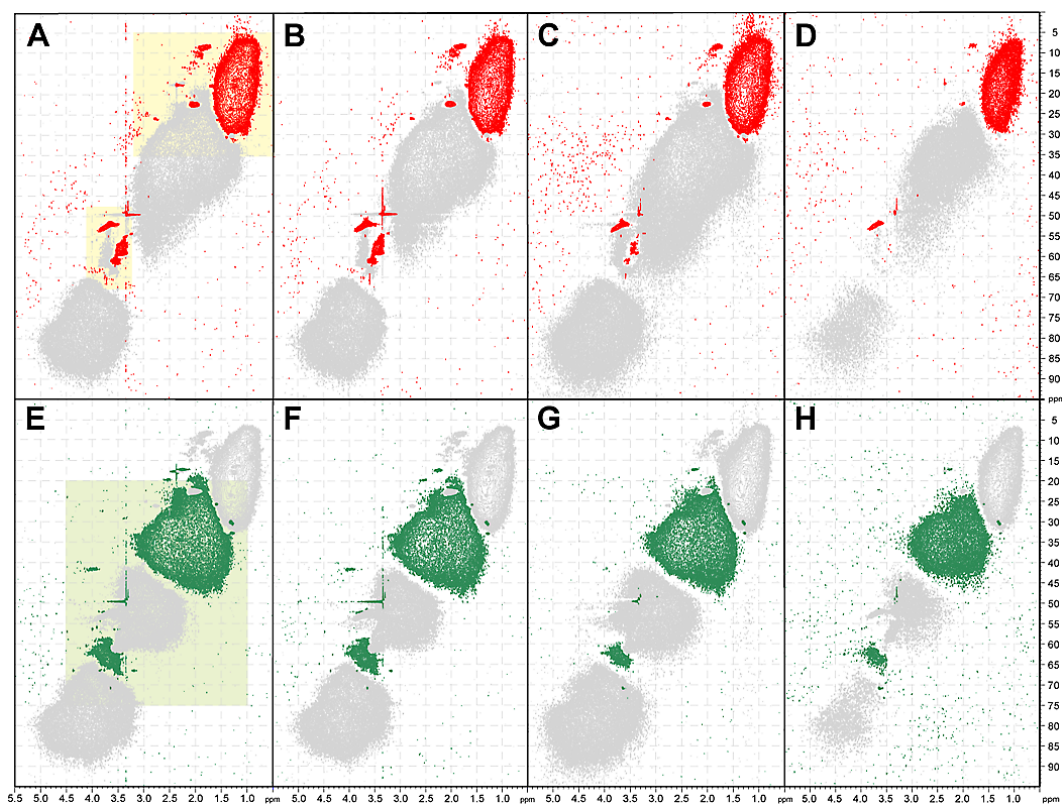
Fig. 7. DEPT-HSQC NMR spectra of four marine SPE-DOM; aliphatic (**HC**C and **HC**X, with X = O, N, S) section with methyl (red) and methylene (green) cross peaks indicated; boxes denote ranges for cross-peak assignments given in Fig. 8, yellow: CH_3-selective, and green: CH_2-selective DEPT-HSQC NMR spectra. Top panel: CH_3-selective DEPT-HSQC NMR spectra (CH_3: red, CH and CH_2: gray); lower panel: CH_2-selective DEPT-HSQC NMR spectra (CH_2: green, CH_3 and CH: gray). **(A, E)** 5 m (near-surface photic zone); **(B, F)** 48 m (fluorescence maximum); **(C, G)** 200 m (upper mesopelagic zone); and **(D, H)** 5446 m (30 m above seafloor).

significant biogenic signatures. In contrast, peptides and carbohydrates are commonly well related to biogenic precursors. Lipids, a rather diverse class of molecules (Graeve and Janssen, 2009; Lipp and Hinrichs, 2009; Cane and Ikeda, 2011), have been extensively processed in marine waters to eventually result in abundant carboxyl-rich alicyclic molecules (CRAM), themselves a very complex mixture (Hertkorn et al., 2006; Lam et al., 2007), thereby resembling TMOC. CRAM have been first elucidated from ultrafiltered marine organic matter (UDOM) (Hertkorn et al., 2006) and were shown to contain an unusually large fraction of carboxylic acids found in a very few known natural products of appreciable size (e.g. >450 Da, a typical size for marine DOM as deduced from FTICR mass spectra).

^{13}C NMR spectra place stringent restrictions on the occurrence and structural characteristics of marine SPE-DOM constituents (Table 3). TMOC abundance in marine SPE-DOM as deduced from ^{13}C NMR spectra likely ranged below one percent of total carbon, similar to the abundance range proposed from FTICR mass spectra (Dittmar and Koch, 2006). This is in accordance to the finding that olefinic carbon in marine SPE-DOM was found more abundant than aromatic carbon and that substantial contributions to aromatic structures might arise from natural products (Blunt et al., 2010). If we regard the C**C**H and **C**OX substructures as characteristic of CRAM, its carbon-based content in marine SPE-DOM ranged from 51 % (SPE-DOM sample from 5 m) to 56 % (SPE-DOM sample from 5446 m). Again, a very large ratio of carboxylic acids (and some methyl esters; Fig. 8c) to total (CRAM-derived) carbon has been found in CRAM, ranging from 0.28 : 1 (SPE-DOM sample from 5 m) to 0.33 : 1 (SPE-DOM sample from 5446 m).

Hence, COX groups had to be proximate to many aliphatic carbon atoms for simple reasons of abundance. Alicyclic geometry with its more numerous pathways of connections between pairs of atoms favoured relative proximity (i.e. small minimum numbers of connecting chemical bonds between arbitrary pairs of atoms) even more. Methyl-edited DEPT-HSQC NMR spectra (Fig. 8a) demonstrated abundant proximity of aliphatic methyl groups (C**C**H$_3$ units) and carbonyl derivatives, because the short range chemical shift anisotropy of the carbonyl group operated on approximately 70 % of aliphatic methyl, inducing downfield chemical shifts from $\delta_H \sim$ 1.0–1.6 ppm (Fig. 8a). Classical aliphatic methyl
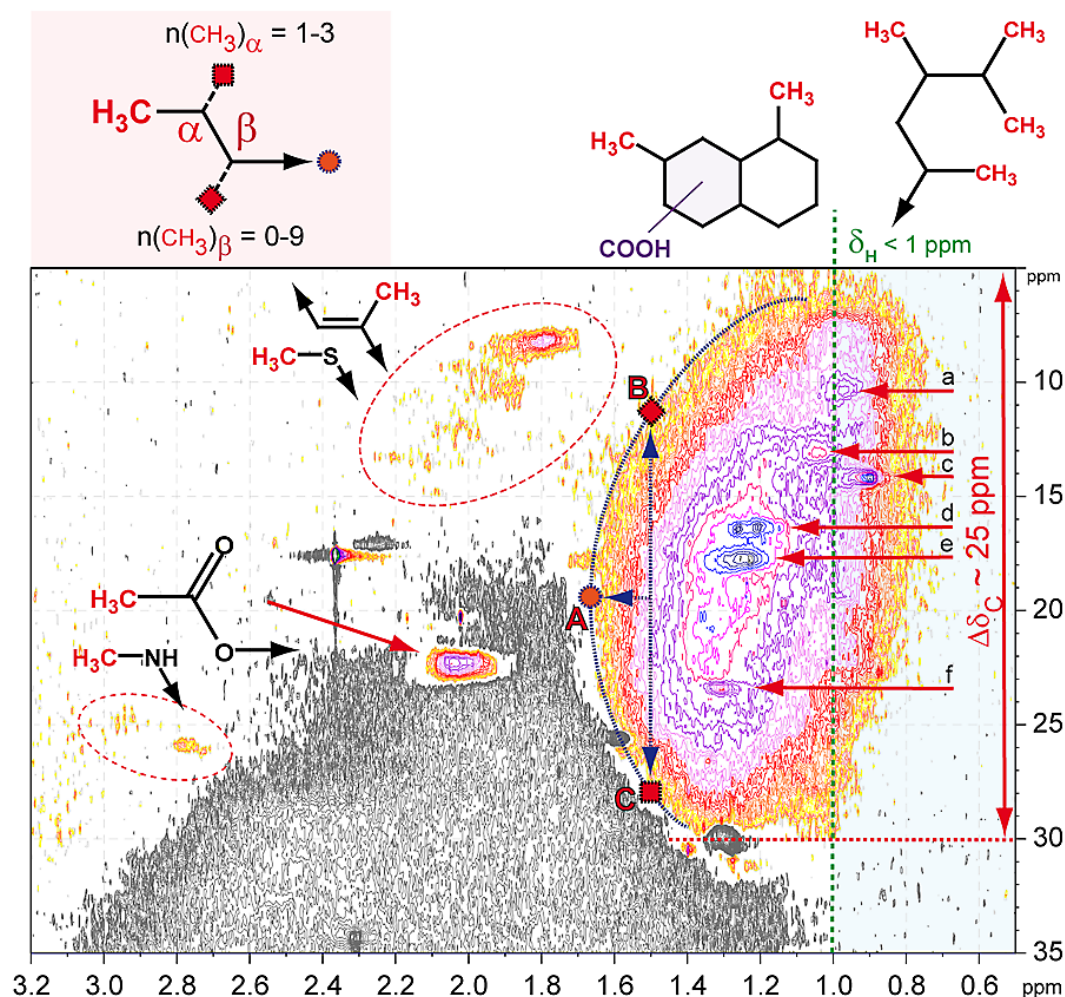
Fig. 8a. DEPT-HSQC NMR spectra of surface marine SPE-DOM at 5m. Section of **H₃C**-C cross peaks with fundamental substructures indicated; blue: the proton chemical shift range ($\delta_H \leq 1$ ppm) corresponding to classical methyl-terminating purely aliphatic units (e.g. peptide side chains) contributed only <15 % of total DEPT-HSQC methyl cross-peak integral (in all four SPE-DOM). The sizable expansion of carbon chemical shift for **H₃C**-C units ($\Delta\delta_C$: 5–30 ppm) indicated near maximum diversity of remote aliphatic substitution, i.e. maximum diversity of aliphatic branching occurred in all four marine SPE-DOM (cf. Fig. 7). The six recognizable intensity maxima of aliphatic methyl (denoted: a–f) likely reflected superposition of remotely substituted common geometries of aliphatic branching. The bulk of aliphatic methyl experienced downfield shift from the chemical shift anisotropy of nearby carbonyl derivatives COX, most likely carboxylic groups, causing downfield proton chemical shifts up to $\delta_H \sim 1.6$ ppm. The depiction of aliphatic branching in ^{1}H and ^{13}C NMR spectra differs considerably: a relative insensitivity of ^{1}H NMR chemical shift with respect to aliphatic branching (negligible aliphatic substituent effects on ^{1}H NMR chemical shift beyond directly bonded carbon) contrasts with sizable aliphatic increments in ^{13}C NMR chemical shifts (substituent ^{13}C NMR chemical shift increments for carbon substitution Cα: +9.1 ppm; Cβ: +9.4 ppm; Cγ: −2.5 ppm; Cδ: 0.3 ppm; Kalinowski, et al., 1984), resulting in strong ^{13}C NMR chemical shift effects of aliphatic substitution at least up to two bonds away in any direction. The positioning of the **H₃C**-C cross peaks results from three main operating effects: alkyl substitution in α-position (H₃C-C$_\alpha$-; three different options) causes increased carbon chemical shift (arrow pointing toward C); alkyl substitution in β-position (H₃C-C-C$_\beta$-; ten different options) causes decreased carbon chemical shift (arrow pointing toward B). Proximate carbonyl derivatives COX (likely carboxylic groups) cause downfield proton chemical shift (arrow pointing toward A). The smooth curvature of the boundary line indicates near-statistical distribution of respective chemical environments A, B, and C. Alicyclic aliphatic geometry (Cho et al., 2011) favours large abundance of proximate COX with respect to given counts of methyl groups, supporting the occurrence of CRAM (carboxyl-rich alicyclic molecules) as abundant contributors to marine SPE-DOM (Hertkorn et al., 2006; Lam et al., 2007; Leenheer et al., 2003). Methyl groups attached to olefins were common; minor suites of S-**CH₃** groups might also have occurred in this cross-peak section. Acetate derivatives and a few minor N-**CH₃** groups complemented the major **H₃C**-C chemical environments shown.
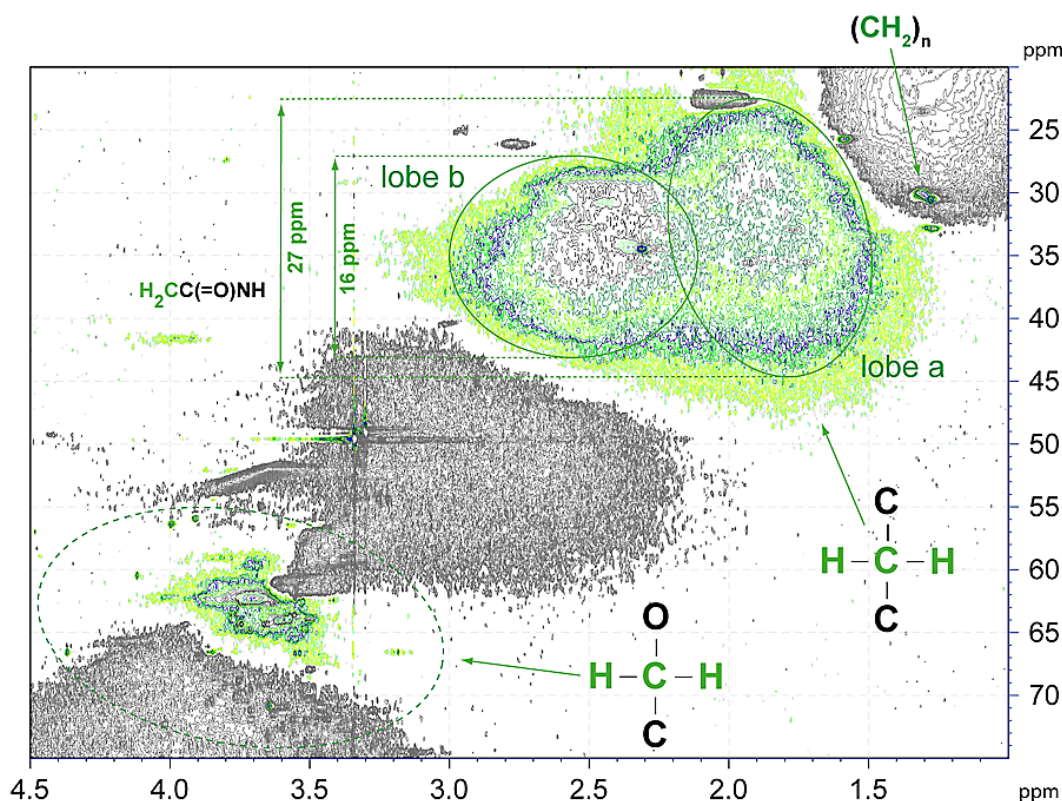
Fig. 8b. DEPT-HSQC NMR spectra of surface marine SPE-DOM at 5 m. Section of $\underline{H_2C}$-Z (Z = C, O, (N, S)) cross peaks. Polymethylene $(CH_2)_n$ experiences the least number of aliphatic neighbours and occupies a low intensity cross peak ($< 1\%$ of methylene cross-peak integral) in a confined area at high field. Carbon bound methylene decompose into two major lobes; the right lobe a (δ_H: 1.5–2.2 ppm) occupied a sizable carbon chemical shift range ($\Delta\delta_C$) of 27 ppm, whereas the lower field lobe b (δ_H: 2.2–3.0 ppm) occupied a smaller carbon chemical shift range ($\Delta\delta_C$) of 16 ppm. These two units differ in the position of COX derivatives with respect to the observed $\underline{H_2C}$-Z unit, which is directly adjacent to lobe b (i.e. C-CH$_2$-COX) and two or more bonds away for lobe a. COX at positions one (α-position) and two (β-position) bonds away from methylene carbon (i.e. C-CH$_2$-C$_x$-COX; $x \geq 1$) will displace aliphatics which otherwise would impose sizable carbon downfield shifts in the range of $\Delta\delta_C \sim 9$ ppm; in addition, proximate COX derivatives will cause downfield proton chemical shift because of chemical shift anisotropy of the carbonyl group (lobe b). COX at positions three (γ-position) bonds away from methylene carbon will cause lower chemical shift anisotropy in proton NMR and obviate a shielding increment for γ-aliphatic substitution ($\Delta\delta_C$: -0.8 ppm), leaving δ_C and δ_H nearly unaltered from standard aliphatic (branched) substitution (lobe a). Several recognizable intensity maxima of aliphatic methylene C-$\underline{CH_2}$-C likely reflected superposition of remotely substituted common geometries of aliphatic branching. Oxomethylene ($\underline{H_2C}$-O) chemical environments in marine SPE-DOM commonly represent carbohydrate side chains of considerable diversity alongside with other minor oxomethylene cross peaks.

groups, like peptide side chains and common lipids, resonating at $\delta_H < 1.0$ ppm, contributed less than 15 % to the C$\underline{CH_3}$ NMR integral (Fig. 8a).

While the vicinity of COX and methyl refers exclusively to spatial proximity without feasible direct bonds in case of carboxylic groups, methylene, methine and quaternary carbon may carry directly bonded COX substituents in marine SPE-DOM (notation used as follows: C$_\delta$-C$_\gamma$-C$_\beta$-C$_\alpha$-COX). Lobe b methylene carbon units (C*-$\underline{CH_2}$-COX; a single carbon C* with possible variance in remote carbon substitution) offer lesser degrees of freedom for variance in remote carbon substitution than lobe a methylene carbon units (C*-$\underline{CH_2}$-C$_n$*-COX; $n \geq 1$; two carbon C* with possible variance in remote carbon substitution). Hence, the overall spread $\Delta\delta$ (^{13}C) is larger for lobe a units ($\Delta\delta(^{13}$C) ~ 27 ppm; cf. Fig. 8b) than for lobe b units ($\Delta\delta(^{13}$C) ~ 18 ppm; cf. Fig. 8b).

Remarkably, methylene edited DEPT-HSQC NMR spectra corroborated these findings and showed two major lobes of extended -C-$\underline{CH_2}$-C- NMR cross peaks with nearly identical total cross-peak integrals, indicating -C-$\underline{H_2C}$-COX units with proximate COX (Fig. 8b, lobe b) and others indicating -C-$\underline{H_2C}$-C$_x$-COX units ($x \geq 1$; Fig. 8b, lobe a) with larger minimum distance between methylene carbon and carbonyl derivatives. Lobe b showed a slightly larger -C-$\underline{CH_2}$-C- NMR cross-peak integral than lobe a; this implies that a majority of the methylene carbon in marine NOM resides in C-CH$_2$-COX units ($\underline{C}$OX occupies α-position with respect to methylene). In contrast to methyl carbon, methylene
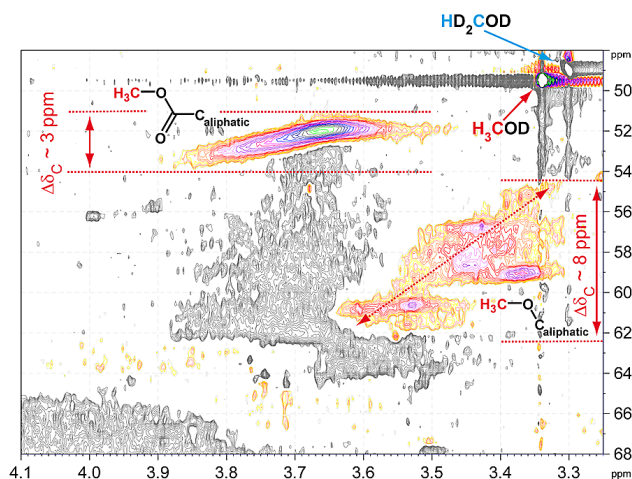
Fig. 8c. DEPT-HSQC NMR spectra of surface marine SPE-DOM at 5 m. Section of $\underline{H_3C}$-O cross peaks with two major substructures indicated: methyl esters and methyl ethers. Methyl ethers were more abundant than in freshwater and soil DOM and occupied a sizable range of carbon chemical shifts (δ_C: 55–62 ppm), given the minimum distance of four bonds from the methyl proton to the first optional variance in substitution ($^4J_{ZH}$ for $\underline{H_3}$C-O-C-$\underline{Z}$ (Z = C, O, (N, S)); likewise, the sizable spread of proton methoxyl chemical shift (δ_H: 3.35–3.65 ppm) indicated substantial chemical diversity of methyl ethers found in marine SPE-DOM. The rather limited bandwidth of carbon chemical shifts in methyl esters ($\Delta\delta_C \sim 3$ ppm) reflects the mandatory minimum distance of five bonds from the methyl proton to the first optional variance in substitution ($^5J_{ZH}$ for $\underline{H_3}$C-O-C(=O)-C-$\underline{Z}$ (Z = C, O, (N, S)); the sizable spread of proton chemical shifts (δ_H: 3.5–3.85 ppm) nevertheless indicated substantial chemical diversity of methyl esters found in marine SPE-DOM. Judging from the one-dimensional ^{1}H NMR spectra (Fig. 2d), the relative disappearance of the DEPT-HSQC methyl ether cross peak from surface to deep marine SPE-DOM (Fig. 7) likely reflected real disappearance of methyl ethers from surface to deep SPE-DOM rather than NMR relaxation imposed bleaching.

carbon offers options of chain elongation in two different directions with a proportionally larger probability of finding (very) proximate COX at otherwise near-statistical distribution of functional groups. It is noteworthy that CH$_2$-COX units cannot be part of alicyclic rings.

The carboxylic NMR resonance appeared very similar for all marine SPE-DOM, with a maximum intensity near $\delta_C \sim 174.3$ ppm, a near-Gaussian intensity distribution across a sizable chemical shift range (range at half height, $\delta_C \sim 171.8$–177.6 ppm), indicating a maximal chemical diversity of COX chemical environments with no visible preference of (remote) substitution. COX from deep SPE-DOM at 5446 m ranged by 0.5 ppm toward lower field with a maximum δ_C of 175 ppm and a chemical shift range at half height of $\delta_C \sim 171.8$–178.2 ppm, possibly indicating a larger fraction of purely aliphatic carboxylic groups like those in classical lipids (cf. JRES NMR spectra; Fig. 5h). In contrast, ultrafiltered marine DOM showed two major carboxylic

acid peaks, one broad hump with maximum amplitude at $\delta_C \sim 177$ ppm and a relatively sharp NMR resonance of lower integral centred at $\delta_C \sim 175$ ppm, which was assigned originating from carboxylated carbohydrates (Hertkorn et al., 2006). The absence of the relatively sharp ^{13}C NMR resonance in marine SPE-DOM implies an extraction selectivity of SPE on the one hand and of ultrafiltration on the other. Solid-state NMR spectra of RO/ED-derived marine organic matter also did not show this relatively sharp ^{13}C NMR resonance, perhaps in part because of intrinsic low resolution of solid state NMR spectroscopy (Koprivnjak et al., 2009).

3.10.1 Depiction and analysis of less common sp^2-hybridized carbon in marine organic matter

Hydrogen atoms bound to sp^2-hybridized carbon (i.e. olefinic and aromatic carbon chemical environments (carbonyl derivatives do not have directly bounded hydrogen except for aldehydes)) in marine SPE-DOM typically accounted for less than 5 % of non-exchangeable proton NMR integral and occupied the chemical shift range of $\delta_H \sim 5$–10 ppm, with small contributions of anomeric protons at $\delta_H < 5.5$ ppm (Figs. 2 and 9, Table 2).

Unsaturated carbon chemical environments in marine DOM have been recognized by means of proton and carbon 1-D NMR spectra (Hertkorn et al., 2006; Lam et al., 2007; Aluwihare et al., 2002) but not further characterized by NMR spectroscopy because of lack of sensitivity. UV/VIS spectra have supplied decisive clues about chromophoric (light-absorbing) and light-emitting (fluorescent) molecules in marine DOM (colored dissolved organic matter, CDOM; Coble, 2007) and thereby provided identification of selected sp^2-hybridized carbon in aromatics (phenols, quinones, pyrrols), olefins, carbonyl derivatives and α,β-unsaturated (polarized) double bonds.

Prospective isolated olefins in marine SPE-DOM likely originate from natural products such as common unsaturated lipids derived from unsaturated fatty acids and, e.g., sterol derivatives. Conjugated olefins occur in linear terpenoids which have been proposed in freshwater DOM (Lam et al., 2007) but commonly occur in marine waters as well (Blunt et al., 2010). A rich diversity of natural products contains α,β-unsaturated molecules, often in conjunction with aromatics (Blunt et al., 2010). Amide moieties in peptides/proteins as well as in amino sugars are common contributors to carbonyl derivatives in marine DOM.

Classical aromatic molecules in marine DOM comprise natural products of diverse origin and substitution (Blunt et al., 2010) and oxygenated, hydroxylated and carboxylated single and small condensed aromatics of possibly thermogenic origin (Dittmar and Koch, 2006; Dittmar and Paeng, 2009; Hockaday et al., 2006). Lignin-derived phenols detected in marine DOM (Hernes and Benner, 2003; Opsahl and Benner, 1997, 1998) are much less abundant than in soil DOM which primarily derives from vascular plants with
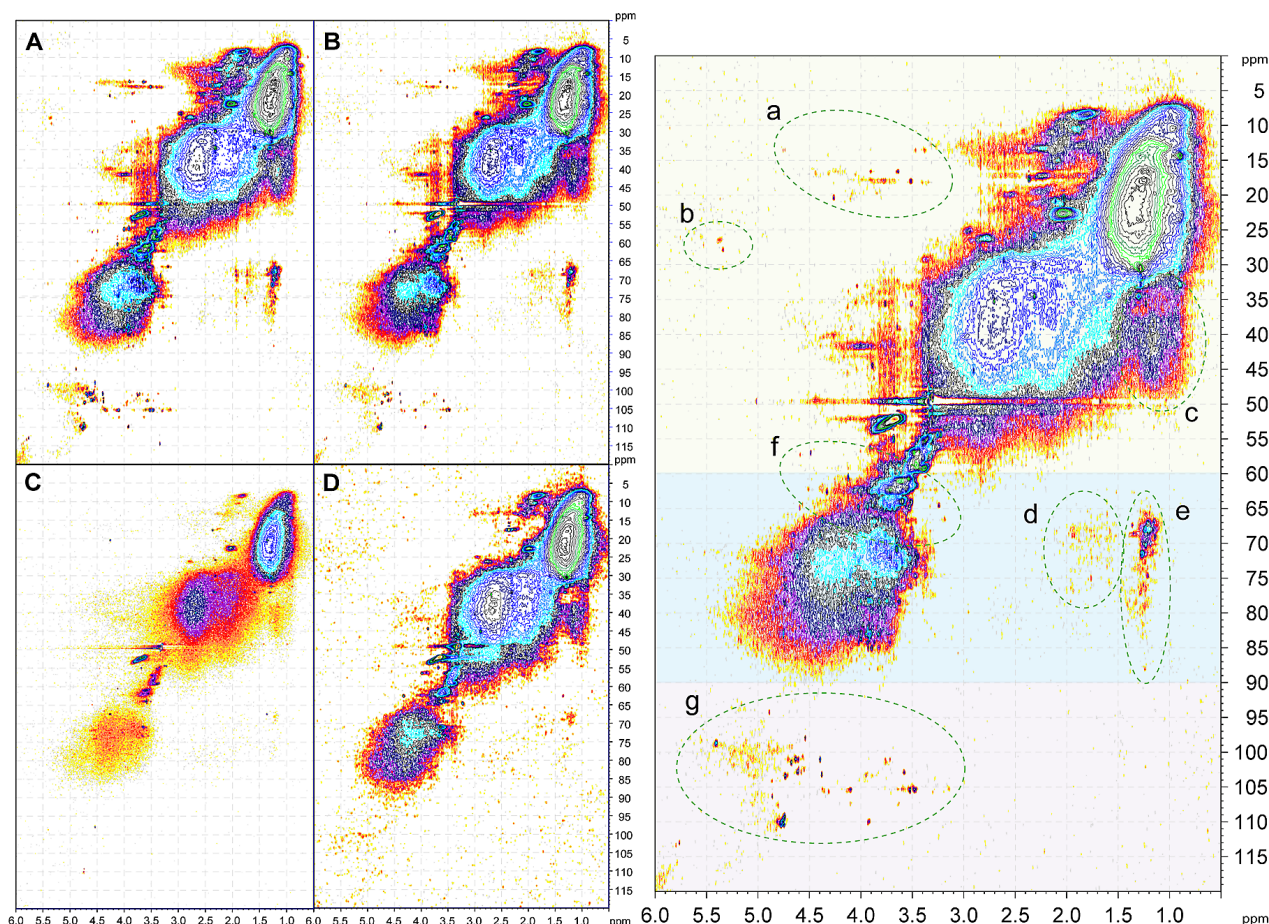
Fig. 9. HSQC-TOCSY NMR spectra of four marine SPE-DOM, aliphatic section of sp^3-hybridized carbon: **(A)** 5 m (near-surface photic zone); **(B)** 48 m (fluorescence maximum); **(C)** 200 m (upper mesopelagic zone); and **(D)** 5446 m (30 m above seafloor). For NMR acquisition parameters, see Table S3. **(E)** HSQC-TOCSY NMR spectrum of surface marine SPE-DOM sample from 48 m. Coarse substructures, connected by ^{n}J$_{HH}$ ($n = 2$–5), are given according to color; green: $\underline{H}$C(C)$\underline{C}$H (δ_C: 0–60 ppm); blue: $\underline{H}$C(C)$\underline{C}$O (δ_C: 60–90 ppm); and purple: $\underline{H}$C(C)H$\underline{C}$O$_2$ (δ_C: 90–110 ppm). Section a: $\underline{H}$C(C)H$\underline{C}$O substructures, like alkylated carbohydrates (Panagiotopoulos et al., 2007); section b: $\underline{H}$C(C)H$\underline{C}$(=O)O substructures, like esters and multiply oxygenated aliphatics; section c: $\underline{H}$C(C)H$\underline{C}$C substructures, like functionalized and strongly branched aliphatics; section d: C$\underline{H}$C(C)H$\underline{C}$O substructures, aliphatics connected to oxygenated carbon, like alkylated carbohydrates and ethers; section e: $\underline{H_3}$C(C)H$\underline{C}$O substructures, methyl connected to oxygenated carbon, like methylated carbohydrates and ethers; section f: $\underline{H_3}$CO(C)H$\underline{C}$O substructures, like methoxyl bound to oxygenated carbon; and section g: CH$\underline{C}$O(C)$\underline{H}$$\underline{C}O_2$ substructures, connecting anomerics in carbohydrates with adjacent rings (significant confirmation tool for carbohydrates).

abundant lignin (Rezende et al., 2010). Nitrogen heterocycles in marine DOM comprise pyridine derivatives (Maie et al., 2006) as natural products and heterocycles with up to several incorporated nitrogen atoms like those occurring in DNA derivatives; nitrogen, sulphur and oxygen in five-membered aromatic rings are further feasible candidates for sp^2-hybridized carbon in marine DOM (Blunt et al., 2010).

Another, more complex assembly of sp^2-hybridized carbon in marine DOM with considerable average ^{14}C age derives from black carbon (Masiello, 2004; Ziolkowski and Druffel, 2010), which ultimately might originate from (natural and anthropogenic) terrestrial burning and biogeochemical weathering (Dickens et al., 2004), transported into the sea via riverine transport (Battin et al., 2009; Dittmar et

al., 2012) and atmospheric deposition (Masiello and Druffel, 1998; Jimenez et al., 2009), and from deep sea infusion by hydrothermal vents and other petrogenic, more diffuse sources (McCollom and Seewald, 2007). Thermogenic marine carbon (TMOC) has been found widely distributed in the ocean and accounts for up to a few percent of total marine organic carbon (Dittmar and Koch, 2006), elevating TMOC to a significant proposed constituent of total marine organic carbon. The susceptibility of TMOC to photodegradation in the surface ocean depends on its aromaticity and degree of condensation, leading to differential photochemical degradation as the major sink of TMOC (Dittmar and Paeng, 2009; Stubbins et al., 2012).
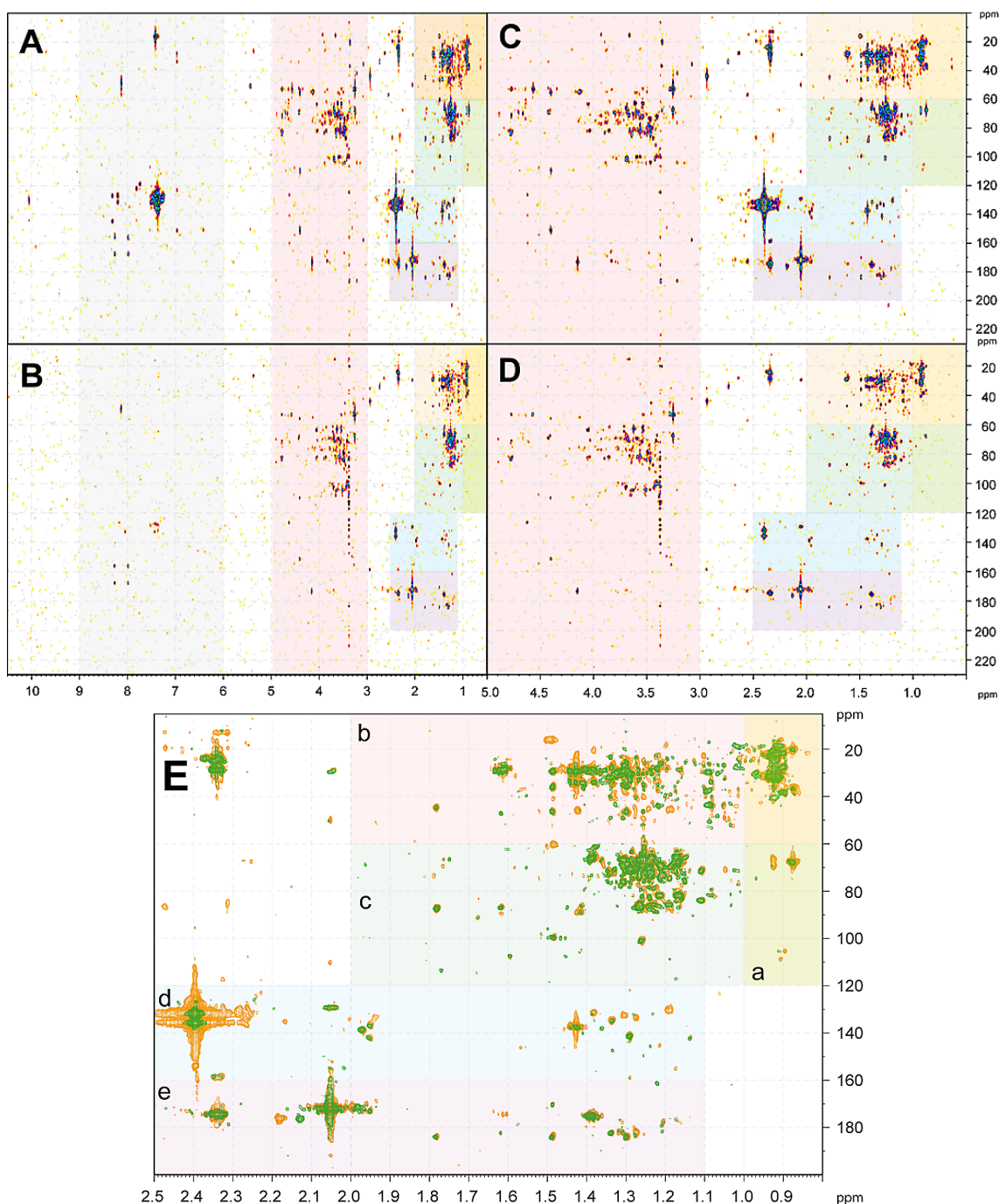
Fig. 10. ^{1}H, ^{13}C HMBC spectra of **(A, C)** surface SPE-DOM at 5 m (near-surface photic zone) and **(B, D)** SPE DOM at 48 m (fluorescence maximum). Color code as provided for **(E)**, with additional oxygenated units (red) $\underline{H}C_n$-$\underline{C}$H-O ($n = 1, 2$; $\delta_H \sim 3$–5 ppm) and unsaturated units (grey) $\underline{H}C_n$-$\underline{C}_{sp^2}$ ($n = 1, 2$; $\delta_H \sim 6$–9 ppm). **(E)** Superposition of surface SPE-DOM at 5 m (orange) and 48 m (green) HMBC aliphatic section cross peaks with substructure regimes indicated in color: section a: HMBC cross peaks $^{2,3}J_{CH}$ connecting methyl with various groups: $\underline{H}_3$C-(C)$\underline{C}$C ($\delta_C < 60$ ppm), $\underline{H}_3$C-(C)$\underline{C}$O ($\delta_C \sim 60$–100 ppm), and $\underline{H}_3$C-(C)$\underline{C}$O$_2$ ($\delta_C \sim 100$–120 ppm); section b: intra-aliphatic HMBC cross peaks $\underline{H}$C(C)$\underline{C}$ ($^{2,3}J_{CH}$); section c: intra-aliphatic HMBC cross peaks $\underline{H}$C(C)$\underline{C}$O ($^{2,3}J_{CH}$); section d: HMBC cross peak connecting aliphatic protons with sp^2-hybridized carbon (olefin or aromatics) $\underline{H}$C$_{al}$(C)$\underline{C}_{sp^2}$ ($^{2,3}J_{CH}$); and section e: HMBC cross peak connecting aliphatic protons with carbonyl carbon (olefin or aromatics) $\underline{H}$C$_{al}$(C)$\underline{C}$(=O)X ($^{2,3}J_{CH}$).

TMOC in marine DOM has at first been identified in FTICR mass spectra because of prevalent hydrogen deficient molecules with a large aromaticity index (Koch and Dittmar, 2006) which cannot be easily explained to have resulted from biochemical precursors. TMOC is likely composed of (condensed) aromatic units like oxygenated and carboxylated polycyclic aromatic hydrocarbons with a few to several contiguous aromatic rings (Hockaday et al., 2006; Dittmar and Koch, 2006; Cheng et al., 2006). Here, appreciable ranges of O / C ratios as deduced from FTICR mass spectra will result in variable carbon oxidation states (Kroll et al., 2011; Cheng et al., 2006), and electronic long-range interactions across extended π-systems (Bauschlicher et al., 2009) will cause different extents of aromaticity (and reactivity) of individual bonds within nominal benzene rings (Aihara et al., 2011). In NMR spectroscopy, carboxylation will induce downfield chemical shifts in both proton and carbon NMR (Perdue et al., 2007). In contrast, oxygenation will induce sizable upfield chemical shifts in both proton and carbon NMR because of strong electron-donating effect in ortho and para positions (Perdue et al., 2007). Owing to extensive conjugation and strong resonance, these cumulative chemical shift effects can operate in remote positions (up to 4–6 bonds away, and further in condensed aromatics) and are therefore difficult to predict in complex molecules. The intrinsic heterogeneity of this inhomogeneous class of TMOC molecules resembles that of carboxyl-rich alicyclic molecules (CRAM), another key contributor of marine DOM (Hertkorn et al., 2006; Lam et al., 2007), and will manifest itself in rather low-resolution NMR signatures (i.e. extended NMR cross peaks in two-dimensional NMR spectra). One-dimensional (¹H and ¹³C) NMR spectra alone will not allow unambiguous structural identification of TMOC because of overlap from nitrogen heterocycles and other strongly electron withdrawing aromatics.

NMR chemical shifts of pure aromatic hydrocarbons occupy a relatively narrow range of ¹³C chemical shifts irrespective of structural arrangements and degree of condensation; protonated carbons range from $\delta_C \sim 120$–135 ppm, whereas quaternary carbons resonate from $\delta_C \sim 135$–143 ppm (Hansen, 1979). In contrast, proton chemical shifts in pure polycyclic aromatic hydrocarbons are rather sensitive to specific steric arrangements. Normal, uncongested hydrogen positions resonate from $\delta_H \sim 7$–8 ppm, depending on position and extent of condensation; larger polycyclic hydrocarbon (PAH) superimpose several deshielding ring currents, resulting in progressive downfield proton NMR chemical shifts. Sterically congested bay and fjord regions impose downfield proton NMR chemical shift depending on the extent of steric hindrance; most pronounced steric congestions in narrow fjord regions produce downfield proton chemical shifts beyond 9 ppm, lesser tight bays like those related to incorporated five-membered rings resonate from $\delta_H \sim 8.6$–8.9 ppm (Tominaga et al., 2010; Williamson et al., 1986).

However, major key substructure regimes within the thermogenic signature of marine DOM can be proposed with predictable NMR chemical shift characteristics (Fig. 11). ¹H, ¹H TOCSY and ¹H, ¹³C HSQC NMR experiments are most appropriate to probe marine DOM signatures of low abundance because their absorptive line shape allows superposition of small individual NMR resonances into aggregated cross peaks which can be processed with adapted apodization function to enhance their apparent S / N ratio (Figs. S1, 12 and 13). Electron-deficient six-membered nitrogen heterocycles produce strong proton and carbon NMR downfield shifts; plausible candidates in marine DOM include natural products derived from pyridine, indole and histidine and more complex compounds derived from nucleic acids and analogues. In contrast, aromatic amines and simple five-membered N-heterocycles, as plausible candidates of chlorophyll degradation, exhibit considerable proton and carbon NMR upfield shifts because of electron-donating capacity (proton and carbon chemical shifts in five-membered heterocycles can be strongly modified by electron-donating and withdrawing substitution).

3.10.2 Conceptual model and NMR chemical shift characteristics for polycyclic aromatic chemical environments of thermogenic origin (TMOC) in marine DOM

A conceptual model to depict the effects of conceivable substitution patterns in black carbon analogous marine thermogenic carbon was proposed in Fig. 11a (atom numbering and computed ¹H and ¹³C chemical shifts, cf. Fig. S6 and Table S4). This model denoted the effects of relative steric congestion (Fig. 11a, PAH narrow and open bay regions A and B), relative condensation (Fig. 11a, substructure D; see also relative downfield ¹H NMR chemical shifts of B2 compared with B1 because of larger aromatic ring current from more extended condensation; Table S4) in unsubstituted PAH hydrocarbon environments, as well as the consequences of substitution with plausible electron-withdrawing (-COOH, N-heterocycles; substructures E1 and E3) and electron-donating (-OH; substructures E2) substituents that may exhibit long-range transmission of NMR-relevant substituent effects across conjugated π-systems.

Within common edge moieties of unsubstituted PAH, steric congestion of proton pairs (Bauschlicher et al., 2009; Tominaga et al., 2010) decreases from narrow fjord regions A (substructures A1, A2, A3) through mid-bay sections B (substructures B1, B2) through unhindered domains C (substructures C1 and C2). Extensive steric congestion (substructures A1 $\sim$ A2 $\sim$ A3 > B1 $\sim$ B2) imposes progressive downfield shift beyond $\delta_H > 9$ ppm, whereas δ_C sustains considerably less relative chemical shift displacement (atom pairs 24/46 as compared with 25/26; cf. Fig. S6, Table S4). Lesser steric hindrance in open bays (sections B) imposed mid-size downfield shifts ($\delta_H \sim 8.6$ ppm) at nearly unaltered δ_C (atom pairs
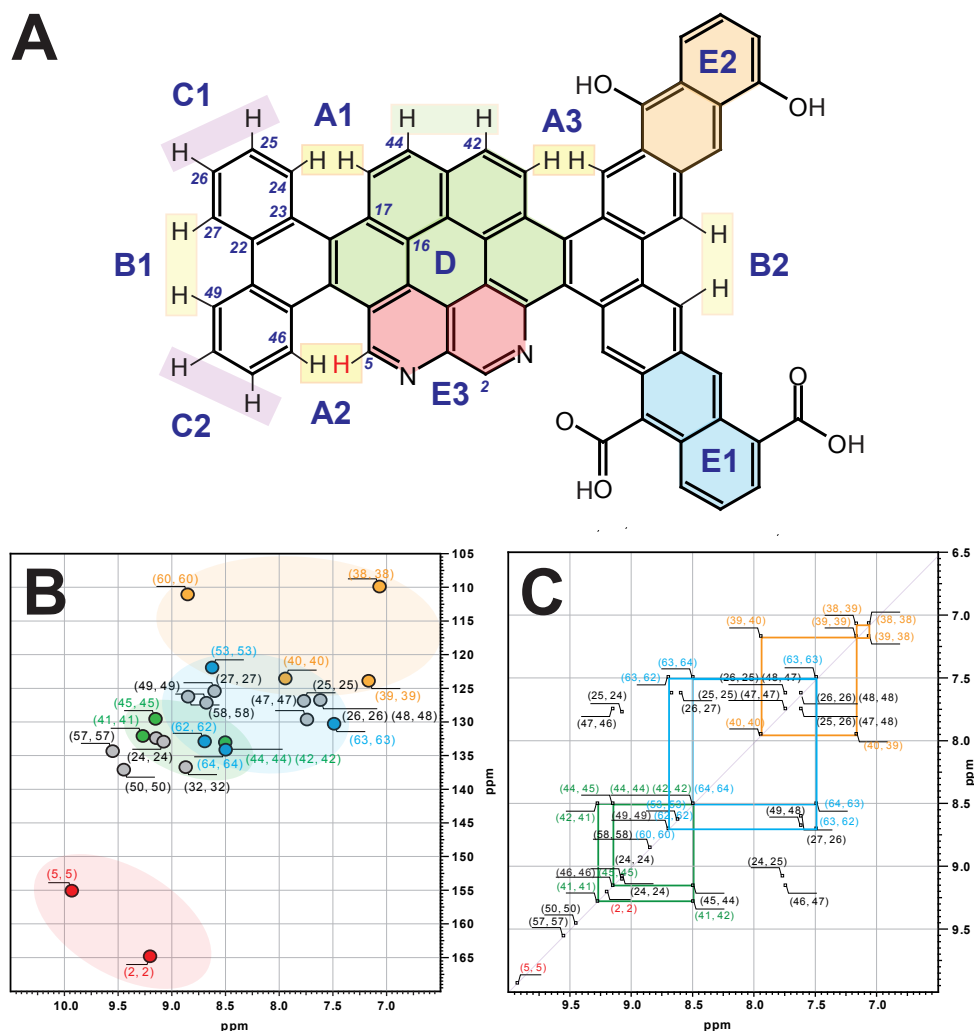
Fig. 11. Conceptual model of polycyclic aromatics to elucidate prospective NMR properties of marine thermogenic carbon (TMOC; cf. text). **(A)** Molecular formula of PAH model $C_{65}H_{34}N_2O_6$ (IUPAC mass: 938.975 Da) with specific chemical environments provided (full numbering scheme, cf. Fig. S6, ^{1}H and ^{13}C NMR chemical shifts: Table S4); narrow polycyclic hydrocarbon (PAH) fjord regions: A1, A2, A3; more relaxed open PAH bay regions: B1 and B2; unconstrained PAH: C1 and C2; condensed PAH: D; specific substitutions patterns as follows: electron withdrawing substituents: E1; electron-donating substitution: E2; N-heterocycles: E3. **(B)** Computed HSQC and **(C)** COSY (TOCSY) NMR spectra of PAH model $C_{65}H_{34}N_2O_6$ with specific positions highlighted (cf. text).

27/49; cf. Fig. S6). Similarly, increased aromatic condensation, which implies superimposed and amplified in-plane deshielding ring currents (Williamson et al., 1986; Tominaga et al., 2010), imposes downfield proton chemical shift (atom pairs 44(42)/25; cf. Fig. S6). Increased condensation implies more numerous long-range carbon–carbon contacts within four bonds, and here, downfield shifts of δ_C may occur (atom pairs 17/23: $\Delta\delta_C \sim 11$ ppm and 16/22: $\Delta\delta_C \sim 1$ ppm; cf. Fig. S6, Table S4).

Heterocyclic nitrogen incorporated into six-membered rings imposes electron-withdrawal and strong deshielding for both δ_H and δ_C (cf. $\delta_{C5/H5} \sim 154.6/9.90$ ppm (fjord region A1), $\delta_{C2/H2} \sim 164.3/9.18$ ppm). In fact, this combination of pronounced proton and carbon downfield chemical

shift might serve as a recognition feature for six-membered N-heterocycles because protonated carbons (methines) in any polycyclic aromatic hydrocarbon rarely resonate beyond $\delta_C \sim 140$ ppm (Hansen, 1979). This even applies in case of additional carboxylic substitution (section E1), which rather imposes significant δ_H downfield displacement for ortho and para positions while barely affecting δ_C. In contrast, electron-donating substituents like hydroxyl or ethers (section E3) which act upon ortho and para positions as well, are mandatory to displace δ_C to <120 ppm; similarly, $\delta_H < 7$ ppm imply presence of oxygen attached to, or incorporated into six-membered rings within PAH (Perdue et al., 2007).

In conclusion, pure hydrocarbon PAH exhibit variable proton chemical shift in dependence of steric crowding and

degree of condensation, both of which induce sizable proton NMR downfield chemical shift while leaving δ_C nearly unchanged. Six membered N-heterocycles will show combinations of downfield chemical shift for protons and carbon not available by any means of electron withdrawing – and donating oxygenation of aromatic hydrocarbons. Here, electron withdrawing substitution (COOH, COOR, CONH) will displace ortho as well as para positions to lower field for both δ_H and δ_C, whereas electron donating substitution will displace ortho and para positions to higher field in both δ_H and δ_C. At first approximation these effects can be considered near additive as known from NMR increment analysis (Perdue et al., 2007).

3.11 NMR characterization of unsaturated chemical environments in marine SPE-DOM

3.11.1 TOCSY NMR spectra

The distinctive sensitivity of TOCSY NMR spectra was perfectly eligible to detect minor and possibly diffuse NMR signatures in less congested spectral regions. Hence, TOCSY cross peaks were ideally suited to determine chemical environments of hydrogen attached to sp^2-hybridized carbon in the chemical shift range of $\delta_H \sim 5$–10 ppm. Their relatively fast transverse NMR relaxation caused by enhanced contributions from chemical shift anisotropy (CSA) suggested the use of apodization functions which improved the S/N ratio at the expense of resolution (Fig. S1) to reveal weak and extended NMR signatures of complex biogeochemical mixtures, like those of TMOC (Fig. 12). Accordingly, high-field NMR spectra have uncovered otherwise elusive extended downfield olefinic and aromatic TOCSY cross peaks in marine SPE-DOM, which provided useful constraints about chemical environments of its sp^2-hybridized carbon (Fig. 12).

3.11.2 HSQC NMR spectra of marine SPE-DOM

The strength of HSQC NMR spectra, which exhibit shorter duration and hence less susceptibility of magnetization loss from fast transverse NMR relaxation than DEPT-HSQC NMR spectra, resides in the detection of low abundant features, in particular when acquired at high S/N ratio with limited F1 resolution and apodization designed for S/N enhancement. Unsaturated chemical environments in marine DOM contain almost exclusively methine and quaternary carbon; terminal methylene ($C=CH_2$), while present in some marine natural products (Blunt et al., 2010), is rather elusive in natural organic matter. Hence, spectral editing is of limited use in the HSQC chemical shift section of sp^2-hybridized carbon ($\delta_C > 90$ ppm). All four marine SPE-DOM revealed significant HSQC cross peaks of unsaturated carbon chemical environments (Fig. 13). Interestingly, transverse relaxation accelerated markedly from surface to deep SPE-DOM,

requiring disproportionally large numbers of scans to acquire meaningful HSQC NMR spectra of deep (5446 m) marine SPE-DOM (Table S3).

3.11.3 Joint HSQC and TOCSY cross-peak assignment of marine SPE-DOM

Both TOCSY and HSQC NMR spectra of marine SPE-DOM shared the same proton NMR chemical shift but indicated different units within: HSQC NMR cross peaks indicated any CH$_n$-X group (n: 1, 2, 3; X: any atom) with directly bound carbon–proton pairs (magnetization transfer via $^1J_{CH}$), whereas TOCSY NMR cross peaks required rather proximate coupled proton pairs (magnetization transfer via $^nJ_{HH}$; $n \sim 2$–5). Saturated molecules with large H/C ratios will exhibit abundant HSQC and TOCSY cross peaks, whereas fused aromatic rings and hydrogen deficient molecules in general will display HSQC cross peaks for any C-H pair even when isolated, but only a few to none TOCSY cross peaks in case of isolated protons (similar considerations applied to the appearance of COSY and JRES cross peaks). Furthermore, individual carbon and hydrogen atoms at polarized double bonds might resonate at widely different HSQC as well as TOCSY cross-peak positions. Olefins and aromatics with extensive aliphatic substitution are in general sterically protected from microbial and enzymatic attack, making them likely candidates for survival especially in aged deep water SPE-DOM. Nevertheless, the proposed HSQC and TOCSY cross-peak assignments of sp^2-hybridized carbon in marine SPE-DOM (Figs. 12 and 13) were in mutual agreement.

3.12 FTICR mass spectra of marine SPE-DOM

3.12.1 Negative electrospray ionization (ESI) FTICR mass spectra of marine SPE-DOM

Ultrahigh resolution Fourier transform ion cyclotron mass spectra (FTICR/MS) of Atlantic Ocean SPE-DOM each provided several thousands of mass peaks (Koch et al., 2005; Kujawinski et al., 2009), of which many hundreds could be assigned to extended CHO, CHNO, CHOS and CHNOS molecular series (Fig. 14 and Table 4) based on excellent mass accuracy and mass resolution. From surface to deep SPE-DOM, slightly increasing numbers of mass peaks occurred, of which similar fractions (near 45 %) were assigned to molecular formulae (Table 4). The relative oxygen content derived from intensity weighted assigned mass peaks was near 36 % for the three near-surface samples and 42 % for the deep sample from 5446 m. This increase of oxygen caused the relative carbon content to decrease from typically 50–52 % (slightly increasing from surface with increasing depth) to 47 % in case of the deep sample 5446 m. Consequently, the computed H/C ratio increase for this deep sample was likely
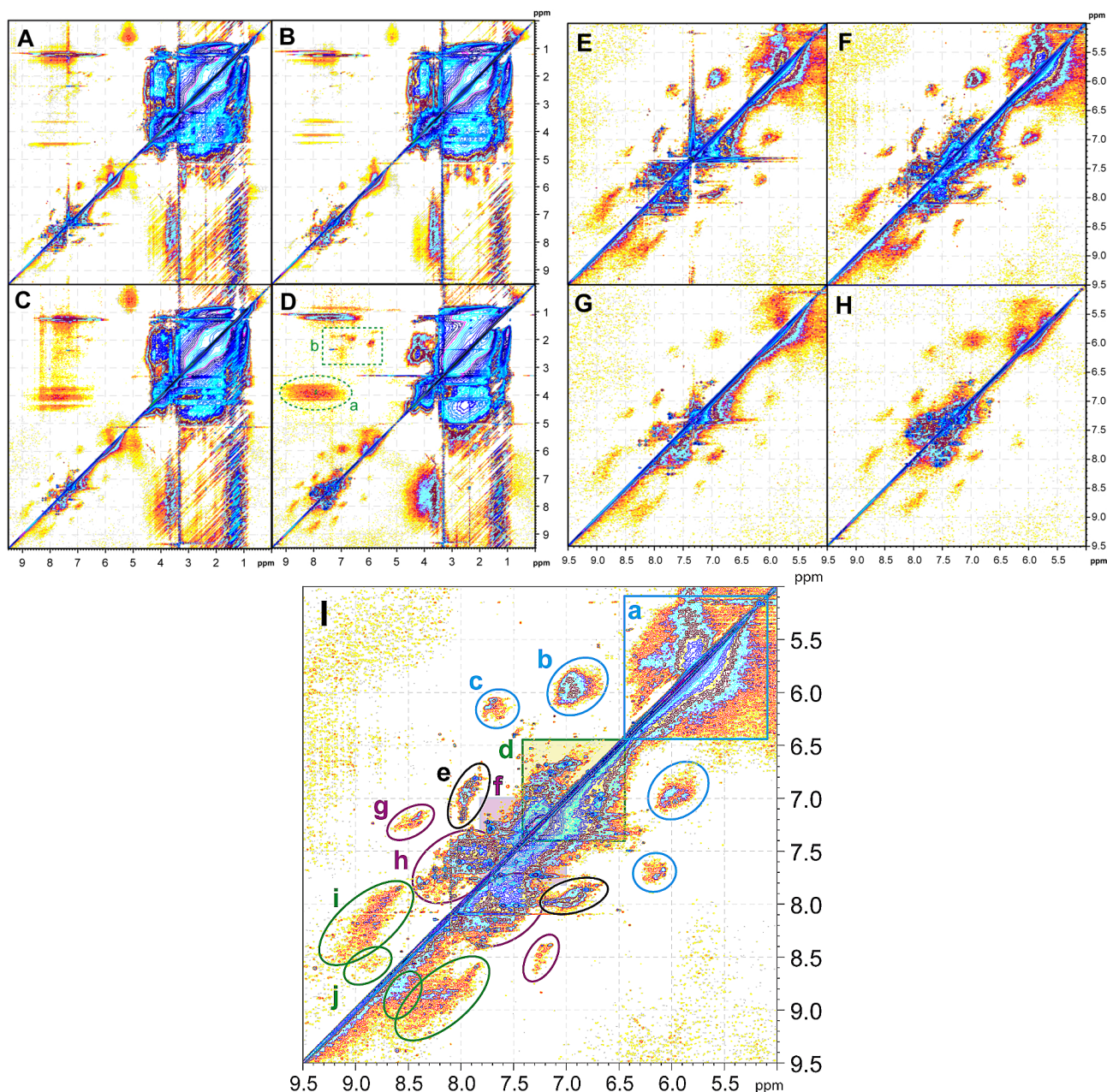
Fig. 12. TOCSY NMR cross peaks of four marine SPE-DOM ((**A, E**): 5 m (near-surface photic zone); (**B, F**) 48 m (fluorescence maximum); (**C, G**) 200 m (upper mesopelagic zone); (**D, H**) 5446 m (30 m above seafloor)) with sensitivity enhanced apodization to emphasize less abundant sp^2-hybridized carbon environments in marine SPE-DOM. (**A–D**) full spectrum $\delta_H = 0$–9.5 ppm; (**E–H**) section of unsaturated (olefinic and aromatic) protons $\delta_H = 5$–9.5 ppm; (**D**) dotted box a: TOCSY cross peaks connecting peptides $\underline{H}$N-C$\underline{H}\alpha$; dotted box b: TOCSY cross peaks connecting olefins and methyl, C$=$$\underline{H}$C-C$\underline{H}_3$. (**I**) unsaturated (olefinic and aromatic) protons in surface SPE-DOM 48 m with substructures denoted as follows: section a: intra-olefinic cross peaks $\underline{H}$C$_{olefin}=$C$_{olefin}\underline{H}$, like in linear terpenoids; section b: α,β-unsaturated double bonds: $\underline{H}$C$_{olefin}=$C$_{olefin}\underline{H}$-(C$=$O)-X; section c: polarized α,β-unsaturated double bonds: $\underline{H}$C$_{olefin}=$C$_{olefin}\underline{H}$-(C$=$O)-X; section d: aromatics $\underline{H}$C$_{aromatic}$-C$_{aromatic}\underline{H}$ with ortho and/or para oxygenated substituents (classic aromatic substitution of natural organic matter); section e: strongly polarized α,β-unsaturated double bonds, also in oxygen-derived heterocycles: $\underline{H}$C$_{olefin}$-C$_{olefin}\underline{H}$-(C$=$O, O)-X; section f: condensed and strongly electron withdrawing aromatics $\underline{H}$C$_{aromatic}$-C$_{aromatic}\underline{H}$ (multiply carboxylated, N-heterocycles); section g: poly-cyclic aromatics, open fjord region (cf. Fig. 11a sections B1, B2), N-heterocycles; section h: polycyclic aromatics, fjord region in polycyclic aromatics, more extended polycyclic aromatics, N-heterocycles; section i: congested fjord region in polycyclic aromatics (cf. Fig. 11a sections A1, A2, A3); and section j: alike section i, and $\underline{H}$C$_{sp2}$-C$_{sp2}\underline{H}$ in condensed polycyclic aromatics.
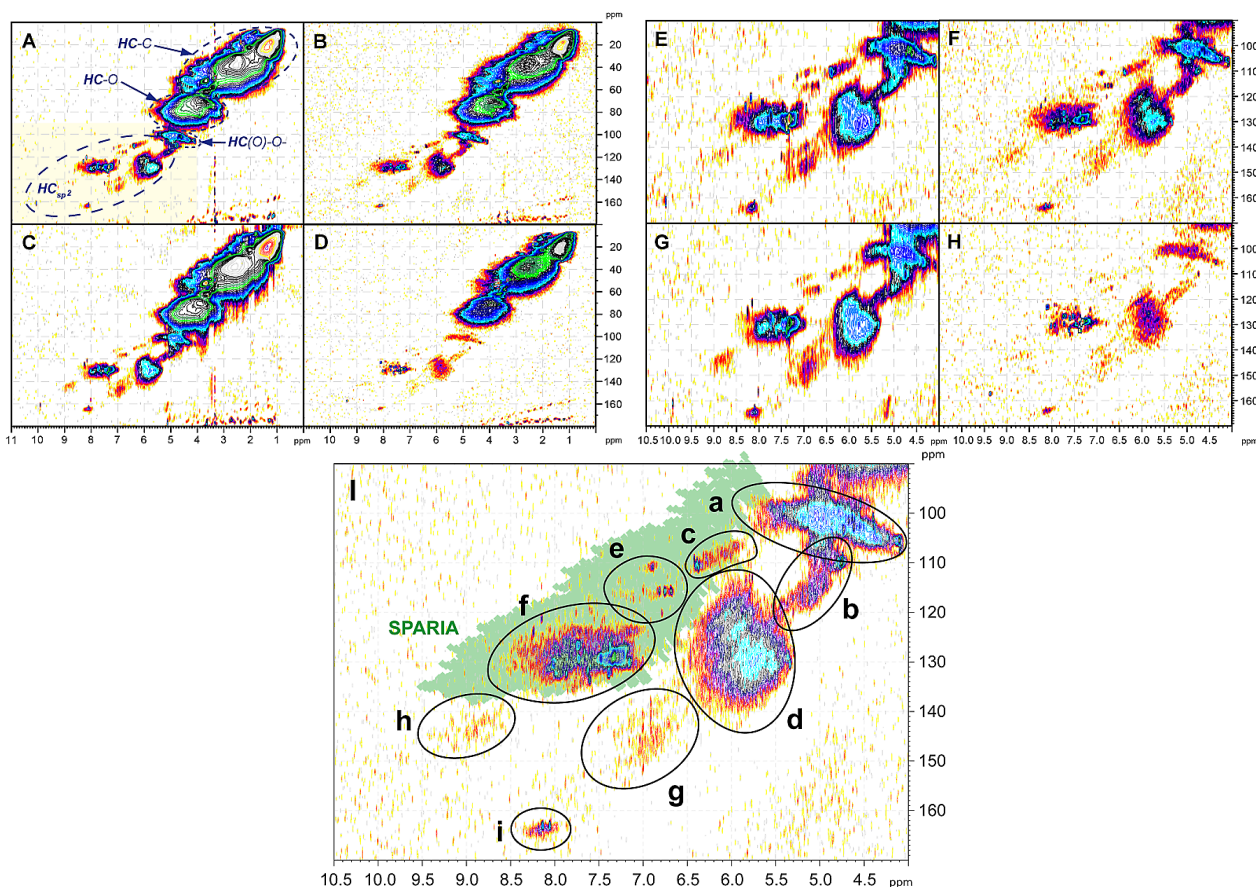
Fig. 13. ^{1}H, ^{13}C HSQC NMR cross peaks of four marine SPE-DOM with **(A)** four major chemical environments indicated ((**A, E**): 5 m (near-surface photic zone); **(B, F)** 48 m (fluorescence maximum); **(C, G)** 200 m (upper mesopelagic zone); **(D, H)** 5446 m (30 m above seafloor)) with sensitivity enhanced apodization to emphasize less abundant sp^2-hybridized carbon environments in marine SPE-DOM. **(A–D)** full spectra $\delta_H = 0$–11 ppm; **(E–H)** section of unsaturated (olefinic and aromatic) protons $\delta_H = 5$–10.5 ppm; **(I)** section of unsaturated (olefinic and aromatic) CH pairs in surface SPE-DOM 48 m (fluorescence maximum) with substructures denoted as follows: section a: anomeric CH in carbohydrates (sp^3-hybridized); section b: isolated olefins; section c: multiply oxygenated aromatics (oxygen heterocycles), olefins; section d: C-conjugated olefins, certain five membered N-, O- and S-heterocycles ($\delta_H < 6.5$ ppm); section e: phenols, classical oxygenated NOM aromatics; section f: classical NOM aromatics with substantial fraction of carbonyl derivatives (likely COOH); at $\delta_H > 8$ ppm: multiply carboxylated aromatics, classical PAH and six-membered nitrogen heterocycles; sterically uncongested polycyclic aromatic hydrocarbons; section g: α,β-unsaturated double bonds for $\delta_C > 140$ ppm, including double bonds adjacent to aromatics: C-$\underline{\mathbf{H}\mathbf{C}}_{\text{olefin}} = \underline{\mathbf{C}}_{\text{olefin}}\underline{\mathbf{H}}$-(C=O), C$_{\text{ar}}$-X; section h: nitrogen heterocycles, heteroatom substituted polycyclic aromatics; and section i: specific nitrogen heterocycles, very likely with more than one nitrogen. The green area highlights the HSQC cross-peak region accessible to single benzene rings substituted by common electron withdrawing, neutral and electron-donating common substituents of natural organic matter; SPARIA: **s**ubstitution **pa**tterns in **a**romatic **r**ings by **i**ncrement **a**nalysis (Perdue et al., 2007).

an indirect consequence of enhanced oxygenation rather than increase of saturation.

The abundance of CHO and CHNO molecular series grew from surface to bottom SPE-DOM, whereas CHOS and especially CHNOS molecular series markedly declined. Visual inspection of entire FTICR mass spectra revealed minor alterations of peak distributions, with extended continual series and a very few large intensity mass peaks, least abundant in the 200 m sample and likely indicative of biological origin. The average mass grew by about 10 Da from surface to deep SPE-DOM, consistent with findings by Flerus et al. (2012).

This at first inconspicuous looking change might reflect in fact major alterations of molecular composition and structure within the various marine SPE-DOM. Any single marine SPE-DOM mass peak represented many isomers, possibly hundreds to thousands of them were projected onto any given mass peak (Hertkorn et al., 2008). This superposition corresponded to a massive intrinsic averaging and considerable alterations of SPE-DOM structure were required to effect in essence marginally looking mass shifts. Expansion of nominal mass sections which were well suited to depict organic molecular diversity (Hertkorn et al., 2008) demonstrated a

Table 4. Counts of mass peaks as computed from negative electrospray 12T FTICR mass spectra for singly charged ions with nitrogen rule check and 500 ppb tolerance.

Members of molecular series	5 m		48 m		200 m		5446 m	
CHO compounds	840	(24.6 %)	772	(24.6 %)	1167	(30.8 %)	1343	(39.3 %)
CHOS compounds	730	(21.4 %)	681	(21.7 %)	700	(18.5 %)	441	(12.9 %)
CHNO compounds	1054	(30.8 %)	976	(31.1 %)	1370	(36.1 %)	1391	(40.7 %)
CHNOS compounds	795	(23.3 %)	711	(22.6 %)	553	(14.6 %)	242	(7.1 %)
Number of assigned mass peaks	3419		3140		3790		3417	
Total number of mass peaks	7301		7244		7940		7537	
Percent of mass peaks attributed to CHO, CHOS, CHNO and CHNOS compositions	46.8 %		43.3 %		47.7 %		45.3 %	
Average H (%)	6.70		6.85		6.88		6.77	
Average C (%)	50.17		50.76		51.70		46.66	
Average O (%)	36.12		35.99		36.03		41.69	
Average N (%)	2.70		2.47		2.18		1.94	
Average S (%)	4.31		3.94		3.21		2.94	
Computed H / C ratio from FTICR mass peaks	1.60		1.62		1.60		1.74	
Computed O / C ratio from FTICR mass peaks	0.54		0.53		0.52		0.67	
Computed C / N ratio from FTICR mass peaks	18.4		20.6		23.7		24.1	
Computed C / S ratio from FTICR mass peaks	11.6		12.9		16.1		15.9	
Average mass, intensity weighted	367.6		366.2		372.1		381.8	

decline in abundance of extensively unsaturated (i.e. aromatic) CHOS compounds from surface to bottom SPE-DOM at otherwise similar mass peak distributions.

The main dissimilarities denoted in van Krevelen diagrams of marine SPE-DOM with depth were observed within the ratios $0.5 < H/C < 1.5$ and $O/C < 0.3$ and primarily concerned medium unsaturated CHOS and CHNOS molecules (Fig. S7). Accordingly, the numbers of (mostly CHO and CHNO) molecules denoted within the ratios $0.65 < H/C < 1.7$ and $0.25 < O/C < 0.7$ were higher in the case of deep marine SPE-DOM (200 m and 5446 m) than in the top layer SPE-DOM (5 m and 48 m). Furthermore, the counts of oxygen atoms in CHO, CHNO and CHOS molecular series increased from top to bottom SPE-DOM, indicative of progressive oxidation, in line with the NMR results (Table 4). Negative ESI mass spectrometry-derived elemental C / N ratios were growing from 18.4 (SPE-DOM sample from 5 m) to 24.1 (SPE-DOM sample from 5446 m), indicative of a slight preference to ionize N-containing molecules over others, however with declining discrimination (cf. Table 1). This divergence indicated again variable chemical environments for CHO and CHNO molecules at different water depths. The MS-derived C / S atomic ratios near continually increased from surface to deep SPE-DOM (Table 4), indicating progressive depletion of sulfur, in line with element analyses (Fig. 20).

3.12.2 Positive electrospray ionization (ESI) FTICR mass spectra of marine SPE-DOM

Positive mode FTICR mass spectra of four marine SPE-DOM showed smooth skewed near-Gaussian bulk envelopes

characteristic of processed organic matter with almost entirely absent conspicuous biosignatures and a singular large mass peak ($m/z = 240.1495$: $C_{15}H_{18}N_3^+$, unknown origin). The relative abundance of mass peaks between $m/z \sim 240$–320 continually decreased from surface SPE-DOM at 5 m (clearly recognizable shoulder in the overall mass peak distribution) to deep SPE-DOM at 200 m and then increased again in case of abyssopelagic SPE-DOM at 5446 m (Fig. 15). In general, ions detected in positive ESI FTICR mass spectra were more carbon-rich (~ 62 % carbon in assigned molecular compositions) than those detected in negative ESI FTICR mass spectra (~ 50 % carbon in assigned molecular compositions) and oxygen-depleted (~ 26 % (positive ions) against 36–42 % oxygen (negative ions) in assigned molecular compositions; Tables 4 and 5). The coverage of CHNO compounds in FTICR mass spectra grew from 30–40 % of assigned molecular compositions in negative ESI mode to 46–51 % in positive ESI mode. The ratio of assigned CHNO / CHO molecular compositions in positive ESI mass spectra of all marine SPE-DOM was near uniform (1.13 ± 0.05; Table 5). Though CHNO compounds appeared more abundant in all positive ESI FTICR mass spectra of marine SPE-DOM, the overall MS-detected nitrogen content in assigned mass peaks ranged near 3 %, only slightly exceeding the nitrogen content deduced from negative ESI FTICR mass spectra (2.5 %).

With the exception of abyssopelagic SPE-DOM at 5446 m, positive ESI FTICR mass spectra showed much fewer CHOS and CHNOS compounds in comparison with negative ESI FTICR mass spectra (Tables 4 and 5). However, structural selectivity for ionization of CHOS and CHNO
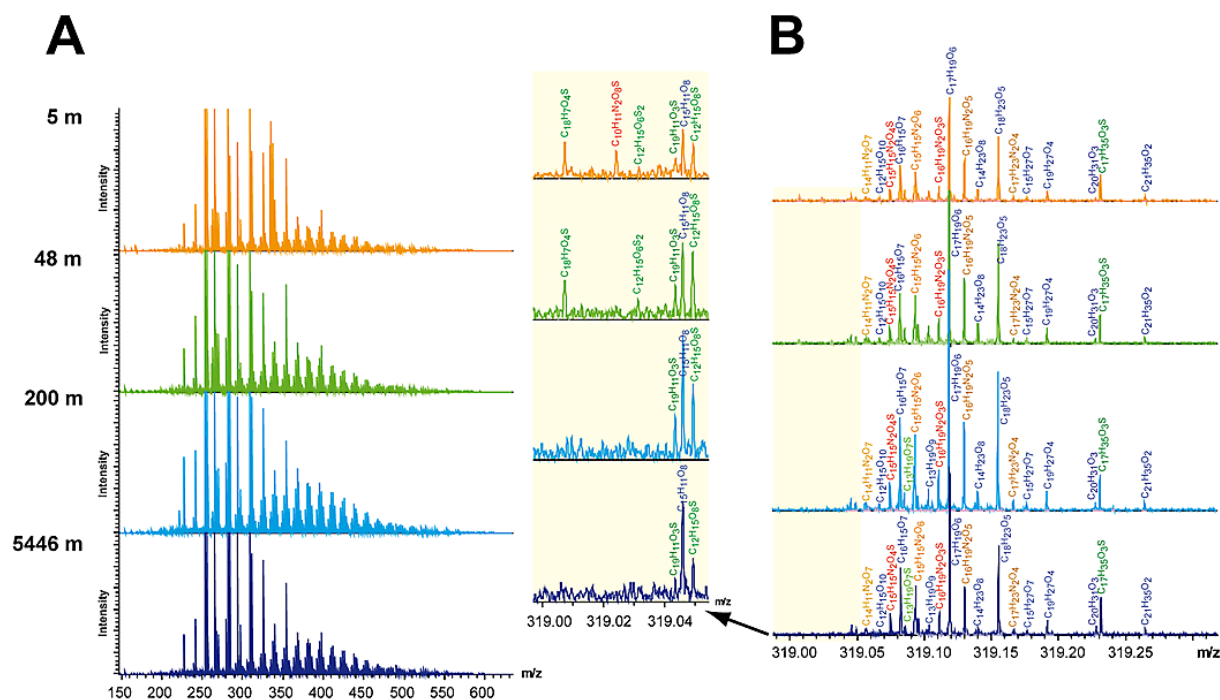
Fig. 14. Negative electrospray 12T FTICR mass spectra of marine SPE-DOM; from top to bottom: 5 m (near-surface photic zone); 48 m (fluorescence maximum); 200 m (upper mesopelagic zone); 5446 m (30 m above seafloor). **(A)** FTICR mass spectra from 150–650 Da; **(B)** expansion of nominal mass 319 for negative ions MH$^-$ with molecular formulae provided on the basis of their mass accuracy and mass resolution (cf. text). Insert **(B)** expansion of the mass segment 319–319.05 Da ($\Delta m = 0.05$ Da) with enhanced relative intensity, indicating mostly CHOS molecules which discriminate between top and bottom marine SPE-DOM.

compounds in various marine SPE-DOM became obvious from non-continual and variable proportions of abundance in positive and negative ESI FTICR mass spectra. The fraction of assigned CHOS compounds in negative ESI FTICR mass spectra decreased from 22 % in surface SPE-DOM to 13 % at a depth of 5446 m (CHNOS compounds: from 23 % to 7 %), whereas in positive ESI FTICR mass spectra, CHOS compounds were somewhat abundant in surface SPE-DOM 5m (5 %), nearly absent in SPE-DOM of intermediate depth (∼ 3 %) but prevalent at maximum depth SPE-DOM (10 %).

Hence, the FTMS-derived abundance patterns of CHOS compounds indicated selective sulfur chemistry in marine SPE-DOM at different depths. A suite of several dozens of specific CHOS compounds of considerable H-deficiency (H/C ratio: 0.7–1.1) and O-deficiency (O/C ratio < 0.3) has been detected exclusively in abyssopelagic SPE-DOM at 5446 m, suggesting prevalence of reduced sulfur (thiols, sulfides, thioethers) present in these CHOS compounds. A specific suite of surface ocean CHOS compounds rapidly declined in abundance with water depth, suggesting surface photochemistry as a main source of then reduced CHOS compounds (cf. discussion of negative ESI FTICR mass spectra). In addition, atmospheric deposition might contribute to the composition of surface marine CHOS compounds (Jimenez et al., 2009; Paytan et al., 2009). The CHOS

compounds found near the ocean seafloor were more numerous and similarly hydrogen-deficient (Fig. 16). In both sites, a wide range of reactions of reduced sulfur with organic matter (Hebting et al., 2006; Kok et al., 2000) might apply; however, the origin of the participating substrates might differ vastly. While surface photochemistry would release reactive sulfur species from reduced sulfur compounds, metal-mediated and biological redox reactions in the seafloor sediment might leach CHOS molecules to bottom marine DOM (Fig. 16). Notably, DOM concentrations in marine sediment pore waters are elevated over bottom water values by up to ten-fold (Hedges, 1992; Burdige et al., 1999). DOC fluxes from marine sediments are related to sediment carbon cycling (preservation and mineralization) and represent an important source of DOC to the oceans, with abyssal DOC flux rates ranging from 0.1 to 0.7 mmol m^{-2} d^{-1} (Burdige et al., 1999). Appreciable diffusive DOC flux from marine sediments across large, level abyssal plains therefore seems quite capable of sustaining an unique deep sea DOM signature near the ocean floor. Release of reduced sulfur species (Hebting et al., 2006) from ocean floor sediments into the bottom seawater column and incorporation into marine DOM can be assessed in further studies by comparative analysis of deep water SPE-DOM obtained at increasing distance from the seafloor.

Table 5. Counts of mass peaks as computed from positive electrospray 12 T FTICR mass spectra for singly charged ions with nitrogen rule check and 500 ppb tolerance.

Members of molecular series	5 m		48 m		200 m		5446 m	
CHO compounds	1650	(35.7 %)	1932	(35.9 %)	1676	(34.2 %)	1321	(31.1 %)
CHOS compounds	212	(4.6 %)	172	(3.2 %)	182	(3.7 %)	428	(10.1 %)
CHNO compounds	2321	(50.3 %)	2666	(51.3 %)	2505	(51.2 %)	1951	(46.0 %)
CHNOS compounds	435	(9.4 %)	608	(8.1 %)	533	(10.9 %)	543	(12.8 %)
Number of assigned mass peaks		4618		5378		4896		4243
Total number of mass peaks		7483		9689		9427		8338
Percent of mass peaks attributed to CHO, CHOS, CHNO and CHNOS compositions		61.7 %		55.5 %		51.9 %		50.9 %
Average H (%)		6.84		6.47		6.28		6.22
Average C (%)		62.03		61.56		61.42		61.86
Average O (%)		25.87		26.55		26.89		25.82
Average N (%)		3.58		3.64		3.70		2.51
Average S (%)		1.69		1.77		1.71		2.59
Computed H / C ratio from FT-ICR mass peaks		1.31		1.24		1.21		1.19
Computed O / C ratio from FT-ICR mass peaks		0.31		0.32		0.33		0.31
Computed C / N ratio from FT-ICR mass peaks		20.2		19.9		19.6		20.6
Computed C / S ratio from FT-ICR mass peaks		98.0		93.2		96.8		63.8
Average mass, intensity weighted		371.4		371.3		381.5		388.7

Both CHO and CHNO positive ions showed expansive contiguous ellipsoids in van Krevelen diagrams with a decent coverage of the C,H,O-compositional space across sizable ranges of H / C (0.7–1.6) and O / C ratios (0.1–0.7; Fig. S8). With the notable exception of abyssopelagic SPE-DOM at 5446 m, only a few CH(N)OS compounds occupied the sector of markedly unsaturated molecular compositions. Coverage in positive ESI FTICR mass spectra extended to lesser oxygenated compositions (O / C ratio < 0.1) than found in negative ESI FTICR mass spectra.

CHNO compounds occupied a slightly lesser range of oxygenation than CHO molecular series and were displaced toward increased H / C ratio. This displacement exceeded the single intrinsic hydrogen carried by any nitrogen into any H / C versus O / C van Krevelen diagram (the formal nitrogen insertion unit in C-C and C-H bonds is -NH-), suggesting less carbon unsaturation in average CHNO ions than found in CHO ions. Otherwise, peptide nitrogen in marine SPE-DOM would carry a single intrinsic oxygen (the O / N ratio within a CONH unit equals one) for any nitrogen atom in case of neutral amino acids.

3.12.3 Comparison of positive and negative ESI FTICR mass spectra of marine SPE-DOM

In general, positive ions were more numerous than negative ions (in fact, mass peaks) for all marine SPE-DOM; less numerous positive ions were observed for deep SPE-DOM at 5446 m (relative decrease by ∼ 10 %) and especially for surface SPE-DOM (decrease by ∼ 20 %; Table 5). The proportion of assigned molecular compositions was somewhat larger for positive than for negative ions, possibly because of

the larger regularity observed within the positive ESI FTICR mass spectra of marine SPE-DOM (Fig. 16).

A combination of factual occurrence and structure-dependent ionization selectivity of positive and negative ESI determines the occupancy of distinct sectors in van Krevelen diagrams for CHO, CHNO, CHOS and CHNOS molecular series. For assessment of ionization selectivity and overall coverage, positive and negative ions present in each of all four marine SPE-DOM were compared (Figs. 16–18 and Table 6).

Abundant CHO, CHOS, and CHNO compositions of probable biochemical heritage were almost exclusively observed in negative ESI FTICR mass spectra, whereas positive ESI FTICR mass spectra showed smooth overall bulk envelopes of processed organic matter with prevalent processed biogeomolecules (Fig. 15).

Positive CHO ions were less oxygenated (O / C ratio: 0.25–0.65) than negative CHO ions (O / C ratio: 0.1–0.7) but occupied a larger range of relative unsaturation (H / C ratio of CHO ions, positive ESI: 0.75–1.7; negative ESI: 1.0–1.65). Similar abundance relationships applied for CHNO ions (Figs. S7 and S8). Negative CHO and CHNO ions showed lesser coverage of the C,H,O-compositional space at low oxygenation (O / C ratio: < 0.25) than positive CHO and CHNO ions. Negative CHOS ions occupied mainly three clusters of oxygen-deficient (O / C ratio < 0.35) compositions with H / C ratios of ∼ 2 (aliphatic sulfonates), 1.3–1.6 (CHOS lipids), and 0.7–1.0 (likely aromatic CHOS compounds with reduced sulphur; Figs. 16 and S8).

Positive and negative electrospray ionization selectivity was very pronounced in FTICR mass spectra of all four

Table 6. Counts of common and unique ions found in all FTICR mass spectra of the four marine SPE-DOM sorted according to molecular series.

Molecular series	Negative ions found in FTICR mass spectra	Sum of all negative ions (common + negative)	Negative ions in all four SPE-DOM	Common ions in all FTICR mass spectra of all four SPE-DOM	Positive ions in all four SPE-DOM	Sum of all positive ions (common + posiive)	Positive ions found in FTICR mass spectra
CHO		767	620	147	830	977	
CHOS		215	180	35	89	124	
CHNO		770	635	135	930	1065	
CHNOS		135	95	40	66	106	
CHO/5 m	840	767	620	147	830	977	1650
CHO/48 m	772	767	620	147	830	977	1932
CHO/200 m	1167	767	620	147	830	977	1676
CHO/5446 m	1343	767	620	147	830	977	1321
CHOS/5 m	730	215	180	35	89	124	212
CHOS/48 m	681	215	180	35	89	124	172
CHOS/200 m	700	215	180	35	89	124	182
CHOS/5446 m	441	215	180	35	89	124	428
CHNO/5 m	1054	770	635	135	930	1065	2321
CHNO/48 m	976	770	635	135	930	1065	2666
CHNO/200 m	1370	770	635	135	930	1065	2505
CHNO/5446 m	1391	770	635	135	930	1065	1951
CHNOS/5 m	795	135	95	40	66	106	435
CHNOS/48 m	711	135	95	40	66	106	608
CHNOS/200 m	553	135	95	40	66	106	533
CHNOS/5446 m	242	135	95	40	66	106	543

marine SPE-DOM and molecular series: with the exception of CHNOS molecules, the number of common ions (found in both negative and positive ESI FTICR mass spectra) was always much smaller than the unique ions (found in either positive or negative FTICR mass spectra; Table 6). This at first implies that multiple heteroatom occurrence in marine SPE-DOM molecules alleviates ionization selectivity. Otherwise, given the respectable size of molecular ions and their supposed polyfunctionality (as derived from NMR properties and count of heteroatoms in assigned molecular compositions), the observed extent of ionization selectivity is remarkable, and for CHO molecular series is qualitatively different from that of CHO molecular series in Suwannee River fulvic acid (Hertkorn et al., 2008). Distinct clustering of common and unique ions, particularly for CHOS and CHNOS compositions, indicate that ionization selectivity depends on the presence of distinct functional groups. Unique ions in general occupy larger areas in van Krevelen diagrams and hence will be more chemically diverse than common ions.

The display of mass resolved H / C elemental ratios according to molecular series (Fig. 16) derived from negative ESI FTICR mass spectra showed about uniform mass distribution for CHO and CHNO molecular series for all marine SPE-DOM but a larger range of relative unsatura-

tion for CHO compared with CHNO molecular series (CHO compounds in abyssopelagic SPE-DOM at 5446 m extended towards larger mass; Fig. 16a). A separate limited number of rather saturated (H / C ratio ≥ 2) and abundant CHOS molecules *distinct in any marine SPE-DOM*, which were likely aliphatic sulfonates, extended to ever increasing mass from top to bottom SPE-DOM and were probably of biological origin in case of 5 m and 48 m SPE-DOM and of unknown provenance in the case of mesopelagic and abyssopelagic SPE-DOM at 200 m and 5446 m.

Extended molecular CHOS series of medium unsaturation (H / C ratio: 1.35 ± 0.2) were observed in negative ESI FTICR mass spectra of the three upper marine SPE-DOM with decreasing abundance according to $48 \, m \approx 5 \, m > 200 \, m$; the fraction with $m/z > 460 \, \text{Da}$ appeared displaced about 80 Da towards higher mass from similarly unsaturated CHO (and CHNO) compositions, suggesting prevalent sulfonation of respective precursors (the exchange of -OH by $-OSO_3H$ accounts for a mass difference of $\Delta m = 79.95682 \, \text{Da}$ for ^{32}S and ^{16}O). The abyssopelagic SPE-DOM at 5446 m lacked the high mass section ($m/z > 500 \, \text{Da}$) of these CHOS molecular series but showed significantly higher abundance of strongly unsaturated (H / C ratio ≤ 1; i.e. aromatic) CHOS molecules from
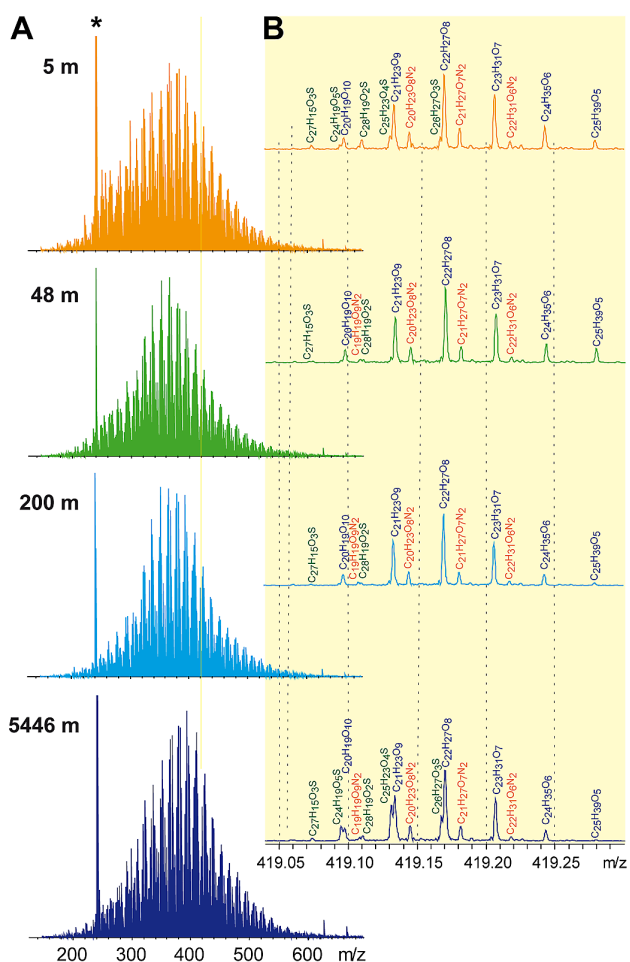
Fig. 15. Positive electrospray 12 T FTICR mass spectra of marine SPE-DOM samples; from top to bottom: 5 m (near-surface photic zone); 48 m (fluorescence maximum); 200 m (upper mesopelagic zone); 5446 m (abyssopelagic, 30 m above seafloor). **(A)** FTICR mass spectra from 150–700 Da; **(B)** expansion of nominal mass 419 for positive ions MH$^+$ (Δm: 419.04–419.31 Da) with molecular formulae provided on the basis of their mass accuracy and mass resolution (cf. text). Asterisk: $m/z = 240.1495$: $C_{15}H_{18}N_3$, unknown origin.

$m/z \sim 350$–530 than found in all other marine SPE-DOM. A specific CHOS chemistry in abyssopelagic SPE-DOM at 5446 m was further indicated in positive ESI FTICR mass spectra in which a suite of several dozen severely unsaturated, aromatic CHOS molecules (H/C ratio ≤ 1) occupied the mass range from $m/z \sim 280$–500 Da. This set of unique CHOS compounds specific to abyssopelagic marine SPE-DOM at 5446 m can be termed *black sulphur* because of its compositional similarity with black carbon and black nitrogen molecules (Knicker, 2010) which all are strongly hydrogen deficient (H/C ratio ≤ 1) and of limited oxygenation (O/C ratio ≤ 0.3; Fig. S8). A subordinated suite of compositionally related CHOS compounds in surface marine SPE-

DOM at 5 m probably originated from photochemical incorporation of reduced sulphur species in susceptible aromatic precursors.

The proportion of unique ions varied according to ionization and molecular series: more numerous positive than negative ions were observed for CHO and CHNO molecular series whereas, with the exception of abyssopelagic SPE-DOM at 5446 m, more numerous CH(N)OS ions were observed in negative ionization modus. The increased scatter of common negative ions as compared with common positive ions probably reflects its larger intrinsic molecular diversity, and a lesser intrinsic averaging from the presence of a larger proportion of biomolecules, in line with the abundance of signature mass peaks in the respective FTICR mass spectra (Figs. 14 and 15). The positioning of negative CHOS ions into three distinct areas likely reflected the intrinsic discontinuity of sulphur chemical environments in marine SPE-DOM.

Cluster analysis, based upon relative intensities of assigned mass peaks, revealed at first decreasing similarity of marine SPE-DOM with growing difference in water depth indicative of the different processes impacting waters from surface to depth (Fig. 15; cf. also proton NMR spectra, Fig. 2; Fig. S3). Comparison of consolidated pairs of surface (5 m and 48 m) and deep (200 m and 5446 m) SPE-DOM mass spectra revealed additional striking compositional variance. Surface SPE-DOM was enriched in certain oxygen-deficient CHOS and CHNOS molecules (O/C ratio < 0.3), with CHOS molecules showing larger H/C ratios than CHNOS molecules. This surprising behaviour (nitrogen carries indirect hydrogen into molecular formulae: i.e. a NH fragment can be inserted into any C-C and C-H bond but not N alone) implied that CHNOS molecules in surface marine SPE-DOM were "even" more unsaturated than CHOS molecules; i.e., they likely contained heterocyclic nitrogen. The observed oxygen deficiency within these molecular series probably excluded sulfates as significant marine SPE-DOM contributors, which also would exhibit considerable water solubility and therefore poorly absorb on PPL resin.

On the contrary, consolidated deep (200 m and 5446 m) marine SPE-DOM contained larger counts of specific CHO and CHNO molecules of intermediate H/C and O/C ratio, indicative of CRAM but also ranging in part into the aromatic realm (Koch and Dittmar, 2006), alongside with a marginal series of oxygen-deficient CHOS molecules; unique CHNOS molecules in deep SPE-DOM were essentially absent. Three CHOS ions ($C_{18}H_7O_4S^-$, $C_{11}H_{11}N_2O_8S^-$ and $C_{12}H_{15}O_6S_2^-$) were found abundant in consolidated deep ocean SPE-DOM (Fig. 17).

The occurrence of oxygen deficient CHOS compounds in surface SPE-DOM could be partly explained by integration of reactive, photoproduced reduced sulfur species such as hydrogen sulfide (H_2S), dimethyl sulfide (($CH_3)_2S$), and carbonyl sulfide ($O=C=S$) into functionalized molecules (Andreae and Crutzen, 1997; Amrani et al., 2007; Pos et al.,
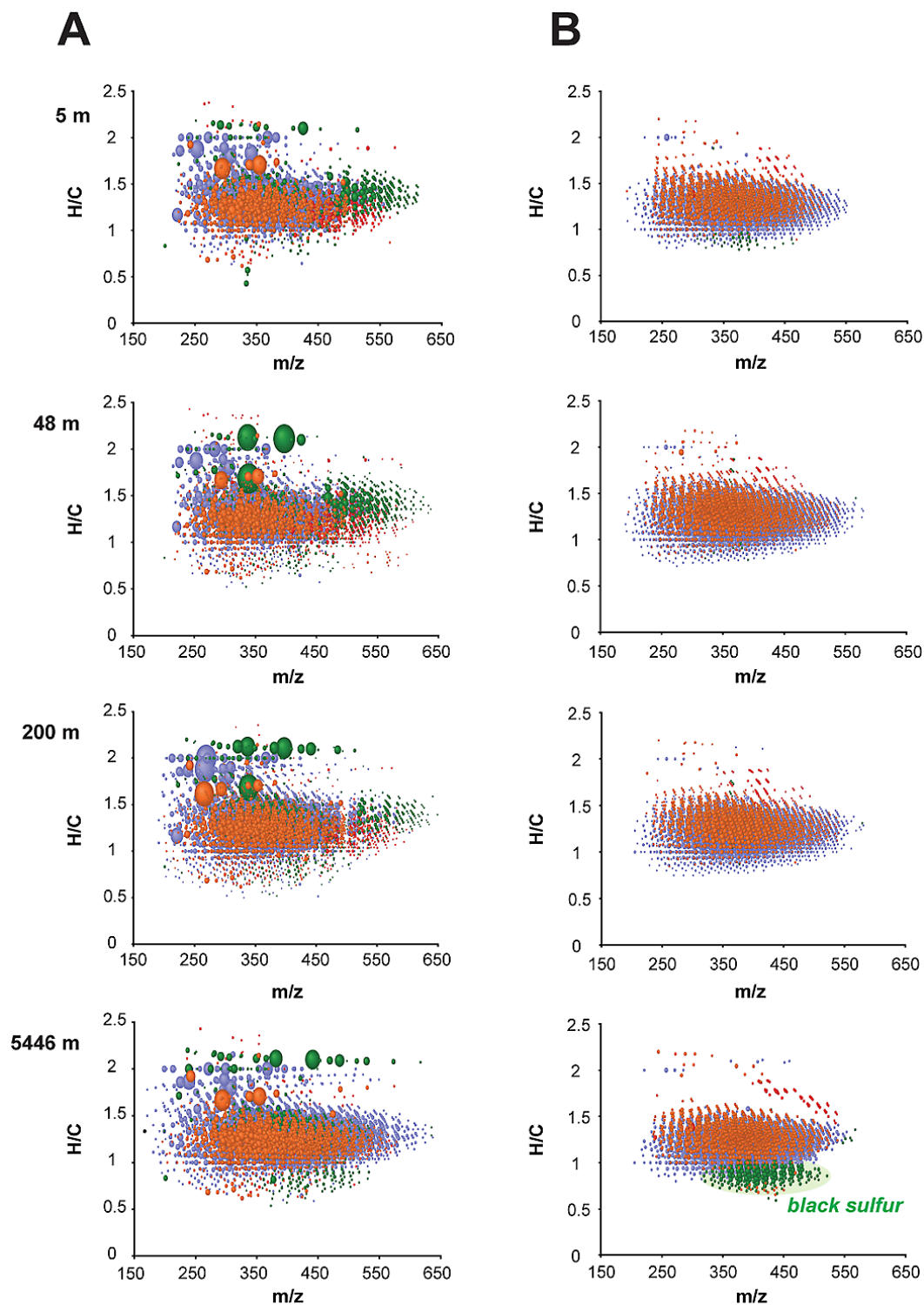
Fig. 16. Mass edited H / C ratios derived from **(A)** negative ESI FTICR mass spectra and **(B)** positive ESI FTICR mass spectra of marine SPE-DOM, assigned in all four marine SPE-DOM to CHO (blue), CHNO (orange), CHOS (green) and CHNOS (red) molecular series. Note the distinct series of aromatic CHOS compounds unique to abyssopelagic marine SPE-DOM at 5446 m which is termed *black sulphur* because of its compositional characteristics (cf. text, Figs. 15 and S8).
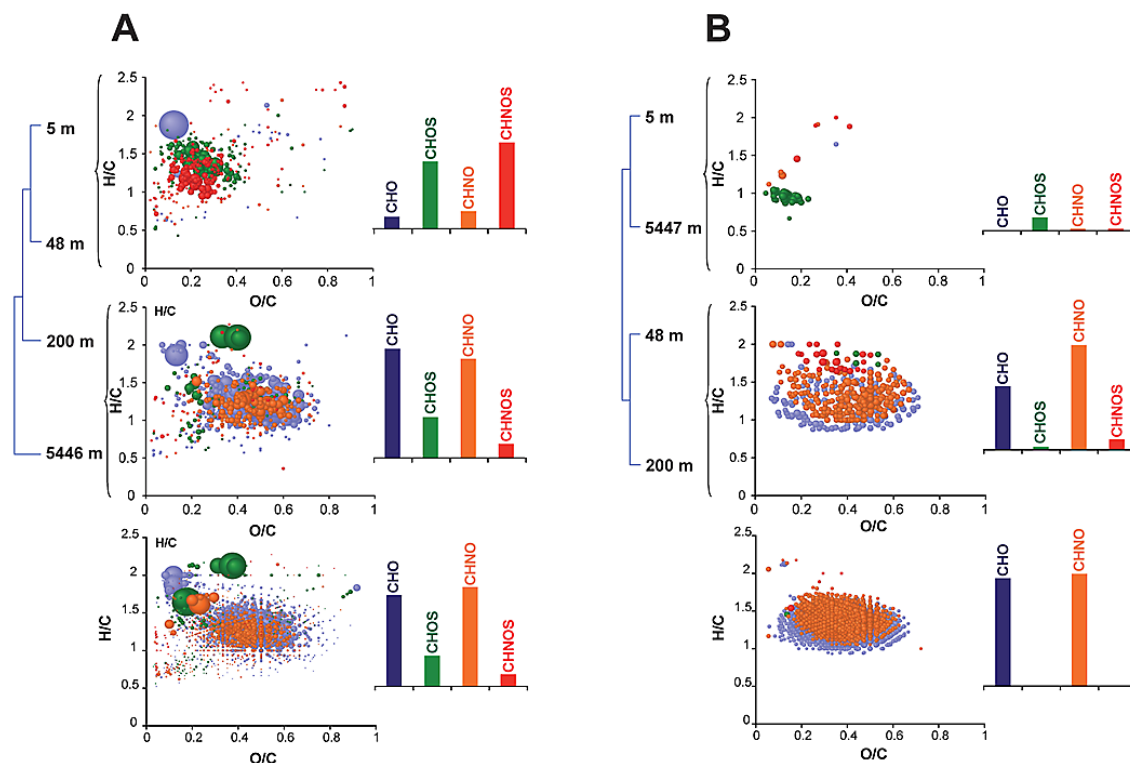
Fig. 17. (A) Negative ESI FTICR mass spectra of marine SPE-DOM; Euclidean clustering diagram based on the similarity values between the merged negative ESI FTICR mass spectra of marine SPE-DOM near surface (5 m, 48 m) and at depth (200 m, 5446 m); circular areas indicate relative mass peak intensity. Top and middle row: van Krevelen diagrams of the unique compositions found in 5 m/48 m SPE-DOM versus 200 m/5446 m SPE-DOM; bottom row: common ions found in negative ESI FTICR mass spectra of all four marine SPE-DOM. **(B)** Positive ESI FTICR mass spectra of marine SPE-DOM; Euclidean clustering diagram based on the similarity values between the merged negative ESI FTICR mass spectra of marine SPE-DOM at extreme depths (5 m, 5446 m) and in between (48 m, 200 m); circular areas indicate relative mass peak intensity. Top and middle row: van Krevelen diagrams of the unique compositions found in 5 m/5446 m SPE-DOM versus 48 m/200 m SPE-DOM; bottom row: common ions found in positive ESI FTICR mass spectra of all four marine SPE-DOM. Note the absence of black sulphur compounds specific to abyssopelagic SPE-DOM at 5446 m (Fig. 16b) in the top row of **(B)** because only unique ions common to both surface and abyssopelagic SPE-DOM are displayed here. Respective right panels: histograms represent relative counts of respective unique and common CHO, CHOS, CHNO and CHNOS molecular series as found in respective van Krevelen diagrams.

1998) under conditions of photochemistry and possibly metal catalysis, assisted by mineral atmospheric deposition (Paytan et al., 2009).

3.13 NMR and FTMS-derived H / C and O / C elemental ratios of marine SPE-DOM

Both NMR and FTICR mass spectra-derived H / C and O / C average elemental ratios of marine SPE-DOM for themselves occupied rather narrow bandwidths with however substantially different positioning (Fig. 19). In relation to elemental ratios derived from NMR spectra, those derived from negative ESI FTICR mass spectra were displaced by +0.3 units in H / C ratio (more saturated) and −0.1 units in O / C ratio (less oxygenated), and those derived from positive ESI FTICR mass spectra were displaced by −0.15 units in H / C ratio (more unsaturated) and −0.4 units in O / C ratio (far less oxygenated).

The proposed NMR-derived mixing model to compute elemental ratios of marine SPE-DOM (Table 3) appeared reasonable and the observed displacement of FTMS derived molecular compositions toward decreased apparent oxidation seemed to contradict the conventional wisdom that electrospray ionization will discriminate in favour of oxygenated compounds relative to, for example, hydrocarbons (Hertkorn et al., 2008). Carbohydrates in marine SPE-DOM, while unambiguously established by NMR signatures, including expansive oxymethylene (OCH$_2$) and anomeric HSQC cross peaks (Figs. 8b and 9), left only very minor signatures in the negative ESI-derived van Krevelen diagrams (none in positive ESI-derived ones), where they should have occupied the section of oxidized ($0.8 < O / C < 1.0$) and fairly saturated ($1.7 < H / C < 2.0$) molecular compositions. Carbohydrates in marine SPE-DOM were supposedly of higher molecular weight (Ohno et al., 2010), corresponding to a lesser volatility and tendency of getting ionized under ESI conditions.
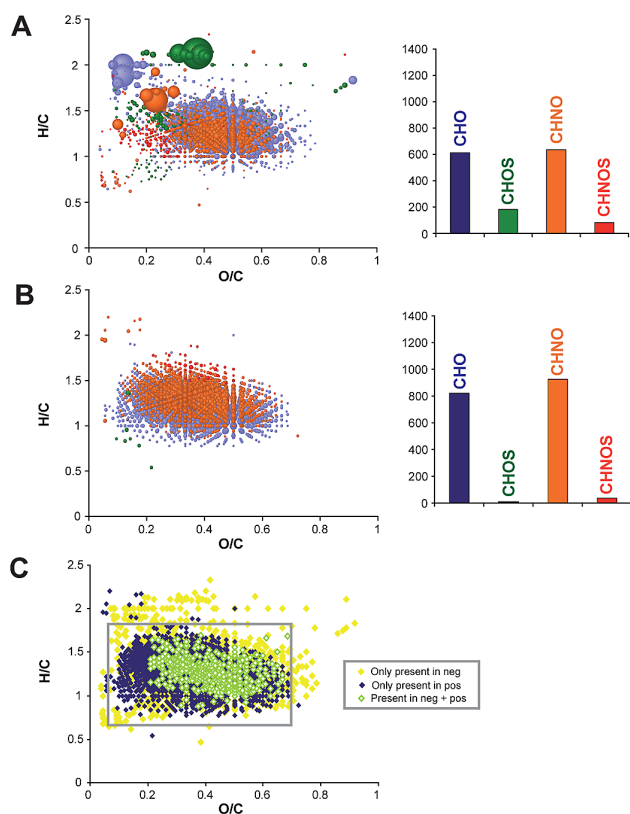
Fig. 18. Van Krevelen diagram derived from consolidated ions observed in all four marine SPE-DOM. **(A)** Common negative ions with (right panel) given counts according to molecular series; **(B)** common positive ions with (right panel) given counts according to molecular series; **(C)** overlay of the respective covered C,H,O-compositional space for consolidated positive (purple) and negative (bright blue) ions from all (CHO, CHNO, CHOS and CHNOS) molecular series.

It could be argued that covalent binding of carbohydrates to other molecules, like peptides (in case of glycoproteins) and lipids (lipopolysaccharides), would have displaced the carbohydrates toward more average H / C and O / C values even if their NMR visible chemical environment would have been preserved. While this might have happened, a faithful representation of all marine SPE-DOM molecules by means of FTICR mass spectra would nevertheless have provided average H / C and O / C ratios in some accordance with NMR data. A displacement of the entire MS-derived compositional space toward lesser O / C ratios seemed to indicate that a sizable fraction of marine SPE-DOM molecules with large O / C ratios were simply not ionized under the employed experimental conditions. Hence, ion suppression was a decisive factor in influencing FTICR mass spectra of the complex marine SPE-DOM fractions. The very pronounced ionization selectivity observed within negative and positive ESI FTICR mass spectra of marine SPE-DOM evidently applies to molecules across the board: in general, oxy-
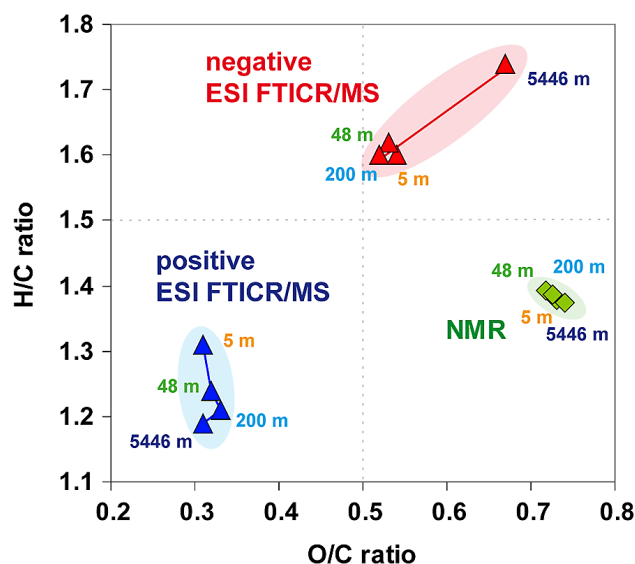

Fig. 19. Average H / C and O / C elemental ratios of marine SPE-DOM as derived from NMR spectroscopy (Table 3), negative ESI (Table 4) and positive ESI (Table 5) FTICR mass spectrometry.

genated SPE-DOM molecules got better ionized in negative ESI mode, whereas unsaturated compounds got better ionized in positive ESI mode. It is conceivable that only a minority of the actually occurring marine SPE-DOM molecules got ionized at all in ESI FTICR mass spectrometry (Hertkorn et al., 2008). Future mass spectrometry studies of marine DOM molecular compositions and structure have to combine several ionization methods, preferentially in conjunction with fractionation, to obtain a realistic depiction of authentic marine DOM molecular complexity.

3.14 The role of metal coordination compounds in the transverse and longitudinal NMR relaxation of marine SPE-DOM

Isolation of marine SPE-DOM imposes less severe chemical alterations than the IHSS-based extraction protocol (International Humic Substances Society). Nevertheless, SPE of marine waters includes an acidification step down to pH ~ 2. Here, metal ions with lesser binding constants to organic matter will be preferentially released from marine DOM during SPE extraction and replaced with protons (Sohrin et al., 2008). Hence, the metals identified in isolated SPE-DOM will not reflect the authentic marine DOM metal composition as found in the ocean (Pohl et al., 2011; Sohrin et al., 2008; Vraspir and Butler, 2009). In addition, isolation of marine SPE-DOM was performed via standard glass bottles without specific care given to metal content (affecting, for example, the quality of Al, B, Na, Si and trace metal analyses). However, large sampling volumes (>50 L of seawater) and concentration factors (Table 1) as well as uniform work-up designed to result in sufficient isolated SPE-DOM for high

quality NMR analyses enabled sensitive metal analyses, too. Hence, determination of metal concentration in SPE-DOM clarified the potential contributions of metal ions to the observed acceleration of transverse NMR relaxation with increasing water depth, which could be twofold. Coordination of SPE-DOM ligands to metal ions will likely reduce molecular mobility of the organic ligands, whereas complexation of SPE-DOM with paramagnetic metal ions (e.g. $Fe^{2/3+}$, Mn^{2+}, $Cu^{+/2+}$) will transfer electron spin density to ligand atoms, which often causes "bleaching" of NMR resonances (Smernik and Oades, 2002; Turano et al., 2010; Bertini et al., 2008; Kleckner and Foster, 2011).

No uniform trends of metal content from surface to deep marine SPE-DOM were identified in the four marine SPE-DOM: some metals were found with a near-uniform distribution throughout the SPE-DOM, whereas others were enriched at depth (Fig. 20; Table S5). Metals associated with life functions (micronutrients for organisms such as Ca, Co, Cu, Fe, K, Mg, Mn, Mo, P, V, Zn) have commonly not been found enriched in the two surface SPE-DOM (5 m and 48 m), which supposedly reflect enhanced proportions of biological activity. Otherwise, thorium, phosphorus and sulfur declined from surface to depth in line with common distribution in marine SPE-DOM. Phosphorus and sulfur attached to SPE-DOM in the form of phosphate and sulfate would increase molecular weight and size, and perhaps attenuate molecular mobility, without clear ^{1}H and ^{13}C NMR signature in the complex SPE-DOM mixture. Near-uniform distribution throughout all SPE-DOM was found for Al, As, Cr, Mo, Sr and Zn. The considerable deviation of the metal / SPE-DOM ratio in comparison with common oceanic metal distribution at various water depths probably indicated variance in metal speciation in the different SPE-DOM, which could have been either related to chemical specificity and/or molecular size selectivity (Pohl et al., 2011; Takeda et al., 2009). Indications for any substantial leaching of metal ions from the bottom sediment were absent; the marginally increased metal concentrations at the abyssopelagic SPE-DOM (5446 m) found for the ions of Ca, Cd, Mg and Zn were considered insignificant in this respect.

In the context of NMR relaxation, the most important ion to assess NMR behaviour was iron (Fe), a paramagnetic and strongly complexing metal (Witter et al., 2000) for which a large contribution for accelerating transverse NMR relaxation could be expected. Remarkably, Fe was found notably enriched in the surface SPE-DOM at 5 m, which nevertheless displayed well resolved NMR spectra (e.g. COSY, cf. Figs. 6 and S5a). Other paramagnetic 3d metals, like V, Cr, Mn, Co and Ni, as well as Cu, were more uniformly distributed and much less abundant than Fe; the abundance of Ni, the second most abundant metal of this series, also declined significantly from surface to deep SPE-DOM (Fig. 20, Table S5). Hence, the acceleration of transverse NMR relaxation from surface to deep SPE-DOM was not primarily caused by metal content of SPE-DOM.

3.15 Molecular detail of marine SPE-DOM as derived from non-target organic structural spectroscopy

Non-target high resolution organic structural spectroscopy (high-field FTICR mass spectrometry and NMR spectroscopy) enabled molecular level characterization of marine SPE-DOM, selected to represent open ocean waters of global significance, with extraordinary coverage of marine organic proton, carbon and heteroatom chemical environments.

The two overwhelmingly present molecular motifs of marine SPE-DOM were extensive aliphatic branching near the statistical limits of molecular diversity and a distinctive average proximity of sp^3-hybridized (hydro)carbon units ($C_n\underline{C}H_{4-n}$; $n = 1$–3) to carbonyl derivatives COX in carboxyl-rich alicyclic molecules (CRAM), suggesting a prevalent alicyclic geometry.

The variance in molecular diversity of the four selected marine SPE-DOM was remarkable for itself and has not been demonstrated before at this level of detail. When scaled to equal total NMR integral, proton NMR spectra showed up to 20 % variance in abundance of major substructures. Hence, quantitative high-field proton NMR spectra with excellent resolution and S / N ratio can be used for future mathematical classification of marine SPE-DOM in comparative studies, even on a large scale. This is remarkable considering the massive intrinsic averaging in one-dimensional NMR spectra, in which a large number of atomic environments project on any single NMR data point, producing smooth bulk NMR envelopes with only a few percent of visibly resolved signatures. The abundance of singly oxygenated aliphatics and acetate derivatives declined from surface to deep marine SPE-DOM, whereas C-based aliphatics and CRAM increased in abundance. Surface marine SPE-DOM contained fewer methyl esters than all other marine SPE-DOM, likely a consequence of photodegradation from direct exposure to sunlight. COSY NMR spectra determined relative concentrations of several hundreds to low thousands of different molecules in a single measurement. Accordingly, COSY NMR spectra represent the most significant molecular classification tool of marine SPE-DOM with respect to structural detail and significance available at present.

All marine SPE-DOM showed similar overall ^{13}C NMR resonance envelopes typical of an intricate mixture of natural organic matter with noticeable peaks of anomeric and aromatic carbon, whereas oxygenated aromatics and ketones were of too low abundance to generate noticeable signals. ^{13}C NMR spectra revealed a continual increase of carboxylic acids and ketones from surface to depth, reflecting a progressive oxygenation of sp^2-hybridized carbon, with a concomitant decline of aliphatic OCH$_n$ substructures. The most significant NMR visible chemical environment representing aliphatic branching is a $C_3\underline{C}H$ methine carbon, followed by a $C_2\underline{C}H_2$ methylene carbon. The fraction of $C_3\underline{C}H$-methine carbon (referred to all methine carbon) continually increased from surface marine SPE-DOM
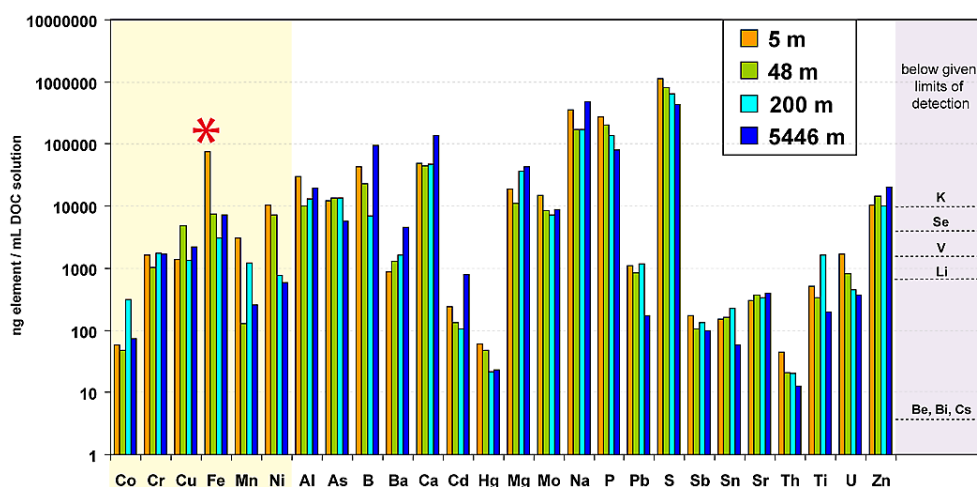
Fig. 20. Content of metals/elements in methanolic SPE-DOM solutions to assess metal contribution to NMR relaxation (note logarithmic display of concentration), yellow: significant metals capable of forming paramagnetic coordination compounds with marine SPE-DOM, with iron (Fe) in surface SPE-DOM at 5 m as the most abundant (asterisk; cf. text); purple background: elements Be, Bi, Cs, K, Li, Se and V were found below detection limits indicated (cf. Table S5).

(45.7 %) to abyssopelagic SPE-DOM (56.7 %). The continually increased proportion of $C_2\underline{C}H_2$-methylene (referred to all methylene carbon) from surface (85 %) to abyssopelagic SPE-DOM (97 %) possibly reflected a partial cumulative deoxygenation of aliphatics as well. COX directly bound to methylene carbon which only can be attached but not incorporated into alicyclic rings appeared indeed a major structural unit of CRAM, possibly covering near half of all $C_2\underline{C}H_2$ methylene units. JRES NMR spectra showed a pronounced alteration of aliphatic cross-peak patterns related to aliphatic branching in lipids: signatures of poly-CH_2-type lipids in abyssopelagic marine SPE-DOM, which supposedly are more susceptible to biodegradation, might indicate sediment leaching of microbial metabolites. The huge diversity of methyl chemical environments extended to $\underline{H_3}\underline{C}$-$C_n$ ($n \geq 1$) and $\underline{H_3}\underline{C}$-$C\underline{H}$-O- units as well; the latter likely indicated presence of a large suite of modified methylated carbohydrates.

All marine SPE-DOM investigated exhibited more abundant olefinic than aromatic sp^2-hybridized carbon. Benzene derivatives were largely attributed to singly and multiply carboxylated species with indications of polycyclic aromatic hydrocarbons, suggesting the presence of thermogenic organic matter (TMOC) at all water depths. A suite of closely related six-membered nitrogen heterocycles with more than one nitrogen occurred in all samples whereas furan, pyrrol and thiophene derivatives were marginal contributors.

The abundance of carbohydrates in marine SPE-DOM was lower than in marine organic matter isolated by ultrafiltration (UF-DOM) and reverse osmosis/electrodialysis (ROED-DOM). The chemical diversity of carbohydrates present in marine SPE-DOM exceeded that found in soil and freshwater organic matter: diversity of anomeric methine indicated the presence of α/β-pyranoses and α/β-furanoses.

With the exception of SPE-DOM at 48 m (fluorescence maximum), in which abundant biosignatures prevail, a general loss of NMR signature and cross-peak integral from surface to deep marine SPE-DOM was observed in all 2-D NMR spectra. Loss of NMR signature can originate from accelerated transverse NMR relaxation, which may result from larger molecular size (either intrinsic of purely organic molecules or initiated by formation of metal coordination compounds and other non-covalent interaction). Straightforward relationships between metal content of isolated SPE-DOM or mass peak distribution and transverse NMR relaxation could not been retrieved. Entropy gain from ever growing molecular diversity of marine SPE-DOM with increasing depth also leaves less disposable NMR signal amplitude for any given chemical environment resulting in an apparent loss of S / N ratio. Progressive disappearance of (NMR) signature patterns will make discrimination of complex mixtures ever more difficult and may be mistaken as an apparent recalcitrance of marine organic matter. Eventually, discrimination capacity for extremely complex supermixtures has to be restored by combination of analytical methods such as separation and organic structural spectroscopy.

In agreement with NMR, FTICR mass spectra showed abundant CHO, CHNO, CHOS and CHNOS molecular series with slightly increasing numbers of mass peaks and average mass from surface to bottom SPE-DOM. CHOS and especially CHNOS negative ions markedly declined. While certain rather aliphatic CHOS and CHNOS compounds were observed solely in surface SPE-DOM, deep marine SPE-DOM was enriched in unique unsaturated and rather oxygenated CHO and CHNO negative ions. With

the exception of abyssopelagic SPE-DOM at 5446 m which showed a peculiar CHOS chemistry of unsaturated carbon and reduced sulphur (black sulphur), CHO and CHNO ions contributed $\sim 87\%$ to total positive electrospray ionization FTICR mass peak integral, with a near-constant ratio of CHNO/CHO molecular compositions near 1.13 ± 0.05. Positive ESI FTICR mass spectra of all marine SPE-DOM showed a larger regularity of CHO and CHNO molecular series than negative ESI FTICR mass spectra.

In essence, resemblance according to NMR and FTMS signatures was most pronounced in-between the two near-surface as well as in-between the two deep sea SPE-DOM, whereas a few unique SPE-DOM signatures in NMR spectra and CHOS chemistry in FTICR mass spectra were found only near the ocean bottom. Oxygenated SPE-DOM molecules were better ionized in negative ESI mode, whereas unsaturated compounds were better ionized in positive ESI mode.

The conformity of key NMR and FTICR/MS signatures in all four marine SPE-DOM suggested the presence of a numerous set of identical molecules throughout the entire ocean column even if the investigated water masses belonged to different oceanic regimes and currents.

4 Conclusions

This study has demonstrated the utility of modern non-target organic structural spectroscopy for the molecular level characterization of solid-phase extracted marine organic matter (SPE-DOM). For example, an extensive NMR study is the only conceivable means to detect the excess abundance of olefinic over aromatic unsaturation in marine SPE-DOM for both proton and carbon chemical environments, which offers novel opportunities for the traceability of the biogeochemical heritage of the oceans.

Marine SPE-DOM comprises molecular features which lead to slow transverse NMR relaxation, likely associated with its marginal metal content and near absence of very large molecules capable of strong interactions with solutes (like carbohydrate-rich marine gels). Slow transverse NMR relaxation is indispensable for the acquisition of highly resolved 2-D NMR spectra. High-field NMR spectroscopy of marine SPE-DOM with cryogenic detection revealed structural (chemical) features of marine SPE-DOM with unsurpassed resolution and sensitivity, however alongside with physical characteristics such as symmetry weighted atom mobilities. Accordingly, these interdependent chemical and physical features have to be recognized in the evaluation of further high-field NMR studies of marine DOM. NMR studies of marine SPE-DOM at different magnetic field strengths B_0 will improve our understanding of NMR relaxation in these complex mixtures (Korzhnev et al., 2004).

While the chemoselectivity of PPL/SPE extraction of marine waters is acknowledged, it will nevertheless act unidi-

rectional on marine waters which all share a DOC/salt ratio of about 1 : 35 000 in mass. Using isolated marine SPE-DOM in conjunction with non-target NMR and FTMS characterization offers the key advantages of a fairly representative marine DOM investigated with exceptional molecular resolution allowing a far reaching description of molecular skeleton and functional groups. While covering the majority of carbon already in the proposed form, this approach is expandable to include advanced ^{15}N NMR and ^{31}P NMR characterization of marine SPE-DOM as well.

In summary, quantitative ^{1}H NMR spectroscopy and ^{1}H,^{1}H COSY NMR spectra appear as the most suitable tools to perform comparative molecular level classification of marine SPE-DOM. While the positions of relative intensity minima and maxima in ^{1}H NMR spectra will often resemble each other, their relative amplitudes will nevertheless vary considerably, allowing structure-selective discrimination of the biogeochemical heritage of the marine water bodies. Relative alterations of major substructure ^{1}H NMR amplitudes in this study were in the 20 % range, a quite substantial variance considering the massive mandatory intrinsic averaging from NMR resonance overlap. ^{1}H,^{1}H COSY NMR spectra of marine SPE-DOM offer the best combination of sensitivity and resolution for comparative pattern recognition studies, whereas the more sensitive ^{1}H,^{1}H TOCSY NMR spectra of marine SPE-DOM produce contiguous aggregated cross peaks with lower usable resolution.

It is noteworthy that the current scientific evaluation of organic molecular complexity rather refers to aspects of biological/biochemical mixtures in which clearly resolved patterns (and their alterations) are readily observed. Any analytical data obtained from characterization of the vastly more complex biogeochemical mixtures are subject to far more extensive intrinsic averaging and necessarily produce less resolved signatures. Even the exceptional mass peak resolution of high-field FTICR mass spectrometry is deceptive, because the ultimate resolution of the C,H,O-compositional space is readily observed in high quality FTICR mass spectra of any DOM (Hertkorn et al., 2008). Here, any single mass peak in FTICR mass spectra of marine SPE-DOM will likely represent thousands of isomers irrespective of the ionization method used.

A mass shift $\Delta m \geq 10 m/z$ for the intensity weighted average of SPE-DOM mass peaks from surface to deep waters across a bandwidth of m/z: 150–800 as observed in negative and positive ESI FTICR mass spectra had to overcome this massive intrinsic averaging and should not be considered insignificant. In an analogy, mass peaks can be thought to represent age groups within a nation's entire population (with any person contributing an equal intensity increment), and mass spectra will represent the age distribution. Then, the observed displacement Δm might be compared with an extension of the individual-related average life-span within a nation's entire population by more than one year. Because Δm and compositional/structural similarity are inversely related,

any MS displacement will represent major structural changes (Hertkorn et al., 2008).

Future non-target molecular DOM characterization by means of NMR and FTICR mass spectrometry will employ full-scale NMR characterization of intact marine DOM in conjunction with fractionation to further resolve this intricate mixture (Gaspar et al., 2010). Then, also FTICR mass spectra will suffer less from intrinsic averaging because lesser numbers of isomeric molecules will be projected onto individual mass peaks (Stenson, 2008). Individual adjustment of NMR acquisition parameters for DOM fractions and comparison of standardized NMR measurements with an educated data base search (Woods et al., 2011, 2012) will enable the resolution, identification and quantification of hundreds to eventually several thousands of individual marine DOM molecules. Finally, the faithful depiction of marine DOM organic complexity will enable a clear perception of oceanic contributions to the global carbon and other element cycles.

As observed in this special issue, unsupervised hierarchical cluster analysis of pigment composition, absorption coefficients and remote sensing reflectance has provided biooptical regimes in the Atlantic Ocean which well correlated with previously established Longhurst biogeographical provinces (Friedline et al., 2012). Furthermore, surface eubacterial communities as deduced from sequencing studies commonly displayed a fair general congruency with the same ecological provinces (Taylor et al., 2011). These significant findings at comparatively low molecular resolution let us anticipate that high-quality molecular level characteristics will carry a wealth of very specific information about the holistic biogeographical heritage of the oceans. Future in-depth functional biodiversity studies with a clear understanding of DOM structure and function might eventually lead to a new level of unified perception of biodiversity and biogeochemistry.

Supplementary material related to this article is available online at: http://www.biogeosciences.net/10/ 1583/2013/bg-10-1583-2013-supplement.pdf.

References

Aihara, J. I., Sekine, R., and Ishida, T.: Electronic and magnetic characteristics of polycyclic aromatic hydrocarbons with factorizable Kekulé structure counts, J. Phys. Chem. A., 115, 9314–9321, 2011.

Aluwihare, L. I., Repeta, D. J., and Chen, R. F.: Chemical composition and cycling of dissolved organic matter in the mid-atlantic bight, Deep-Sea Res. Pt. II, 49, 4421–4437, 2002.

Amrani, A., Turner, J. W., Ma, Q. S., Tang, Y. C., and Hatcher, P. G.: Formation of sulfur and nitrogen cross-linked macromolecules under aqueous conditions, Geochim. Cosmochim. Ac., 71, 4141–4160, 2007.

Andreae, M. O. and Crutzen, P. J.: Atmospheric aerosols: Biogeochemical sources and role in atmospheric chemistry, Science, 276, 1052-1058, 1997.

Battin, T. J., Luyssaert, S., Kaplan, L. A., Aufdenkampe, A. K., Richter, A., and Tranvik, L. J.: The boundless carbon cycle, Nat. Geosci., 2, 598–600, 2009.

Bauschlicher, C. W., Peeters, E., and Allamandola, L. J.: The infrared spectra of very large irregular polycyclic aromatic hydrocarbons (PAHs): Observational probes of astronomical pah geometry, size, and charge, Astrophys. J., 697, 311–327, 2009.

Benner, R.: Chemical composition and reactivity, in: Biogeochemistry of marine dissolved organic matter, edited by: Hansell, D. A. and Carlson, C. A., Academic Press, 59–90, 2002.

Bertini, I., Luchinat, C., Parigi, G., and Pierattelli, R.: Perspectives in paramagnetic NMR of metalloproteins, Dalton T., 2008, 3782–3790, 2008.

Blunt, J. W., Copp, B. R., Munro, M. H. G., Northcote, P. T., and Prinsep, M. R.: Marine natural products, Nat. Prod. Rep., 27, 165–237, 2010.

Buddrus, J., Burba, P., Lambert, J., and Herzog, H.: Quantification of partial structures of aquatic humic substances by one- and two-dimensional solution ^{13}C nuclear magnetic resonance spectroscopy, Anal. Chem., 61, 628–631, 1989.

Burdige, D. J., Berelson, W. M., Coale, K. H., McManus, J., and Johnson, K. S.: Fluxes of dissolved organic carbon from California continental margin sediments, Geochim. Cosmochim. Ac., 63, 1507–1515, 1999.

Cane, D. E. and Ikeda, H.: Exploration and mining of the bacterial terpenome, Acc. Chem. Res., 45, 463–472, 2011.

Carlson, C. A., Del Giorgio, P. A., and Herndl, G. J.: Microbes and the Dissipation of Energy and Respiration: From Cells to Ecosystems, Oceanography, 20, 89–100, 2007.

Cavanagh, J., Fairbrother, W. J., Palmer III, A. G., Rance, M., and Skelton, N. J.: Protein NMR Spectroscopy, Elsevier, Burlington, USA, 2007.

Cheng, C. H., Lehmann, J., Thies, J. E., Burton, S. D., and Engelhard, M. H.: Oxidation of black carbon by biotic and abiotic processes, Org. Geochem., 37, 1477–1488, 2006.

Cho, Y., Kim, Y. H., and Kim, S.: Planar limit-assisted structural interpretation of saturates/aromatics/resins/asphaltenes fractionated crude oil compounds observed by fourier transform ion cyclotron resonance mass spectrometry, Anal. Chem., 83, 6068–6073, 2011.

Coble, P. G.: Marine optical biogeochemistry: The chemistry of ocean color, Chem. Rev., 107, 402–418, 2007.

Crouch, R. C., Llanos, W., Mehr, K. G., Hadden, C. E., Russell, D. J., and Martin, G. E.: Applications of cryogenic NMR probe

technology to long-range ^{1}H-^{15}N 2-D NMR studies at natural abundance, Magn. Reson. Chem., 39, 555–558, 2001.

Del Giorgio, P. A., Cole, J. J., and Cimbleris, A.: Respiration rates in bacteria exceed phytoplankton production in unproductive aquatic systems, Nature, 385, 148–151, 1997.

Dickens, A. F., Gelinas, Y., Masiello, C. A., Wakeham, S., and Hedges, J. I.: Reburial of fossil organic carbon in marine sediments, Nature, 427, 336–339, 2004.

Dittmar, T. and Kattner, G.: Recalcitrant dissolved organic matter in the ocean: Major contribution of small amphiphilics, Mar. Chem., 82, 115–123, 2003a.

Dittmar, T. and Kattner, G.: The biogeochemistry of the river and shelf ecosystem of the arctic ocean: A review, Mar. Chem., 83, 103–120, 2003b.

Dittmar, T. and Koch, B. P.: Thermogenic organic matter dissolved in the abyssal ocean, Mar. Chem., 102, 208–217, 2006.

Dittmar, T. and Paeng, J.: A heat-induced molecular signature in marine dissolved organic matter, Nat. Geosci., 2, 175–179, 2009.

Dittmar, T., Koch, B., Hertkorn, N., and Kattner, G.: A simple and efficient method for the solid-phase extraction of dissolved organic matter (spe-DOM) from seawater, Limnol. Oceanogr.-Meth., 6, 230–235, 2008.

Dittmar, T., Rezende, C. E., Manecki, M., Niggemann, J., Ovalle, A. R. C., and Bernardes, M. C.: Continuous flux of dissolved black carbon from a vanished tropical forest biome, Nat. Geosci., 5, 618–622, 2012.

Einsiedl, F., Hertkorn, N., Wolf, M., Frommberger, M., Schmitt-Kopplin, P., and Koch, B. P.: Rapid biotic molecular transformation of fulvic acids in a karst aquifer, Geochim. Cosmochim. Ac., 71, 5474–5482, 2007.

Falco, C., Caballero, F. P., Babonneau, F., Gervais, C., Laurent, G., Titirici, M.-M., and Baccile, N.: Hydrothermal Carbon from Biomass: Structural Differences between Hydrothermal and Pyrolyzed Carbons via Solid State NMR, Langmuir, 27, 14460–14471, 2011.

Flerus, R., Koch, B. P., Schmitt-Kopplin, P., Witt, M., and Kattner, G.: Molecular level investigation of reactions between dissolved organic matter and extraction solvents using FT-ICR MS, Mar. Chem., 124, 100–107, 2011.

Flerus, R., Lechtenfeld, O. J., Koch, B. P., McCallister, S. L., Schmitt-Kopplin, P., Benner, R., Kaiser, K., and Kattner, G.: A molecular perspective on the ageing of marine dissolved organic matter, Biogeosciences, 9, 1935–1955, doi:10.5194/bg-9-1935-2012, 2012.

Friedline, C. J., Franklin, R. B., McCallister, S. L., and Rivera, M. C.: Bacterial assemblages of the eastern Atlantic Ocean reveal both vertical and latitudinal biogeographic signatures, Biogeosciences, 9, 2177–2193, doi:10.5194/bg-9-2177-2012, 2012.

Gaspar, A., Harir, M., Hertkorn, N., and Schmitt-Kopplin, P.: Preparative free-flow electrophoretic offline ESI-Fourier transform ion cyclotron resonance/MS analysis of Suwannee River fulvic acid, Electrophoresis, 31, 2070–2079, 2010.

Geider, R. J., Delucia, E. H., Falkowski, P. G., Finzi, A. C., Grime, J. P., Grace, J., Kana, T. M., La Roche, J., Long, S. P., Osborne, B. A., Platt, T., Prentice, I. C., Raven, J. A., Schlesinger, W. H., Smetacek, V., Stuart, V., Sathyendranath, S., Thomas, R. B., Vogelmann, T. C., Williams, P., and Woodward, I. F.: Primary Productivity of Planet Earth: Biological Determinants and Physical Constraints in Terrestrial and Aquatic Habitats, Glob. Change

Biol., 7, 849–882, 2001.

Gilbert, J. A., Steele, J. A., Caporaso, J. G., Steinbrück, L., Reeder, J., Temperton, B., Huse, S., McHardy, A. C., Knight, R., Joint, I., Somerfield, P., Fuhrman, J. A., and Field, D.: Defining seasonal marine microbial community dynamics, ISME J., 6, 298–308, 2012.

Graeve, M. and Janssen, D.: Improved separation and quantification of neutral and polar lipid classes by HPLC-ELSD using a monolithic silica phase: Application to exceptional marine lipids, J. Chromatogr. B., 877, 1815–1819, 2009.

Hansell, D. A.: Dissolved organic matter in the ocean, Oceanography, 22, 202–211, 2009.

Hansell, D. A.: Recalcitrant Dissolved Organic Carbon Fractions, Annu. Rev. Mar. Sci., 5, 421–445, doi:10.1146/annurev-marine-120710-100757, 2013.

Hansell, D. A. and Carlson, C. A.: Deep-ocean gradients in the concentration of dissolved organic carbon, Nature, 395, 263–266, 1998.

Hansen, P. E.: ^{13}C NMR of Polycyclic Aromatic Compounds. A Review, Org. Magn. Reson., 12, 109–142, 1979.

Hansman, R. L., Griffin, S., Watson, J. T., Druffel, E. R. M., Ingalls, A. E., Pearson, A., Aluwihare, L. I.: The radiocarbon signature of microorganisms in the mesopelagic ocean, P. Natl. Acad. Sci. USA, 106, 6513–6518, 2009.

Hebting, Y., Schaeffer, P., Behrens, A., Adam, P., Schmitt, G., Schneckenburger, P., Bernasconi, S. M., and Albrecht, P.: Biomarker evidence for a major preservation pathway of sedimentary organic carbon, Science, 312, 1627–1631, 2006.

Hedges, J. I.: Global biogeochemical cycles: progress and problems, Org. Geochem., 39, 67–93, 1992.

Hedges, J. I. and Oades, J. M.: Comparative organic geochemistries of soils and marine sediments, Org. Geochem., 27, 319–361, 1997.

Hedges, J. I., Baldock, J. A., Gelinas, Y., Lee, C., Peterson, M., and Wakeham, S. G.: Evidence for non-selective preservation of organic matter in sinking marine particles, Nature, 409, 801–804, 2001.

Hedges, J. I., Baldock, J. A., Gelinas, Y., Lee, C., Peterson, M. L., and Wakeham, S. G.: The biochemical and elemental compositions of marine plankton: A NMR perspective, Mar. Chem., 78, 47–63, 2002.

Hernes, P. J. and Benner, R.: Photochemical and microbial degradation of dissolved lignin phenols: Implications for the fate of terrigenous dissolved organic matter in marine environments, J. Geophys. Res., 108, 3291, doi:10.1029/2002JC001421, 2003.

Hernes, P. J. and Benner, R.: Terrigenous organic matter sources and reactivity in the North Atlantic Ocean and a comparison to the Arctic and Pacific Oceans, Mar. Chem., 100, 66–79, 2006.

Hertkorn, N. and Kettrup, A.: Molecular level structural analysis of natural organic matter and of humic substances by multinuclear and higher dimensional NMR spectroscopy, in: Use of humic substances to remediate polluted environments: From theory to practice, edited by: Perminova, I., Hatfield, K., and Hertkorn, N., Springer Netherlands, 391–435, 2005.

Hertkorn, N., Benner, R., Frommberger, M., Schmitt-Kopplin, P., Witt, M., Kaiser, K., Kettrup, A., and Hedges, J. I.: Characterization of a major refractory component of marine dissolved organic matter, Geochim. Cosmochim. Ac., 70, 2990–3010, 2006.

Hertkorn, N., Ruecker, C., Meringer, M., Gugisch, R., Fromm-berger, M., Perdue, E. M., Witt, M., and Schmitt-Kopplin, P.: High-precision frequency measurements: Indispensable tools at the core of the molecular-level analysis of complex systems, Anal. Bioanal. Chem., 389, 1311–1327, 2007.

Hertkorn, N., Frommberger, M., Witt, M., Koch, B. P., Schmitt-Kopplin, P., and Perdue, E. M.: Natural organic matter and the event horizon of mass spectrometry, Anal. Chem., 80, 8908–8919, 2008.

Hockaday, W. C., Grannas, A. M., Kim, S., and Hatcher, P. G.: Direct molecular evidence for the degradation and mobility of black carbon in soils from ultrahigh-resolution mass spectral analysis of dissolved organic matter from a fire-impacted forest soil, Org. Geochem., 37, 501–510, 2006.

Hopkinson, C. S. and Vallino, J. J.: Efficient export of carbon to the deep ocean through dissolved organic matter, Nature, 433, 142–145, 2005.

Jiao, N., Herndl, G. J., Hansell, D. A., Benner, R., Kattner, G., Wilhelm, S. W., Kirchman, D. L., Weinbauer, M. G., Luo, T. W., Chen, F., and Azam, F.: Microbial production of recalcitrant dissolved organic matter: Long-term carbon storage in the global ocean, Nat. Rev. Microbiol., 8, 593–599, 2010.

Jimenez, J. L., Canagaratna, M. R., Donahue, N. M., Prevot, A. S. H., Zhang, Q., Kroll, J. H., DeCarlo, P. F., Allan, J. D., Coe, H., Ng, N. L., Aiken, A. C., Docherty, K. S., Ulbrich, I. M., Grieshop, A. P., Robinson, A. L., Duplissy, J., Smith, J. D., Wilson, K. R., Lanz, V. A., Hueglin, C., Sun, Y. L., Tian, J., Laaksonen, A., Raatikainen, T., Rautiainen, J., Vaattovaara, P., Ehn, M., Kulmala, M., Tomlinson, J. M., Collins, D. R., Cubison, M. J., Dunlea, E. J., Huffman, J. A., Onasch, T. B., Alfarra, M. R., Williams, P. I., Bower, K., Kondo, Y., Schneider, J., Drewnick, F., Borrmann, S., Weimer, S., Demerjian, K., Salcedo, D., Cottrell, L., Griffin, R., Takami, A., Miyoshi, T., Hatakeyama, S., Shimono, A., Sun, J. Y., Zhang, Y. M., Dzepina, K., Kimmel, J. R., Sueper, D., Jayne, J. T., Herndon, S. C., Trimborn, A. M., Williams, L. R., Wood, E. C., Middlebrook, A. M., Kolb, C. E., Baltensperger, U., and Worsnop, D. R.: Evolution of organic aerosols in the atmosphere, Science, 326, 1525–1529, 2009.

Kaiser, E., Simpson, A. J., Dria, K. J., Sulzberger, B., and Hatcher, P. G.: Solid-state and multidimensional solution-state NMR of solid phase extracted and ultrafiltered riverine dissolved organic matter, Environ. Sci. Technol., 37, 2929–2935, 2003.

Kaiser, K. and Benner, R.: Organic matter transformations in the upper mesopelagic zone of the North Pacific: Chemical composition and linkages to microbial community structure, J. Geophys. Res., 117, C01023, doi:10.1029/2011JC007141, 2012.

Kelleher, B. P. and Simpson, A. J.: Humic substances in soils: Are they really chemically distinct?, Environ. Sci. Technol., 40, 4605–4611, 2006.

Kleckner, I. R. and Foster, M. P.: An introduction to NMR-based approaches for measuring protein dynamics, BBA-Proteins Proteom., 1814, 942–968, 2011.

Knicker, H.: "Black nitrogen" – an important fraction in determining the recalcitrance of charcoal, Org. Geochem., 41, 947–950, 2010.

Koch, B. P. and Dittmar, T.: From mass to structure: An aromaticity index for high-resolution mass data of natural organic matter, Rapid. Commun. Mass. Sp., 20, 926–932, 2006.

Koch, B. P. and Kattner, G.: Sources and rapid biogeochemical transformation of dissolved organic matter in the Atlantic surface ocean, Biogeosciences, 9, 2597–2602, doi:10.5194/bg-9-2597-2012, 2012.

Koch, B. P., Witt, M. R., Engbrodt, R., Dittmar, T., and Kattner, G.: Molecular formulae of marine and terrigenous dissolved organic matter detected by electrospray ionization fourier transform ion cyclotron resonance mass spectrometry, Geochim. Cosmochim. Ac., 69, 3299–3308, 2005.

Kok, M. D, Schouten, S., and Sinninghe Damsté, J. S.: Formation of insoluble, nonhydrolyzable, sulfur-rich macromolecules via incorporation of inorganic sulphur species into algal carbohydrates, Geochim. Cosmochim. Ac., 15, 2689–2699, 2000.

Koprivnjak, J. F., Pfromm, P. H., Ingall, E., Vetter, T. A., Schmitt-Kopplin, P., Hertkorn, N., Frommberger, M., Knicker, H., and Perdue, E. M.: Chemical and spectroscopic characterization of marine dissolved organic matter isolated using coupled reverse osmosis-electrodialysis, Geochim. Cosmochim. Ac., 73, 4215–4231, 2009.

Korzhnev, D. M., Salvatella, X., Vendruscolo, M., Di Nardo, A. A., Davidson, A. R., Dobson, C. M., and Kay, L. E.: Low-populated folding intermediates of Fyn SH3 characterized by relaxation dispersion NMR, Nature, 430, 586–590, 2004.

Kovalevskii, D. V., Permin, A. B., Perminova, I. V., and Petrosyan, V. S.: Recovery of conditions for quantitative measuring the NMR spectra of humic acids, Vestn. Mosk. U. Khim., 41, 39–42, 2000.

Kroll, J. H., Donahue, N. M., Jimenez, J. L., Kessler, S. H., Canagaratna, M. R., Wilson, K. R., Altieri, K. E., Mazzoleni, L. R., Wozniak, A. S., Bluhm, H., Mysak, E. R., Smith, J. D., Kolb, C. E., and Worsnop, D. R.: Carbon oxidation state as a metric for describing the chemistry of atmospheric organic aerosol, Nat. Chem., 3, 133–139, 2011.

Kujawinski, E. B.: Electrospray ionization fourier transform ion cyclotron resonance mass spectrometry (ESI FT-ICR MS): Characterization of complex environmental mixtures, Environ. Forensics, 3, 207–216, 2002.

Kujawinski, E. B.: The Impact of Microbial Metabolism on Marine Dissolved Organic Matter, Annu. Rev. Mar. Sci., 3, 567–599, 2011.

Kujawinski, E. B., Longnecker, K., Blough, N. V., Del Vecchio, R., Finlay, L., Kitner, J. B., and Giovannoni, S. J.: Identification of possible source markers in marine dissolved organic matter using ultrahigh resolution mass spectrometry, Geochim. Cosmochim. Ac., 73, 4384–4399, 2009.

Lam, B., Baer, A., Alaee, M., Lefebvre, B., Moser, A., Williams, A., and Simpson, A. J.: Major structural components in freshwater dissolved organic matter, Environ. Sci. Technol., 41, 8240–8247, 2007.

Leenheer, J. A., Nanny, M. A., and McIntyre, C.: Terpenoids as major precursors of dissolved organic matter in landfill leachates, surface water, and groundwater, Environ. Sci. Technol., 37, 2323–2331, 2003.

Lipp, J. S. and Hinrichs, K. U.: Structural diversity and fate of intact polar lipids in marine sediments, Geochim. Cosmochim. Ac., 73, 6816–6833, 2009.

Mahieu, N., Powlson, D. S., and Randall, E. W.: Statistical analysis of published carbon-13 CPMAS NMR spectra of soil organic matter, Soil Sci. Soc. Am. J., 63, 307–319, 1999.

Maie, N., Parish, K. J., Watanabe, A., Knicker, H., Benner, R., Abe, T., Kaiser, K., and Jaffe, R.: Chemical characteristics of dissolved organic nitrogen in an oligotrophic subtropical coastal ecosystem, Geochim. Cosmochim. Ac., 70, 4491–4506, 2006.

Mao, J. D., Kong, X. Q., Schmidt-Rohr, K., Pignatello, J. J., and Perdue, E. M.: Advanced Solid-State NMR Characterization of Marine Dissolved Organic Matter Isolated Using the Coupled Reverse Osmosis/Electrodialysis Method, Environ. Sci. Technol., 46, 5806–5814, 2012.

Martin, G. E., Hilton, B. D., Moskau, D., Freytag, N., Kessler, K., and Colson, K.: Long-range ^{1}H-^{15}N heteronuclear shift correlation across wide F1 spectral windows, Magn. Reson. Chem., 48, 935–937, 2010.

Masiello, C. A.: New directions in black carbon organic geochemistry, Mar. Chem., 92, 201–213, 2004.

Masiello, C. A. and Druffel, E. R. M.: Black carbon in deep-sea sediments, Science, 280, 1911–1913, 1998.

McCaul, M. V., Sutton, D., Simpson, A. J., Spence, A., McNally, D. J., Moran, B. W., Goel, A., O'Connor, B., Hart, K., and Kelleher, B. P.: Composition of dissolved organic matter within a lacustrine environment, Environ. Chem., 8, 146–154, 2011.

McCollom, T. M. and Seewald, J. S.: Abiotic synthesis of organic compounds in deep-sea hydrothermal environments, Chem. Rev., 107, 382–401, 2007.

McKee, G. A. and Hatcher, P. G.: Alkyl amides in two organic-rich anoxic sediments: A possible new abiotic route for N sequestration, Geochim. Cosmochim. Ac., 74, 6436–6450, 2010.

Mopper, K., Stubbins, A., Ritchie, J. D., Bialk, H. M., and Hatcher, P. G.: Advanced instrumental approaches for characterization of marine dissolved organic matter: Extraction techniques, mass spectrometry, and nuclear magnetic resonance spectroscopy, Chem. Rev., 107, 419–442, 2007.

Moskau, D.: Application of real time digital filters in NMR spectroscopy, Concept. Magnetic Res., 15, 164–176, 2002.

Nagata, T., Tamburini, C., Arístegui, J., Baltar, F., Bochdansky, A. B., Fonda-Umani, S., Kukuda, H., Gogou, A., Hansell, D. A., Hansman, R. L., Herndl, G. J., Panagiotopoulos, C., Reinthaler, T., Sohrin, R., Verdugo, P., Yamada, N., Yamashita, Y., Yokokawa, T., and Bartlett, D. H.: Emerging concepts on microbial processes in the bathypelagic ocean – ecology, biogeochemistry, and genomics, Deep-Sea Res. Pt. II, 57, 1519–1536, 2010.

Ohno, T., He, Z. Q., Sleighter, R. L., Honeycutt, C. W., and Hatcher, P. G.: Ultrahigh resolution mass spectrometry and indicator species analysis to identify marker components of soil- and plant biomass-derived organic matter fractions, Environ. Sci. Technol., 44, 8594–8600, 2010.

Opsahl, S. and Benner, R..: Distribution and cycling of terrigenous dissolved organic matter in the ocean, Nature, 386, 480–482, 1997.

Opsahl, S. and Benner, R..: Photochemical reactivity of dissolved lignin in river and ocean waters, Limnol. Oceanogr., 43, 1297–1304, 1998.

Panagiotopoulos, C., Repeta, D. J., and Johnson, C. G.: Characterization of methyl sugars, 3-deoxysugars and methyl deoxysugars in marine high molecular weight dissolved organic matter, Org. Geochem., 38, 884–896, 2007.

Paytan, A., Mackey, K. R. M., Chen, Y., Lima, I. D., Doney, S. C., Mahowald, N., Labiosa, R., and Post, A. F.: Toxicity of atmospheric aerosols on marine phytoplankton, P. Natl. Acad. Sci. USA, 106, 4601–4605, 2009.

Perdue, E. M., Hertkorn, N., and Kettrup, A.: Substitution patterns in aromatic rings by increment analysis. Model development and application to natural organic matter, Anal. Chem., 79, 1010–1021, 2007.

Pohl, C., Croot, P. L., Hennings, U., Daberkow, T., Budeus, G., and v. d. Loeff, M. R.: Synoptic transects on the distribution of trace elements (Hg, Pb, Cd, Cu, Ni, Zn, Co, Mn, Fe, and Al) in surface waters of the Northern- and Southern East Atlantic, J. Mar. Syst., 84, 28–41, 2011.

Pos, W. H., Riemer, D. D., and Zika, R. G.: Carbonyl sulfide (OCS) and carbon monoxide (CO) in natural waters: Evidence of a coupled production pathway, Mar. Chem., 62, 89–101, 1998.

Repeta, D. J., Quan, T. M., Aluwihare, L. I., and Accardi, A. M.: Chemical characterization of high molecular weight dissolved organic matter in fresh and marine waters, Geochim. Cosmochim. Ac, 66, 955–962, 2002.

Rezende, C. E., Pfeiffer, W. C., Martinelli, L. A., Tsamakis, E., Hedges, J. I., and Keil, R. G.: Lignin phenols used to infer organic matter sources to Sepetiba Bay – RJ, Brasil, Estuar. Coast. Shelf. Sci., 87, 479–486, 2010.

Ritchie, J. D. and Perdue, E. M.: Analytical constraints on acidic functional groups in humic substances, Org. Geochem., 39, 783–799, 2008.

Schmidt, F., Elvert, M., Koch, B. P., Witt, M., and Hinrichs, K.-U.: Molecular characterization of dissolved organic matter in pore water of continental shelf sediments, Geochim. Cosmochim. Ac., 73, 3337–3358, 2009.

Schmidt, F., Koch, B. P., Elvert, M., Schmidt, G., Witt, M., and Hinrichs, K. U.: Diagenetic transformation of dissolved organic nitrogen compounds under contrasting sedimentary redox conditions in the black sea, Environ. Sci. Technol., 45, 5223–5229, 2011.

Schmitt-Kopplin, P., Hertkorn, N., Schulten, H. R., and Kettrup, A.: Structural changes in a dissolved soil humic acid during photochemical degradation processes under O_2 and N_2 atmosphere, Environ. Sci. Technol., 32, 2531–2541, 1998.

Schmitt-Kopplin, P., Gabelica, Z., Gougeon, R. D., Fekete, A., Kanawati, B., Harir, M., Gebefuegi, I., Eckel, G., and Hertkorn, N.: High molecular diversity of extraterrestrial organic matter in murchison meteorite revealed 40 years after its fall, P. Natl. Acad. Sci. USA, 107, 2763–2768, 2010a.

Schmitt-Kopplin, P., Gelencser, A., Dabek-Zlotorzynska, E., Kiss, G., Hertkorn, N., Harir, M., Hong, Y., and Gebefuegi, I.: Analysis of the unresolved organic fraction in atmospheric aerosols with ultrahigh-resolution mass spectrometry and nuclear magnetic resonance spectroscopy: Organosulfates as photochemical smog constituents, Anal. Chem., 82, 8017–8026, 2010b.

Simpson, A. J. and Brown, S. A.: Purge NMR: Effective and easy solvent suppression, J. Magn. Reson., 175, 340–346, 2005.

Simpson, A. J., Kingery, W. L., Hayes, M. H. B., Spraul, M., Humpfer, E., Dvortsak, P., Kerssebaum, R., Godejohann, M., and Hofmann, M.: Molecular structures and associations of humic substances in the terrestrial environment, Naturwissenschaften, 89, 84–88, 2002.

Simpson, A. J., McNally, D. J., and Simpson, M. J.: NMR spectroscopy in environmental research: From molecular interactions to global processes, Prog. Nucl. Mag. Res. Sp., 58, 97–175, 2011.

Smernik, R. J. and Oades, J. M.: Paramagnetic effects on solid state ^{13}C nuclear magnetic resonance spectra of soil organic matter, J. Environ. Qual., 31, 414–420, 2002.

Sohrin, Y., Urushihara, S., Nakatsuka, S., Kono, T., Higo, E., Minami, T., Norisuye, K., and Umetani, S.: Multielemental determination of Geotraces Key trace metals in seawater by ICPMS after preconcentration using an ethylenediaminetriacetic acid chelating resin, Anal. Chem., 80, 6267–6273, 2008.

Stenson, A. C.: Reversed-Phase Chromatography Fractionation Tailored to Mass Spectral Characterization of Humic Substances, Environ. Sci. Technol., 42, 2060–2065, 2008.

Stenson, A. C., Marshall, A. G., and Cooper, W. T.: Exact masses and chemical formulas of individual Suwannee River fulvic acids from ultrahigh resolution electrospray ionization Fourier Transform ion cyclotron resonance mass spectra, Anal. Chem., 75, 1275–1284, 2003.

Stubbins, A., Niggemann, J., and Dittmar, T.: Photo-lability of deep ocean dissolved black carbon, Biogeosciences, 9, 1661–1670, doi:10.5194/bg-9-1661-2012, 2012.

Takeda, A., Tsukada, H., Takaku, Y., and Hisamatsu, S.: Fractionation of metal complexes with dissolved organic matter in a rhizosphere soil solution of a humus-rich andosol using size exclusion chromatography with inductively coupled plasma-mass spectrometry, Soil. Sci. Plant. Nutr., 55, 349–357, 2009.

Taylor, B. B., Torrecilla, E., Bernhardt, A., Taylor, M. H., Peeken, I., Röttgers, R., Piera, J., and Bracher, A.: Bio-optical provinces in the eastern Atlantic Ocean and their biogeographical relevance, Biogeosciences, 8, 3609–3629, doi:10.5194/bg-8-3609-2011, 2011.

Tomczak, M. and Godfrey, J. S.: Regional Oceanography: An Introduction, 2nd Edn., Daya Publishing House, Delhi, 390 pp., 2003.

Tominaga, K., Sakamoto, Y., Fujimaki, Y., Takekawa, M., and Ohshima, S.: Structural analysis of hepta-, nona-, and undecacyclic aromatic hydrocarbons by NMR spectroscopy, Polycycl. Aromat. Comp., 30, 274–286, 2010.

Turano, P., Lalli, D., Felli, I. C., Theil, E. C., and Bertini, I.: NMR reveals pathway for ferric mineral precursors to the central cavity of ferritin, P. Natl. Acad. Sci. USA, 107, 545–550, 2010.

Tziotis, D., Hertkorn, N., and Schmitt-Kopplin, P.: Kendrick-analogous network visualisation of ion cyclotron resonance Fourier transform mass spectra: improved options for the assignment of elemental compositions and the classification of organic molecular complexity, Eur. J. Mass Spectrom., 17, 415–421, 2011.

Vraspir, J. M. and Butler, A.: Chemistry of marine ligands and siderophores, Annu. Rev. Mar. Sci., 1, 43–63, 2009.

Walker, B. D., Beaupre, S. R., Guilderson, T. P., Druffel, E. R. M., and McCarthy, M. D.: Large-volume ultrafiltration for the study of radiocarbon signatures and size vs. age relationships in marine dissolved organic matter, Geochim. Cosmochim. Ac., 75, 5187–5202, 2011.

Williamson, D. S., Cremonesi, P., Cavalieri, E., Nagel, D. L., Markin, R. S., and Cohen, S. M.: Assignment of ^{1}H NMR Spectra of Polycyclic Aromatic Hydrocarbons by Multiple Quantum Filtration, J. Org. Chem., 51, 5210–5213, 1986.

Witter, A. E., Hutchins, D. A., Butler, A., and Luther, G. W.: Determination of conditional stability constants and kinetic constants for strong model Fe-binding ligands in seawater, Mar. Chem., 69, 1–17, 2000.

Woods, G. C., Simpson, M. J., Koerner, P. J., Napoli, A., and Simpson, A. J.: HILIC-NMR: Toward the identification of individual molecular components in dissolved organic matter, Environ. Sci. Technol., 45, 3880–3886, 2011.

Woods, G. C., Simpson, M. J., and Simpson, A. J.: Oxidized sterols as a significant component of dissolved organic matter: Evidence from 2D HPLC in combination with 2D and 3D NMR spectroscopy, Water Res., 46, 3398–3408, 2012.

Xia, Y. L., Moran, S., Nikonowicz, E. P., and Gao, X. L.: Z-restored spin-echo ^{13}C 1d spectrum of straight baseline free of hump, dip and roll, Magn. Reson. Chem., 46, 432–435, 2008.

Zepp, R. G., Erickson, D. J., Paul, N. D., and Sulzberger, B.: Effects of solar UV radiation and climate change on biogeochemical cycling: Interactions and feedbacks, Photoch. Photobio. Sci., 10, 261–279, 2011.

Ziolkowski, L. A. and Druffel, E. R. M.: Aged black carbon identified in marine dissolved organic carbon, Geophys. Res. Lett., 37, L16601, doi:10.1029/2010GL043963, 2010.